AD-A036 498 NAVAL WEAPONS CENTER CHINA LAKE CALIF F/G 1/3
GATOR/AV-8A ENVIRONMENTAL CAPTIVE FLIGHT VIBRATION RESPONSE TES--ETC(U)
FEB 77 K T KATSUMOTO, W W PARMENTER
UNCLASSIFIED NWC-TP-5883 NL

1 OF 2
AD-A
036 498

GATOR/AV-8A ENVIRONMENTAL CAPTIVE FLIGHT VIBRATION RESPONSE TESTS

NAVAL WEAPONS CENTER
CHINA LAKE, CALIFORNIA

FEBRUARY 1977

NWC TP 5883

GATOR/AV-8A Environmental Captive Flight Vibration Response Tests

by
K. T. Katsumoto
and
W. W. Parmenter
Propulsion Development Department

FEBRUARY 1977

Naval Weapons Center
CHINA LAKE, CALIFORNIA 93555

UNCLASSIFIED

SECURITY CLASSIFICATION OF THIS PAGE (When Data Entered)

REPORT DOCUMENTATION PAGE		READ INSTRUCTIONS BEFORE COMPLETING FORM
1. REPORT NUMBER NWC TP 5883	2. GOVT ACCESSION NO.	3. RECIPIENT'S CATALOG NUMBER
4. TITLE (and Subtitle) GATOR/AV-8A ENVIRONMENTAL CAPTIVE FLIGHT VIBRATION RESPONSE TESTS		5. TYPE OF REPORT & PERIOD COVERED Final Report October 1974-January 1976 6. PERFORMING ORG. REPORT NUMBER
7. AUTHOR(s) K. T. Katsumoto W. W. Parmenter		8. CONTRACT OR GRANT NUMBER(s)
9. PERFORMING ORGANIZATION NAME AND ADDRESS Naval Weapons Center China Lake, CA 93555		10. PROGRAM ELEMENT, PROJECT, TASK AREA & WORK UNIT NUMBERS A532-5323/008-D/WMW170000
11. CONTROLLING OFFICE NAME AND ADDRESS Naval Air Systems Command Washington, D.C.		12. REPORT DATE February 1977 13. NUMBER OF PAGES 102
14. MONITORING AGENCY NAME & ADDRESS(if different from Controlling Office)		15. SECURITY CLASS. (of this report) UNCLASSIFIED 15a. DECLASSIFICATION/DOWNGRADING SCHEDULE

16. DISTRIBUTION STATEMENT (of this Report)

Approved for public release, distribution unlimited.

17. DISTRIBUTION STATEMENT (of the abstract entered in Block 20, if different from Report)

18. SUPPLEMENTARY NOTES

19. KEY WORDS (Continue on reverse side if necessary and identify by block number)

Environmental Criteria Determination
Captive Flight Vibration Response
Component/Mine Response
Vibration Data Analysis
Spectral Analysis
Dynamic Data Instrumentation/Measurement/Analysis

20. ABSTRACT (Continue on reverse side if necessary and identify by block number)

See back of this form.

DD FORM 1 JAN 73 1473 EDITION OF 1 NOV 65 IS OBSOLETE
S/N 0102-014-6601

UNCLASSIFIED

SECURITY CLASSIFICATION OF THIS PAGE (When Data Entered)

(U) *GATOR/AV-8A Environmental Captive Flight Vibration Response Tests*, by K. T. Katsumoto and W. W. Parmenter. China Lake, Calif., Naval Weapons Center, February 1977 102 pp. (NWC TP 5883, publication UNCLASSIFIED.)

(U) A series of flights using an AV-8A aircraft and the GATOR weapon (Navy version, Mk 7 dispenser) were made. Vibration and acoustic responses were measured for this externally carried ordnance during typical flight conditions. Acceleration power spectral density plots are presented and test levels are recommended.

Naval Weapons Center

AN ACTIVITY OF THE NAVAL MATERIAL COMMAND

R. G. Freeman, III, Rear Adm., USN ..... Commander
G. L. Hollingsworth ..... Technical Director

FOREWORD

This effort was authorized by the Naval Air Systems Command under the Airtask A532-5323/008-D/6-WMW170000, Joint Service Program for Air Delivered Antipersonnel and Antivehicle Target-Activated Munitions Systems. The work described was performed during the period of October 1974 to January 1976. This publication is a final report on environmental captive flight vibration tests conducted with the GATOR Weapon System under actual flight conditions using an AV-8A aircraft. Dynamic and thermal response data are presented in considerable detail.

This report has been reviewed for technical accuracy by M. L. Braithwaite.

Released by
G. W. LEONARD, *Head*
Propulsion Development Department
1 September 1976

Under authority of
G. L. HOLLINGSWORTH,
Technical Director

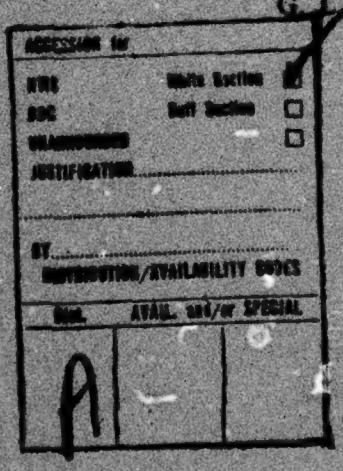

NWC Technical Publication 5883

Published by ..... Propulsion Development Department
Collation ..... Cover, 53 leaves
First printing ..... 185 unnumbered copies

CONTENTS

ACKNOWLEDGMENT

The able assistance of Mr. P. Mercado in the data acquisition system installation, calibration, and flight conduct is gratefully acknowledged.

Special mention must be made of the efforts of the pilot, LT Mickey Taylor. Through his quick response and willingness, the flight tests were efficiently performed.

The authors wish to extend their thanks to Mr. J. L. Bateman for his assistance in the report documentation and editing.

INTRODUCTION

In formulating a captive-flight vibration qualification test for a tactical weapon, the weapon developer will most likely turn to the existing specification MIL-STD-810C, Method 514.2, Procedure II, for energy levels and time limits. However, where a novel type of weapon delivery platform is involved, the calculated test levels *may* or *may not* be appropriate. This is because the dynamic prediction techniques of MIL-STD-810C are based upon information derived from data relative to recent conventional weapon systems and delivery methods. If prediction techniques other than those outlined are used then even less credibility can be afforded to the dynamic test levels. Such a situation existed relative to the AV-8A Harrier aircraft. This vehicle is a relatively new weapon delivery platform having a design using thrust vector control (TVC) techniques for maneuvers. The dynamic environment induced by an aircraft of this type had not been measured prior to the effort reported herein. Of concern were the weapon environments affected by the exhaust from the jet engine nozzles. These nozzles are relatively close to the inboard pylon wing stations.

A test program was devised to conduct a series of evaluation tests.[1] Accordingly, a GATOR weapon (Navy version, Mk 7 dispenser) was instrumented and the dynamic environment was measured while the test unit was carried by the AV-8A aircraft. The test flights were conducted from the Naval Air Facility (NAF), Naval Weapons Center (NWC), China Lake, California, on 11 and 12 August 1975. This report describes the tests and presents the results of the captive flight vibration response tests.

WEAPON DESCRIPTION

The GATOR air-Delivered Target-Activated Weapon System is comprised of five major variations as shown in Figure 1. The particular weapon configuration used for this flight test effort is identified as the SUU-58(X1-1)/B and is shown in Figure 2. This is the Navy Mk 7 Mod 3 dispenser containing the KMU-428 (X1-1)/B adapter kit, the BLU-91/B and BLU-92/B mines, and a Mk 339 fuze. All of the GATOR mines used were N-2 ballistic dummy mines (constructed in accordance with Air Force Drawing X734045, Code Identification 18894, which is an early development version). A typical dummy mine is shown in Figure 3. With the 54 assembled mines, dunnage, fuze, dispenser, and internally mounted instrumentation, the 13.2 inch (33.5 cm) diameter by 12 feet (360 cm) long weapon had a total weight of 437 pounds (197 kg). The center of gravity was 9 inches (23 cm) aft of the forward lug.

---

[1] Naval Weapons Center. *Captive Flight Environmental Vibration Measurements of the GATOR Weapon Carried by the AV-8A (Harrier) Aircraft* by W. W. Parmenter. China Lake, CA, NWC, October 1974. (NWC Memo Reg 4533-052-75, publication UNCLASSIFIED.)

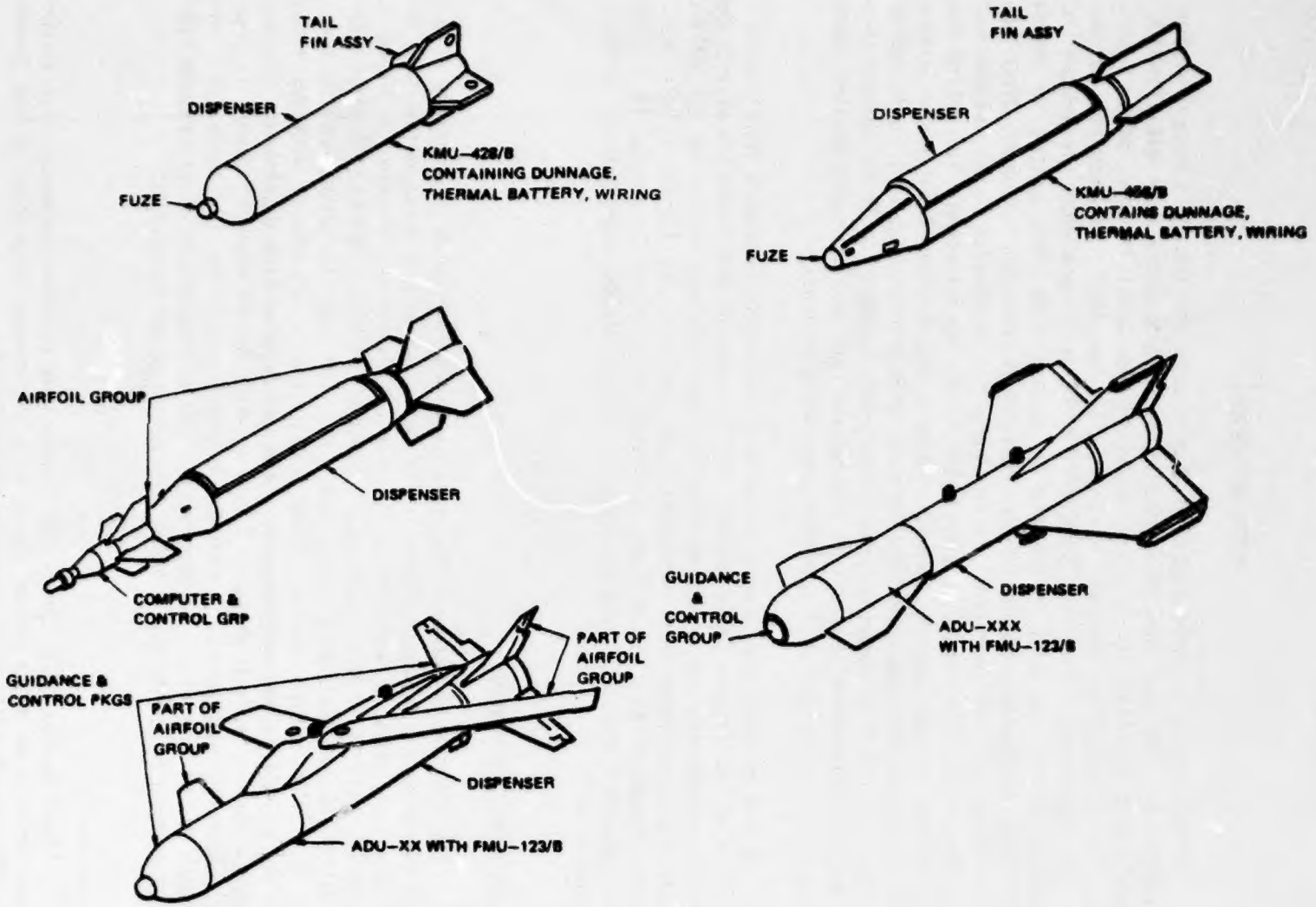

FIGURE 1. Major GATOR Weapon System Variations.

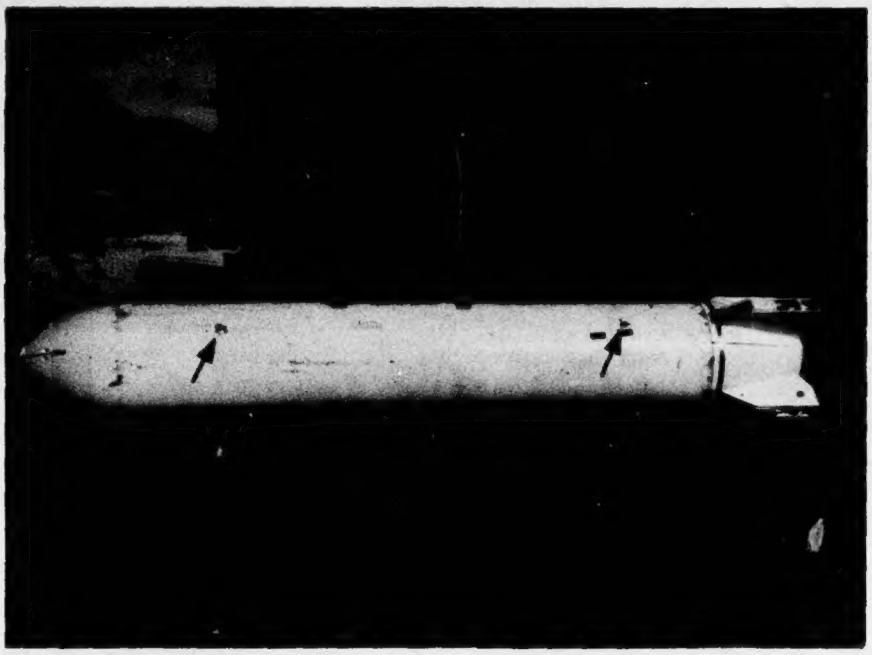

FIGURE 2. Instrumented GATOR Weapon System.(Arrows indicate location of two of the surface microphones.)

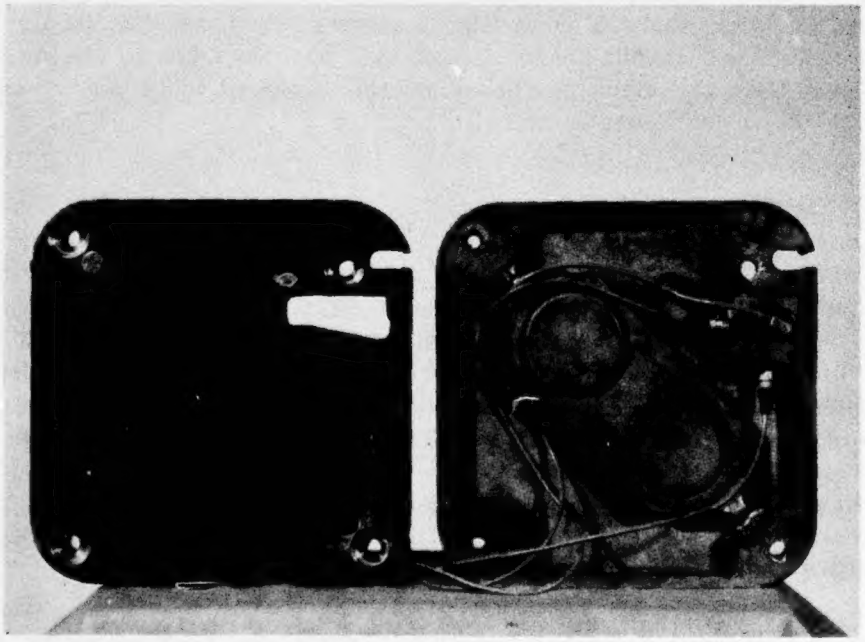

FIGURE 3. Typical Dummy GATOR Mine Used in This Test Effort. (The triaxial accelerometer with leads is shown.)

DATA ACQUISITION SYSTEM

The data acquisition system used for the captive flight tests was completely self-contained within the instrumented GATOR weapon and the Weapon Environmental Measuring Acquisition System (WEMAS) pod. A block diagram of the data acquisition system is presented in Figure 4. Dynamic data were transmitted from the instrumented GATOR weapon located on the starboard wing to the WEMAS pod on the portside wing. Within the WEMAS pod, a receiver and a 1-inch wide, 14-channel magnetic tape recorder acquired the dynamic data. The WEMAS pod has been fully documented.[2]

The instrumentation used along with the component characteristics are given in Table 1. The upper frequency response of the equipment limited the accelerometer and microphone data to 2,000 and 10,000 Hz, respectively. This limitation also coincided with the current typical limitations on environmental laboratory testing equipment capability and MIL-STD-810C.

MINE INSTRUMENTATION AND LOADING

The charge amplifiers, subcarrier oscillators (SCO), mixers, and other signal conditioning components were mounted within nine of the dummy GATOR mines. These particular mines were loaded at the aft end of the GATOR dispenser to allow for ease of access to the instrumentation for checkout and calibration purposes. Photographs of this installation and loading operation are shown in Figures 5, 6, and 7. All of the data signals were routed within the instrumented weapon. Transducer cables were low-noise shielded wires. Dental cement or an insulated mount was used for attachment of the transducers. In all instances, care was taken to electrically isolate the transducer cases and eliminate the occurrence of ground loops. System component locations are shown in Figures 8 through 11.

CALIBRATION TECHNIQUE

Calibration of the entire assembled data acquisition system was performed by the insertion of known voltage levels into the inputs of the charge amplifiers. The signal was a 1-kHz sinusoid of 10 *g* (0-peak) for the accelerometers and 165 dB and 2 kHz for the microphones. These respective calibration signals were amplified, multiplexed, transmitted, received, and recorded using the exact instrumentation components previously described. During the subsequent data reduction process, these multiplexed calibration signals were discriminated and digitized and used to provide input calibration values for converting digitized flight data to engineering units. Thus, the digital spectral analysis plot outputs had calibrated axes from the entire system calibration for each particular transducer.

---

[2] Naval Weapons Center. *Weapon Environmental Measuring Acquisition System,* by W. W. Parmenter, China Lake, CA, NWC, July 1974. (NWC TP 5579, publication UNCLASSIFIED.)

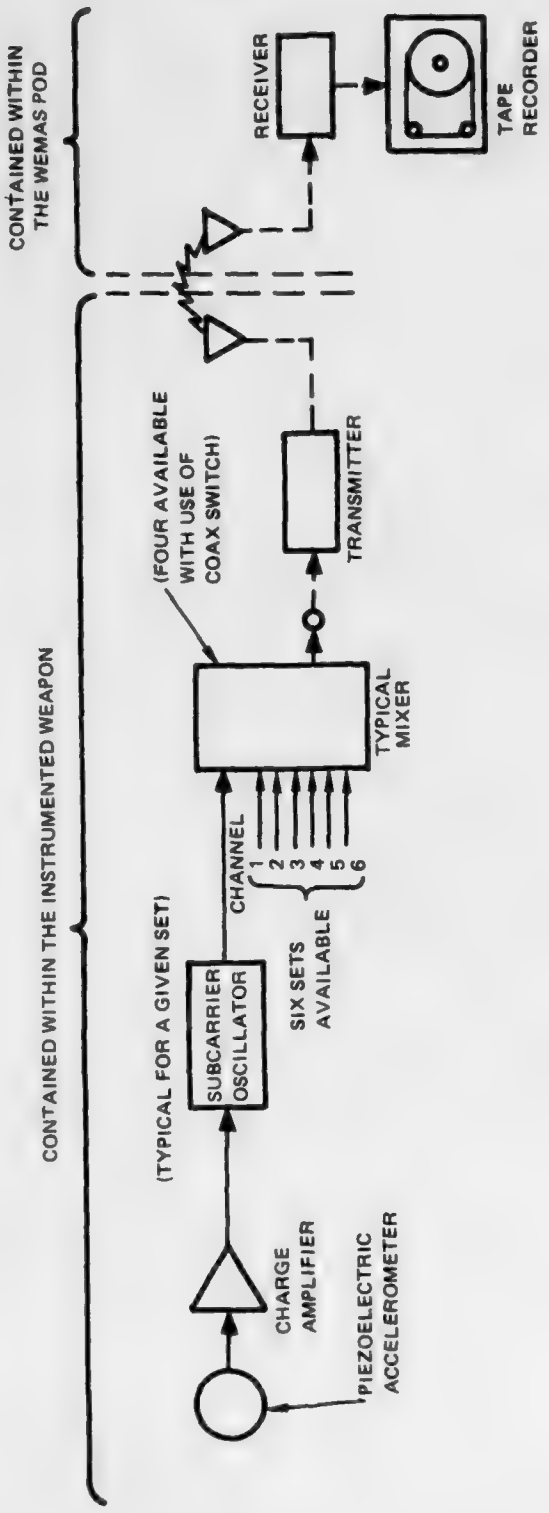

FIGURE 4. Data Acquisition Schematic.

TABLE 1. Item Description and Frequency Response of Instrumentation Used.

Type of instrument	Manufacturer	Model number	Frequency response
Accelerometer	Endevco	2221 D	2 to 7,000 Hz (±5%)
Accelerometer	Endevco	2223	3 to 4,000 Hz (±5%)
Microphone	Endevco	2510 M4A	2 to 10,000 Hz (±2 dB)
Charge amplifier (vibration)	Endevco	2640 M14	5 to 20,000 Hz (±5%)
Charge amplifier (acoustic)	Endevco	2640 M67	5 to 20,000 Hz (±5%)
VCO (vibration)	IED	CSO 335	0 to 2,000 Hz[a]
VCO (acoustic)	IED	CSO 300 C	0 to 8,000 Hz[b]
Mixer amplifier (vibration)	IED	CMA 435 A	0.05 to 200 kHz
Mixer amplifier (acoustic)	IED	CMA 400 C	0.2 to 500 kHz
Transmitter	Conic	CTM-UHF 400-5	0.01 to 500 kHz (±1.5 dB)
Receiver	Babcock	BCR 100 A	0.01 to 200 kHz (±1.5 dB)
Tape Recorder	Ampex	AR-700	0.15 to 150 kHz at 30 in/sec and 0.3 to 300 kHz at 60 in/sec (±3 dB, direct record electronics)

[a] Frequency response with ±4-kHz deviation and a modulation index of 2.

[b] Frequency response with ±16-kHz deviation and a modulation index of 2.

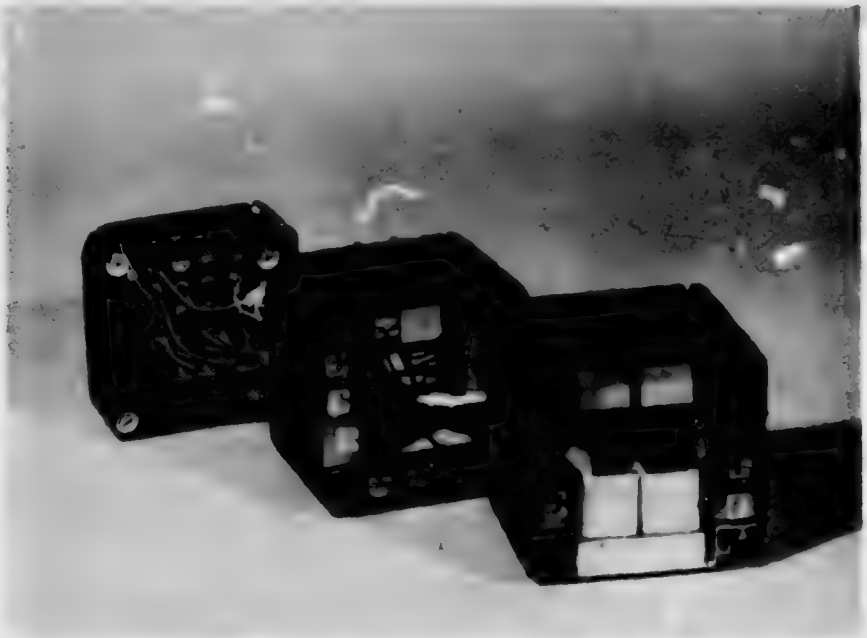

FIGURE 5. Dummy GATOR Mines with Signal Conditioning Electronics Installed.

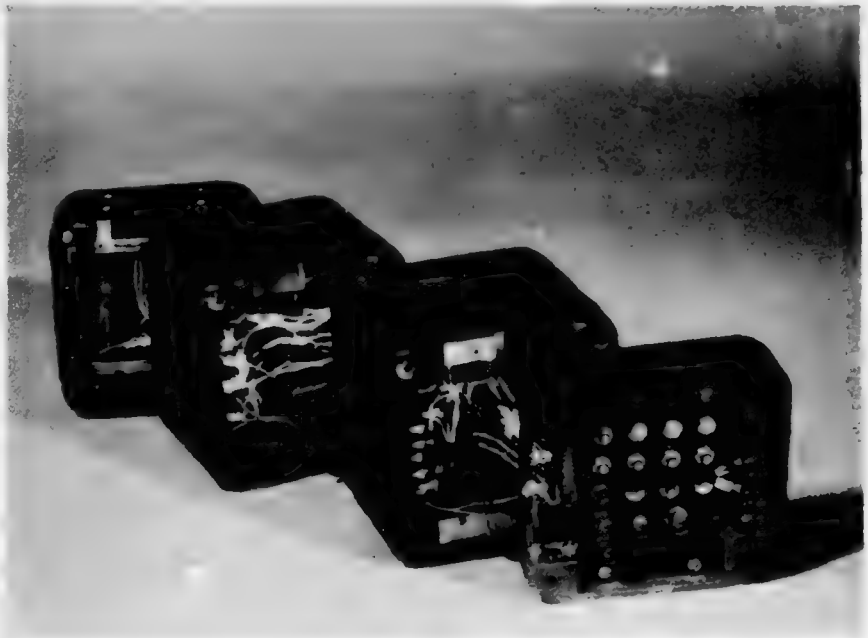

FIGURE 6. Dummy GATOR Mines with Signal Conditioning Electronics and Associated Hardware Installed.

FIGURE 7. Mk 7 Dispenser Being Loaded with Dummy GATOR Mines for Vibration Tests.

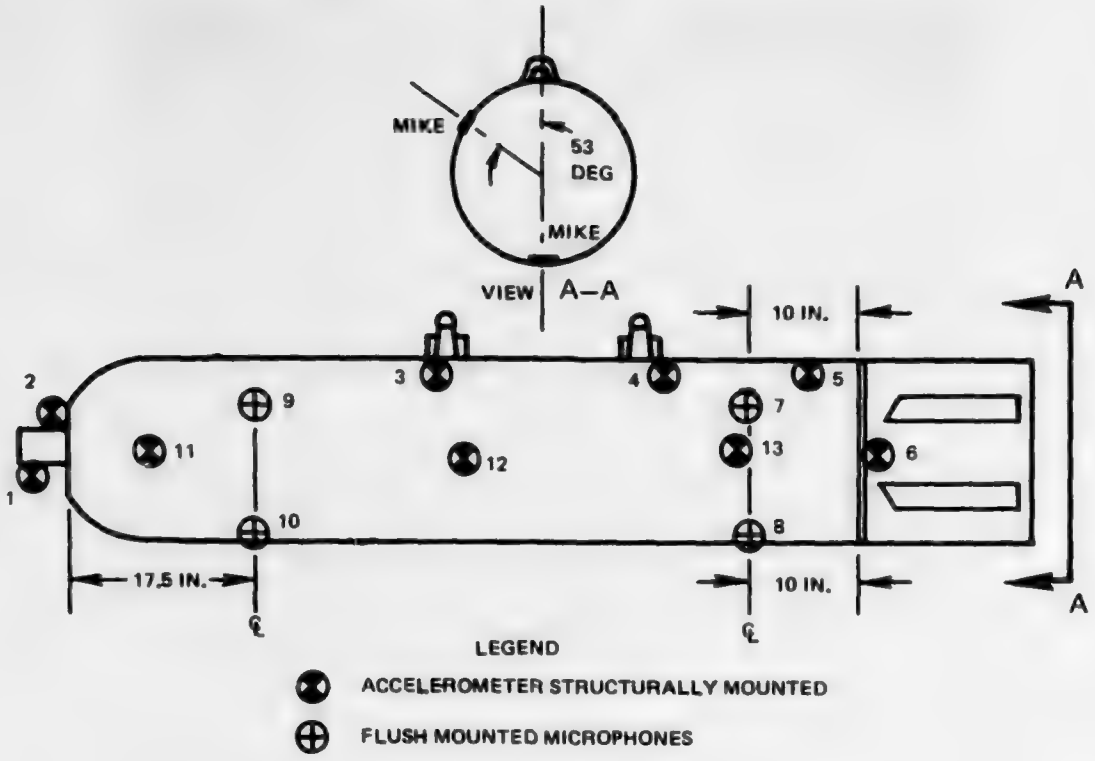

NO.	COMPONENT	LOCATION
1	TRIAXIAL ACCELEROMETER	FUZE
2	BIAXIAL ACCELEROMETER	FRONT OF STORE, ON FORWARD BULKHEAD
3	BIAXIAL ACCELEROMETER	UNDER FWD LUG ON STRONGBACK
4	TRIAXIAL ACCELEROMETER	UNDER AFT LUG ON STRONGBACK
5	BIAXIAL ACCELEROMETER	AFT END OF DISPENSER BODY
6	TRIAXIAL ACCELEROMETER	TAILCONE FWD BULKHEAD
7	MICROPHONE, FLUSH MOUNT	53 DEG CCW FROM TOP DEAD CENTER LOOKING FORWARD AT 25% POINT ON STORE
8	MICROPHONE, FLUSH MOUNT	BOTTOM SIDE AFT AT 25% POINT ON STORE
9	MICROPHONE, FLUSH MOUNT	53 DEG CCW FROM TOP DEAD CENTER LOOKING FORWARD AT 25% POINT ON STORE
10	MICROPHONE, FLUSH MOUNT	BOTTOM SIDE FWD AT 25% POINT ON STORE
11	TRIAXIAL ACCELEROMETER	FWD MINE IN PACKAGE, BOTTOM
12	TRIAXIAL ACCELEROMETER	CENTER MINE IN PACKAGE, BOTTOM
13	TRIAXIAL ACCELEROMETER	MINE NEAR AFT END OF PACKAGE, BOTTOM

FIGURE 8. Illustration of Instrumentation Locations.

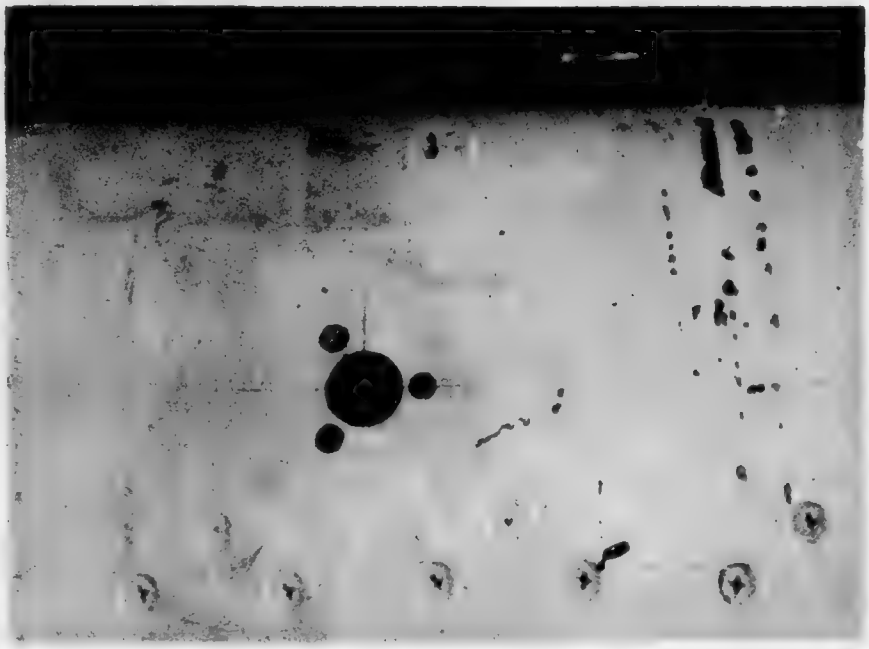

FIGURE 9. Close-Up View of a Flush-Mounted Microphone on the GATOR Weapon.

FIGURE 10. Forward End of an Inert, Instrumented, GATOR Weapon. (Arrow indicates location of accelerometers mounted on fuze and on bulkhead.)

FIGURE 11. Portion of the Tail Section of a Mk 7 Dispenser Used for GATOR Weapon Captive Flight Test. (The transmitter can be seen near the bottom of the photograph; a triaxial accelerometer can be seen mounted on the bulkhead above the transmitter.)

PREFLIGHT LABORATORY TESTS

As an additional verification of the data acquisition system, the assembled instrumented GATOR weapon was subjected to laboratory random vibration. Vibratory forces from an electrodynamic vibration exciter were exerted into the weapon by a 3/4-inch driver rod attached to a collar. The collar was arbitrarily clamped to the aft end of the weapon as shown in Figure 12. From prior experience, an excitation technique and location such as this had provided adequate response-controlled tests for other weapons when simulating captive flight vibration. The weapon was attached to an Aero 7/A bomb rack which in turn was suspended from an overhead frame using elastic cords. Figure 13 shows the overall test site setup for the transverse axis. The data from the instrumented GATOR weapon were transmitted to the WEMAS pod as shown in Figure 14.

The test employed the technique of controlled-response with the control accelerometer located near the aft bomb lug on the GATOR weapon strongback. The test level at the control accelerometer was arbitrarily chosen to be 0.002 g^2 Hz from

FIGURE 12. Mechanical Linkage Between Shaker and GATOR Weapon Used for Laboratory Vibration Tests.

FIGURE 13. GATOR Weapon Test Setup for Laboratory Vibration Test in the Transverse Axis.

FIGURE 14. Test Setup for GATOR Weapon Laboratory Vibration Test in the Vertical Axis. (The WEMAS pod to which vibration data was transmitted can be seen in the foreground.)

10 to 2,000 Hz. The acquisition system was found to be functioning properly except for three accelerometer channels. The arrival of the test aircraft precluded any repair possibility and it was judged that there were enough remaining data channels to proceed with the flight tests.

CAPTIVE FLIGHT TESTS

The aircraft used to conduct this study was the AV-8A (BuNo 159232) from VMA 513, U.S. Marine Corps Air Station, Cherry Point, North Carolina. The fully-instrumented GATOR weapon was attached to the starboard inboard wing station (ERU-119 rack) of the aircraft as shown in Figure 15. The WEMAS pod was suspended from the portside inboard wing station as shown in Figures 16 and 17.

A total of seven data flights were conducted since one transmitter/receiver was used and only one multiplexed signal could be transmitted at a time. Table 2 is a summary of the captive flight conditions. Table 3 presents information relative to transducer application for each particular flight. The normal flight-issue cassette recorder, located in the console panel of the Harrier aircraft, was inoperable for this particular aircraft during the tests. Thus, a ground receiving station at NAF was used

FIGURE 15. GATOR Weapon Installed on the Starboard Side Inboard Wing Station of the AV-8A Harrier Aircraft.

FIGURE 16. WEMAS Instrumentation Pod Mounted on the Portside Inboard Wing Station of the AV-8A Harrier Aircraft.

FIGURE 17. WEMAS Instrumentation Pod Mounted on the Harrier AV-8A Aircraft.

TABLE 2. Flight Conditions During Data Collection (Typical).

Maneuver	Speed, knots	Nozzle vector, degree	Altitude, ft[a](MSL)	Power, %	Remarks
Take-off	NA	NA	2,200	100	Rolling, short and normal
Flight	500	NA	10,000	100	Level
	537-540	NA	5,000	100	
	400	45		80	
	300	81		80	
	250	81		100	
	300	98.5		80	
Flight	250	98.5	5,000	100	Level
Landing	30-35	75	2,200	Variable	Vertical, rolling
Landing	0-5	81	2,200	Variable	Hover

NOTE: NA = not available.
MSL = mean sea level.

[a] 2,200 ft (660 meters)
10,000 ft (3,000 meters)
5,000 ft (1,500 meters)

TABLE 3. Transducer Application Per Flight Test.

SCO center frequency, kHz	Transducer location	Sensitive axis
Data Link No. 1 (Flight One) Accelerometers		
32±4	Blank	
48±4	Aft mine	Longitudinal
64±4	Aft mine	Transverse
80±4	Aft mine	Vertical
96±4	Center mine	Longitudinal
112±4	Center mine	Transverse
Data Link No. 2 (Flight Two) Accelerometers		
32±4	Fuze	Vertical
48±4	Fuze	Longitudinal
64±4	Forward bulkhead	Vertical
80±4	Forward lug	Vertical
96±4	Forward lug	Transverse
112±4	Aft lug	Transverse
Data Link No. 3 (Flight Three) Accelerometers		
32±4	Blank	
48±4	Aft bulkhead	Vertical
64±4	Aft bulkhead	Transverse
80±4	Tail assembly	Vertical
96±4	Tail assembly	Transverse
112±4	Aft lug	Vertical
Data Link No. 4 (Flight Four) Accelerometers		
32±4	Fuze	Transverse
48±4	Forward bulkhead	Transverse
64±4	Forward mine	Vertical
80±4	Forward mine	Transverse
96±4	Forward mine	Longitudinal
112±4	Center mine	Vertical
Data Link No. 5 (Flight Five) Accelerometers		
32±4	Blank	
48±4		
64±4		
80±4		
96±4	Aft lug	Longitudinal
112±4	Tail assembly	Longitudinal
Data Link No. 6 (Flight Six) Microphones		
128±16	Aft, 53 degrees	Dispenser surface
192±16	Aft, bottom	Dispenser surface
Data Link No. 7 (Flight Seven) Microphones		
128±16	Forward, 53 degrees	Dispenser surface
192±16	Forward, bottom	Dispenser surface

to record the pilot's voice during the flight events which was later correlated with the data signals recorded by the WEMAS pod. As a back-up system, the ground station also received and recorded the data signals from the instrumented weapon.

During a given test flight, data signals from six preselected piezoelectric accelerometers (out of a total of 24 such devices) were amplified and frequency-multiplexed using Inter-Range Instrumentation Group (IRIG) compatible constant bandwidth SCOs. This complex signal was transmitted, received, and then recorded. Similarly, the four microphone signals were acquired. Tape recorder speed was 30 in/sec for the accelerometer data and 60 in/sec for the microphone data. In addition to the data, an IRIG-B time code signal and 50-kHz sinusoidal reference signal were recorded. The time code signal was an aid to subsequent data editing and reduction processing; the 50-kHz sinusoidal signal was used as a reference during data playback to provide compensation for tape speed variation.

DATA ANALYSIS METHODOLOGY

The complex analog-recorded data signal was discriminated and oscillograph records were obtained, as outlined in the schematic shown in Figure 18. Marks were made on these oscillograph records to correlate between the pilot's comments and the flight conditions. The oscillograph records were visually edited, and the IRIG-B time intervals noted at areas of importance for subsequent digitizing and performance of spectral analysis.

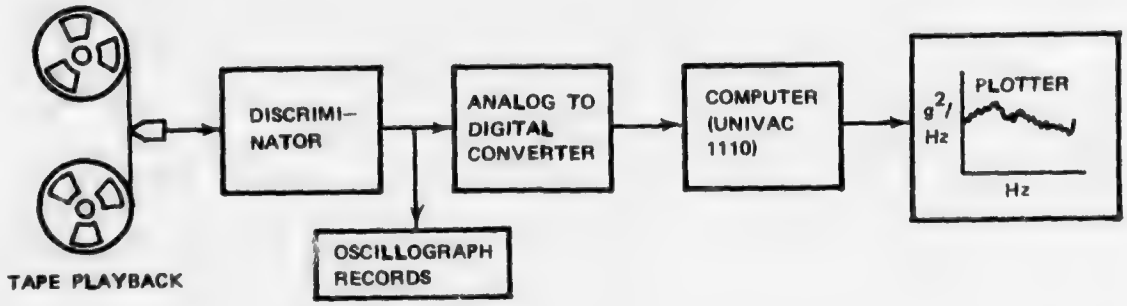

FIGURE 18. Block Diagram of Data Reduction System for Multiplexed Data.

ACCELEROMETER DATA

The digitizing was performed by the Digital Development Branch, Systems Development Department, NWC. The tape speed during playback was one-half the original recorded tape speed; the effective sampling rate with respect to the original recordings was 10,000 samples per second. Tape compensation technique was used during the analog-to-digital conversion process.

The computer program, VIBAN 3, was originally developed by the Manned Space Flight Center, Houston, Texas, and has since been installed at NWC to operate with the UNIVAC 1110. The VIBAN 3 program has been fully documented.[3]

For all of the computer plots shown in this report, 2,000 data points or 0.2 second of data were used, and the effective filter bandwidth was 7.3 Hz. The calibration signals for the data system were digitized to provide conversion factors for the plots of the computer program.

ACOUSTIC DATA

A Time/Data Real Time Analyzer, Model 100, was used to perform analysis upon selected time intervals of interest. A Digital Electronics Corporation computer, Model PDP 11/20, was programmed to yield sound pressure levels and spectra plots. Data were inputed using a 8.5 kHz low-pass filter with a 96-dB/octave rolloff.

TEST RESULTS

The selected power spectral density (PSD) plots, presented in the Appendixes, are only a small portion of the total analyses performed. Oscillograph records of the data signals always showed an increase in signal levels with dynamic pressure. (This effect has been reported in several prior measurement programs of other tactical weapons during external carriage, and thus provides confirmation of the reliability of these data.) Appendix A contains acceleration PSD plots for (1) the maximum attained free-stream dynamic pressure (about 850 psf) at 540 knots and 5,000 feet; and (2) a Harrier aircraft nozzle deflection setting of 81 degrees at 250 knots and 5,000 feet. The flow effect from the vectored nozzle impinging upon the weapon is readily apparent when comparing these spectra for a common accelerometer location. The vibration responses of the mines within the dispenser (and the dispenser itself) are significantly higher during a low-speed vectored nozzle flight condition than a maximum speed flight at a straight and level flight condition.

---

[3] Naval Weapons Center. *User's Manual for the NWC Spectral Analysis Computer Program*, by R. G. Christiansen and R. F. Klever. China Lake, CA, NWC, 15 November 1972. (NWC TP 5327, publication UNCLASSIFIED.)

Appendix B presents acceleration PSD plots obtained during the hover and rolling vertical landing conditions. RMS time history plots for the acoustic data are presented in Appendix C along with the PSD plots. The rolloff effect of the 8.5-kHz filter can be readily observed in these acoustic PSD plots. The effect of increased acoustic levels during a vectored flight versus a maximum straight and level flight condition can again be readily observed in these plots.

The acceleration PSD plots obtained from the laboratory tests are presented in Appendix D. These laboratory responses compare favorably to the response levels measured during the maximum free-stream dynamic pressure flight condition with the Harrier aircraft. The spectra do not compare as well, since no attempt was made to shape the spectra during the laboratory vibration tests. Another laboratory test iteration, with the knowledge of the flight spectra shapes would provide even better correlations.

Finally, overall g RMS levels during the selected laboratory and flight conditions are tabulated in Appendix E.

CONCLUSIONS AND RECOMMENDATIONS

The maximum observed PSD levels were enveloped and are presented in Figures 19, 20, and 21. These enveloped curves can be used to provide spectra at the various major structural points on the weapon and at the denoted components. An overall acoustic level of 160 dB is adequate for test purposes. Thus, the resulting enveloped acceleration spectra can be used in the development of a specification for the response-control vibration levels during qualification of the Navy version of the GATOR weapon.

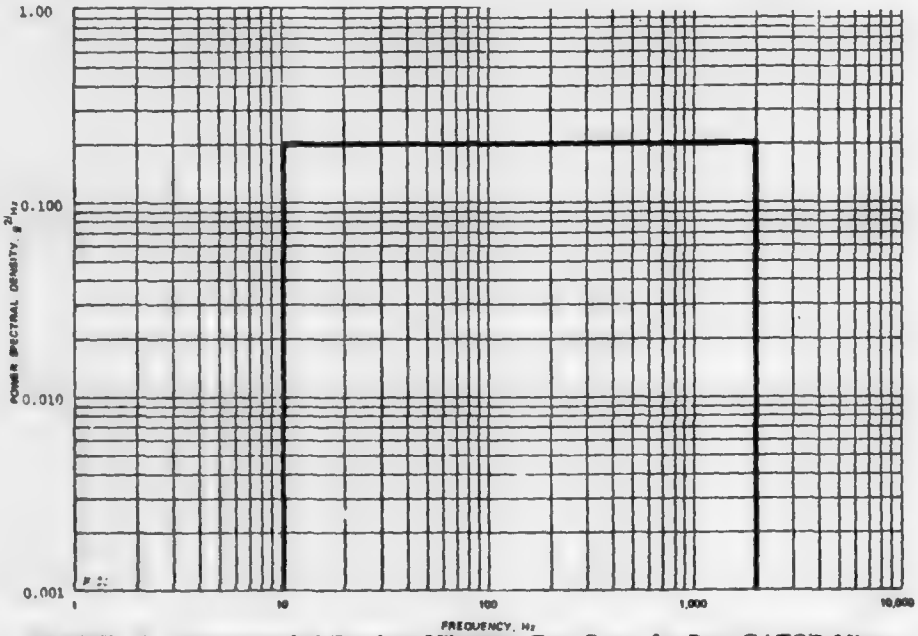

FIGURE 19. Recommended Random Vibration Test Curve for Bare GATOR Mines, all Axes.

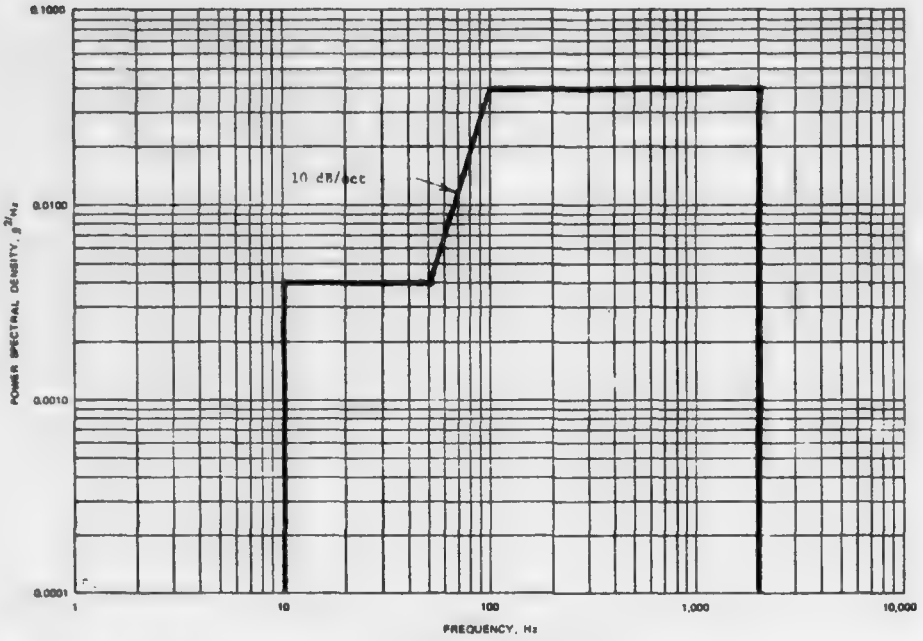

FIGURE 20. Recommended Random Vibration Test Levels for Bare Fuzes for GATOR Weapons, Transverse and Vertical Axes.

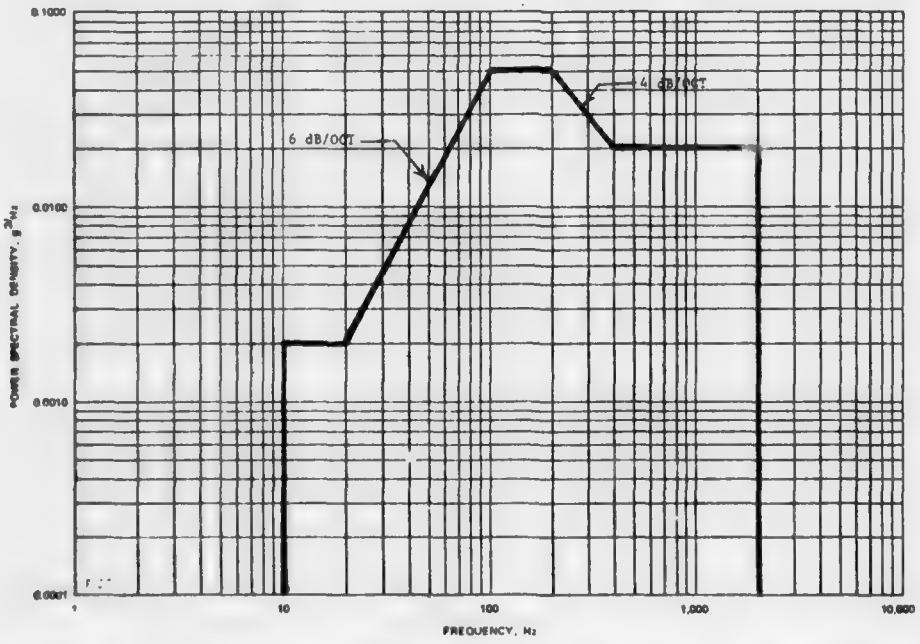

FIGURE 21. Recommended Random Vibration Test Levels for Testing All-Up GATOR Weapons, Transverse and Vertical Axes.

Appendix A

Acceleration PSD Plots:
Captive Flight Tests at Maximum Speed
(Figures A-1 through A-20)
and
250 Knots with 81 Degree Nozzle Deflection
(Figures A-21 through A-39)

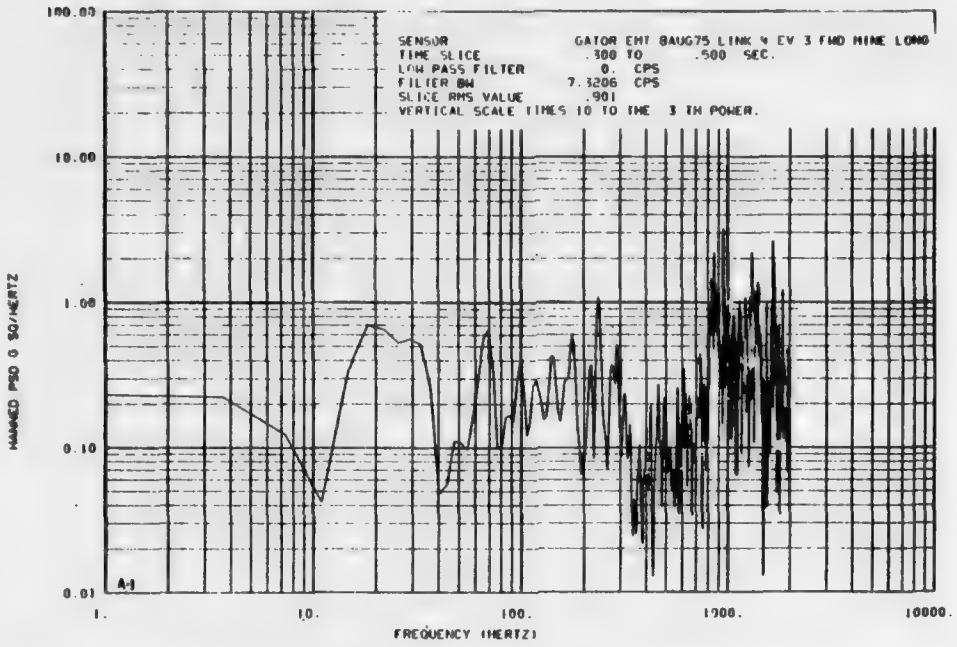

FIGURE A-1. PSD Plot Derived from Data Recorded During Flight at Maximum Speed at 5,000 Ft MSL.

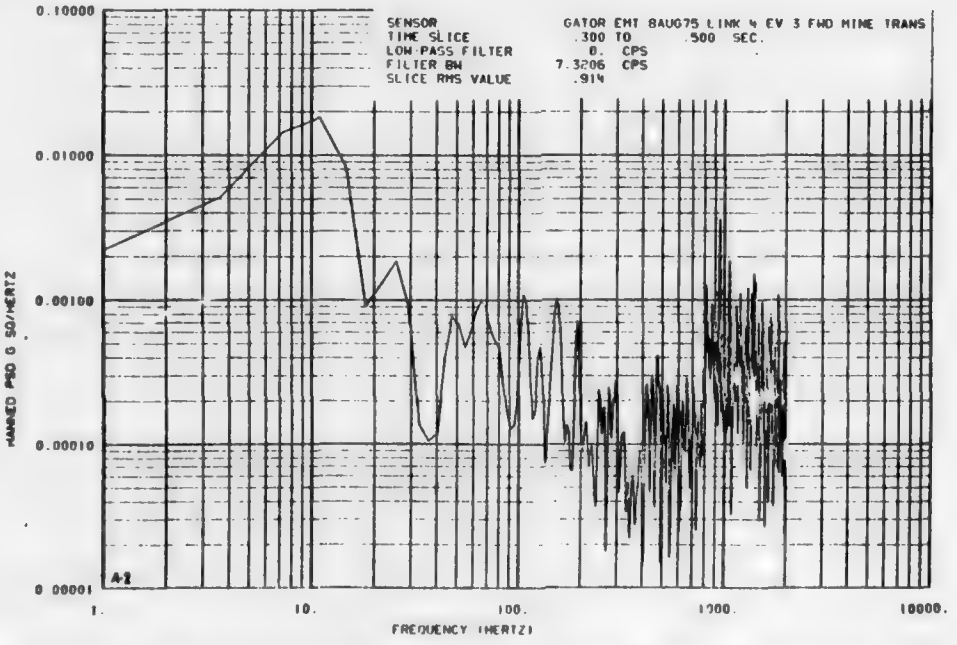

FIGURE A-2. PSD Plot Derived from Data Recorded During Flight at Maximum Speed at 5,000 Ft MSL.

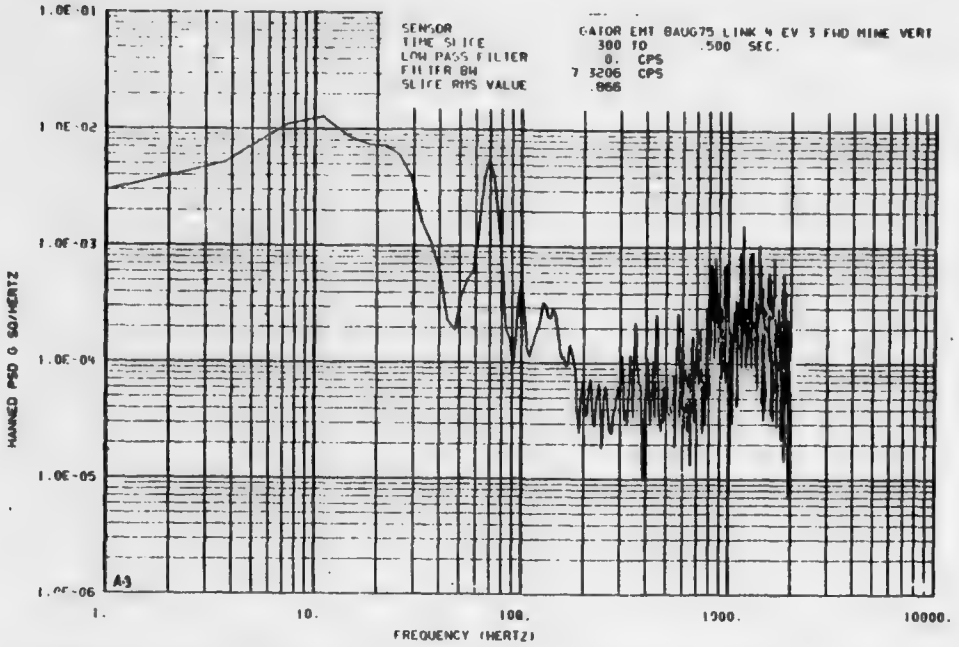

FIGURE A-3. PSD Plot Derived from Data Recorded During Flight at Maximum Speed at 5,000 Ft MSL.

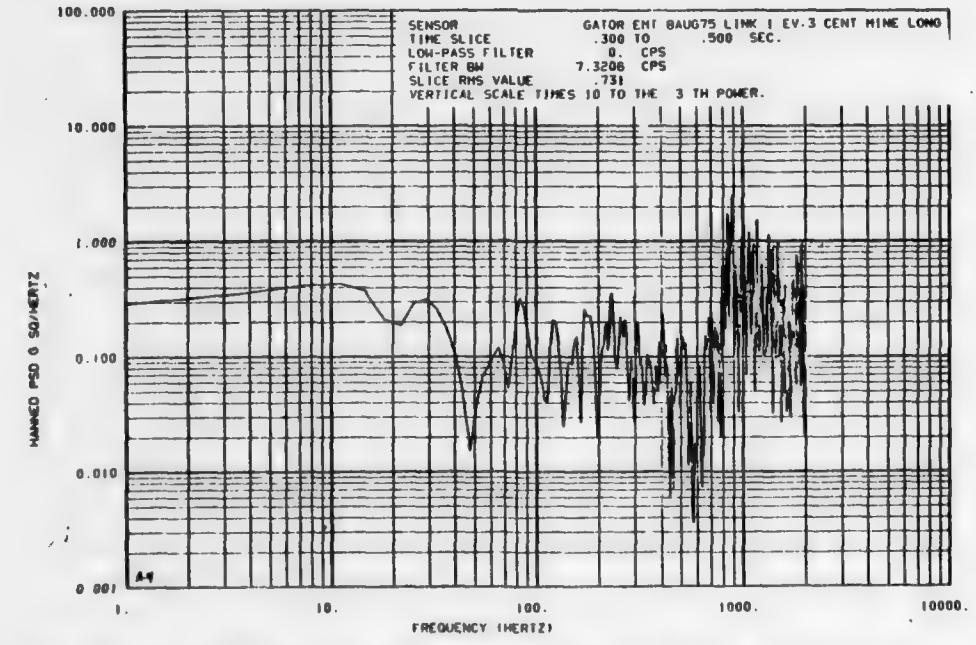

FIGURE A-4. PSD Plot Derived from Data Recorded During Flight at Maximum Speed at 5,000 Ft MSL.

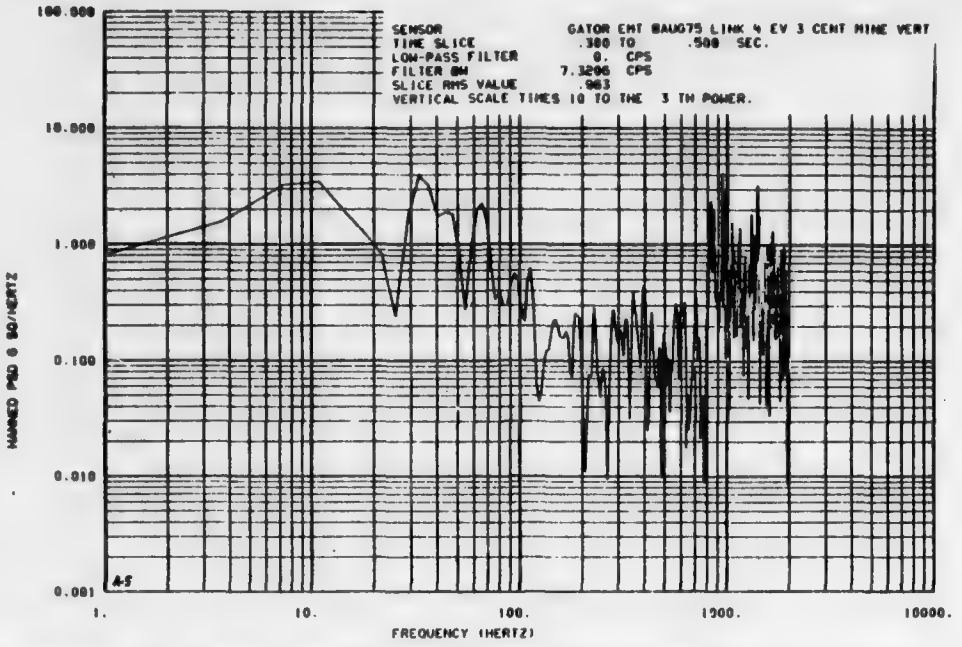

FIGURE A-5. PSD Plot Derived from Data Recorded During Flight at Maximum Speed at 5,000 Ft MSL.

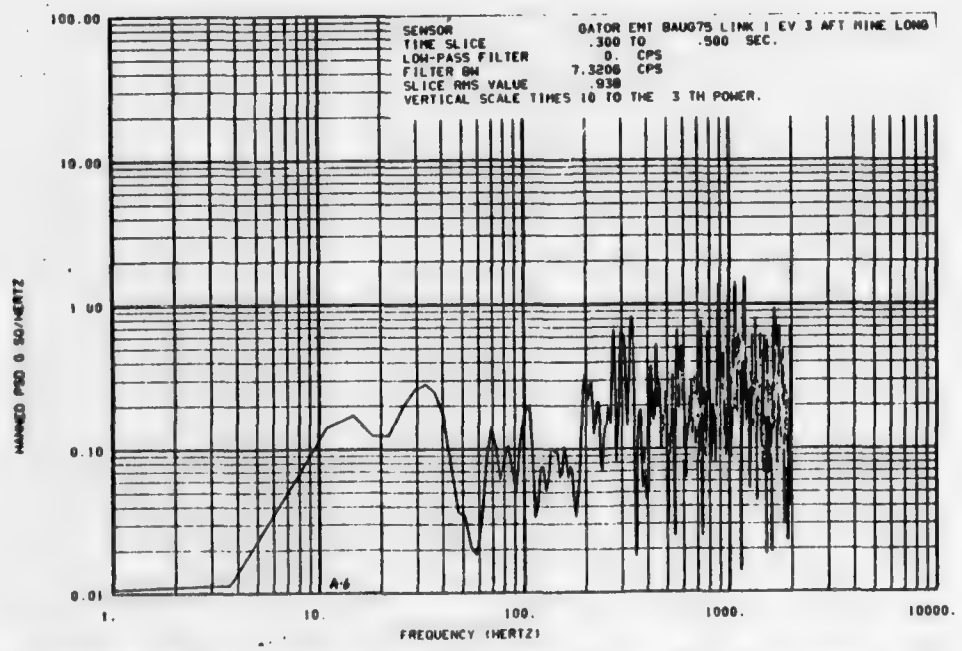

FIGURE A-6. PSD Plot Derived from Data Recorded During Flight at Maximum Speed at 5,000 Ft MSL.

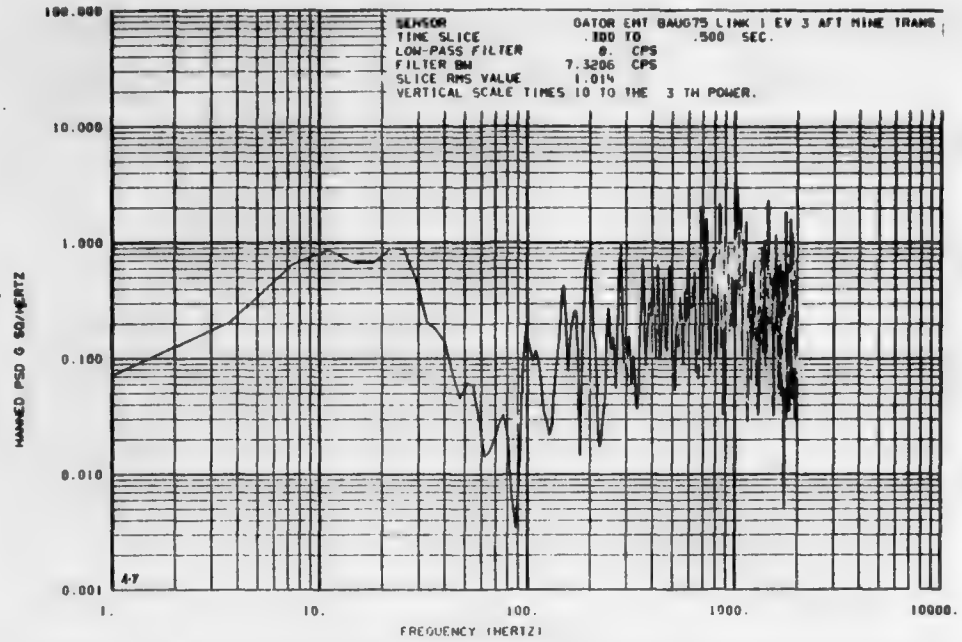

FIGURE A-7. PSD Plot Derived from Data Recorded During Flight at Maximum Speed at 5,000 Ft MSL.

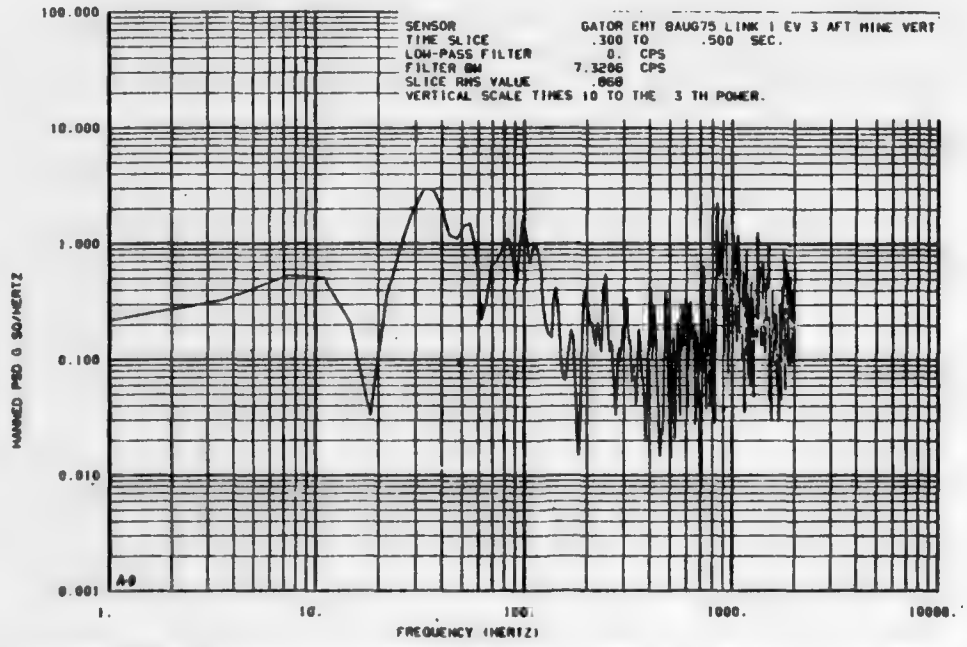

FIGURE A-8. PSD Plot Derived from Data Recorded During Flight at Maximum Speed at 5,000 Ft MSL.

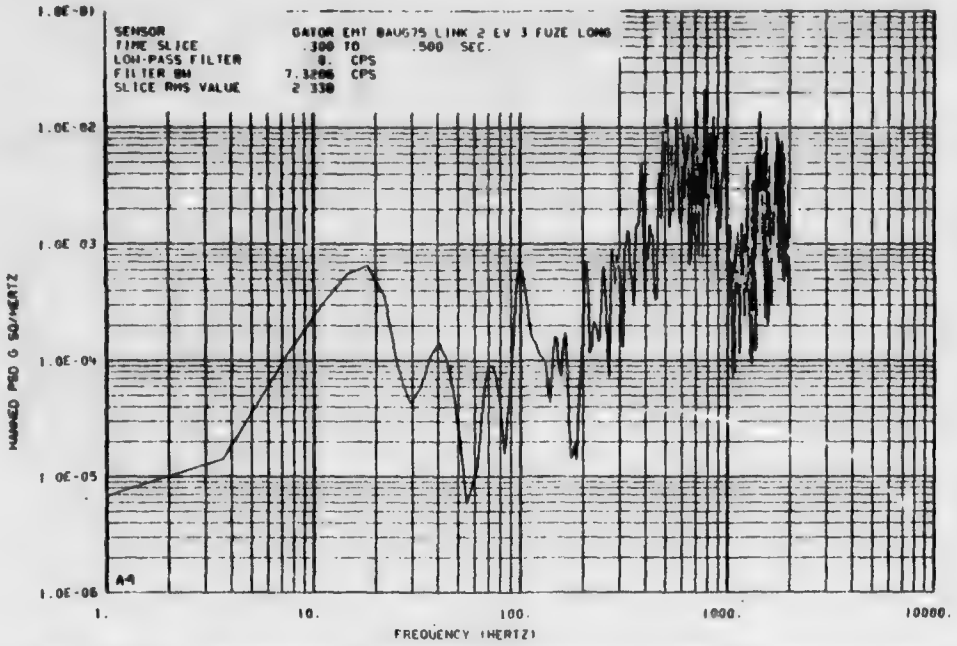

FIGURE A-9. PSD Plot Derived from Data Recorded During Flight at Maximum Speed at 5,000 Ft MSL.

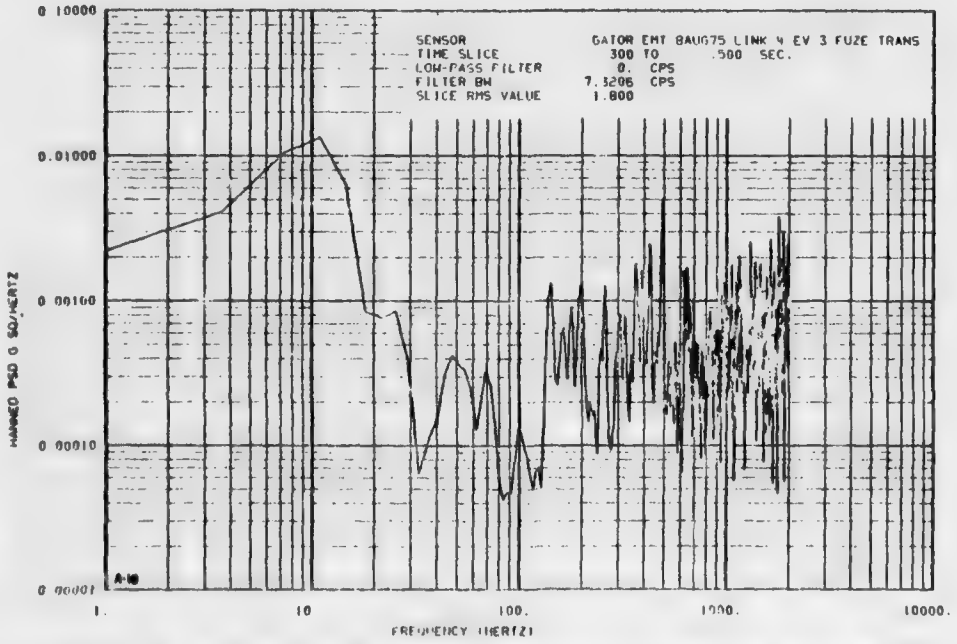

FIGURE A-10. PSD Plot Derived from Data Recorded During Flight at Maximum Speed at 5,000 Ft MSL.

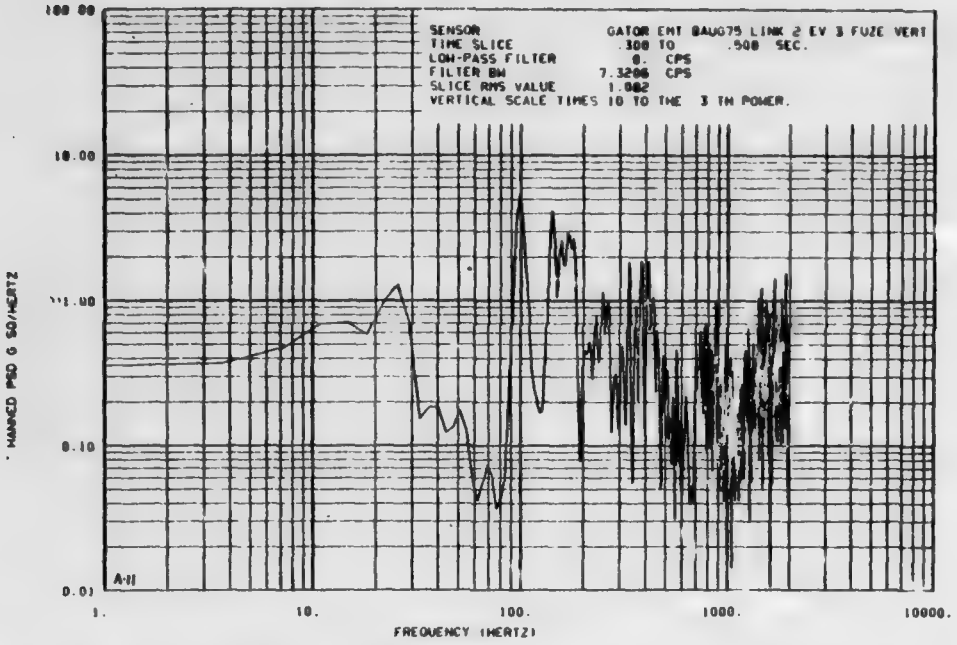

FIGURE A-11. PSD Plot Derived from Data Recorded During Flight at Maximum Speed at 5,000 Ft MSL.

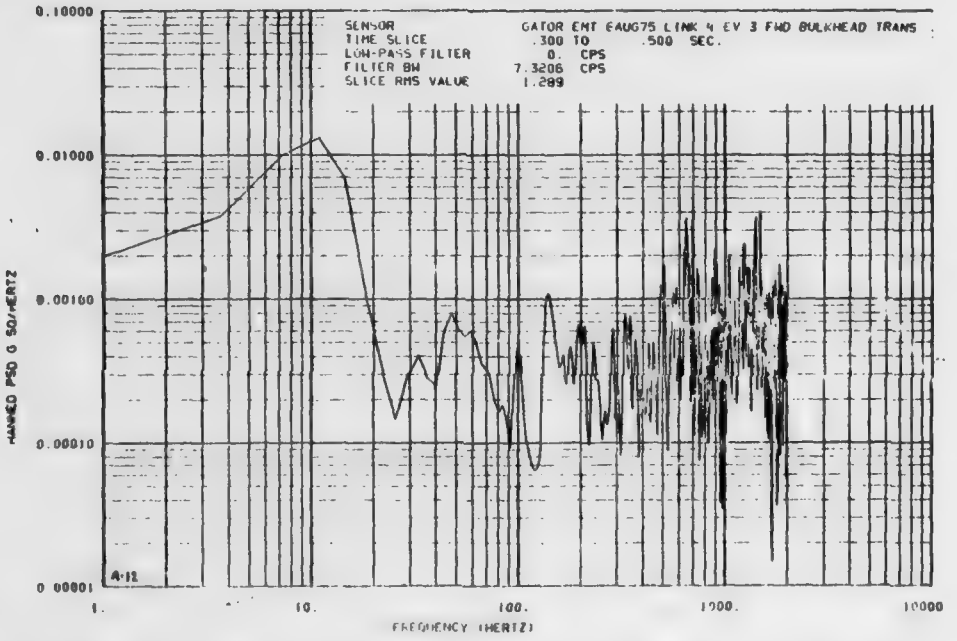

FIGURE A-12. PSD Plot Derived from Data Recorded During Flight at Maximum Speed at 5,000 Ft MSL.

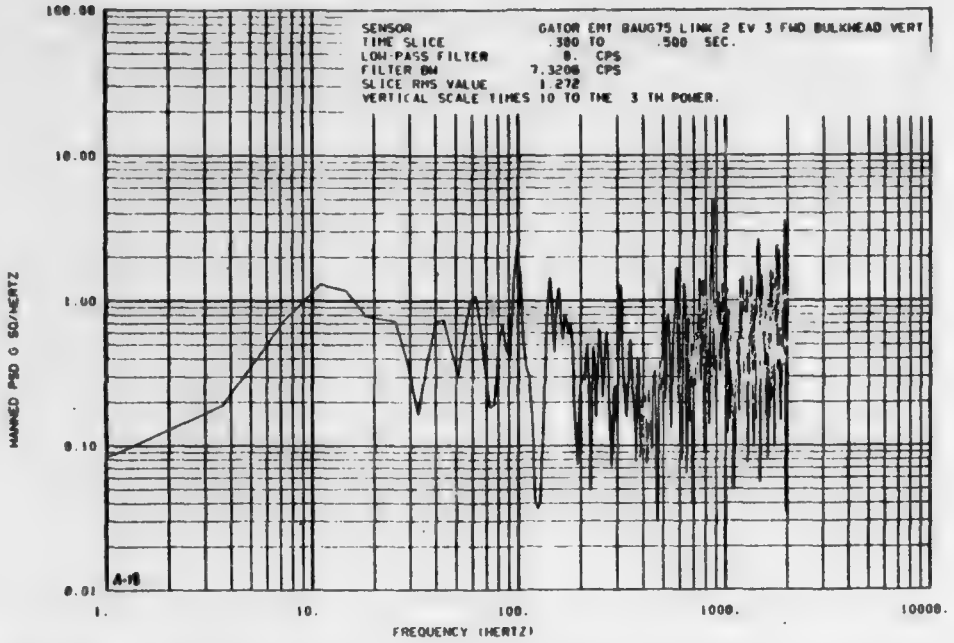

FIGURE A-13. PSD Plot Derived from Data Recorded During Flight at Maximum Speed at 5,000 Ft MSL.

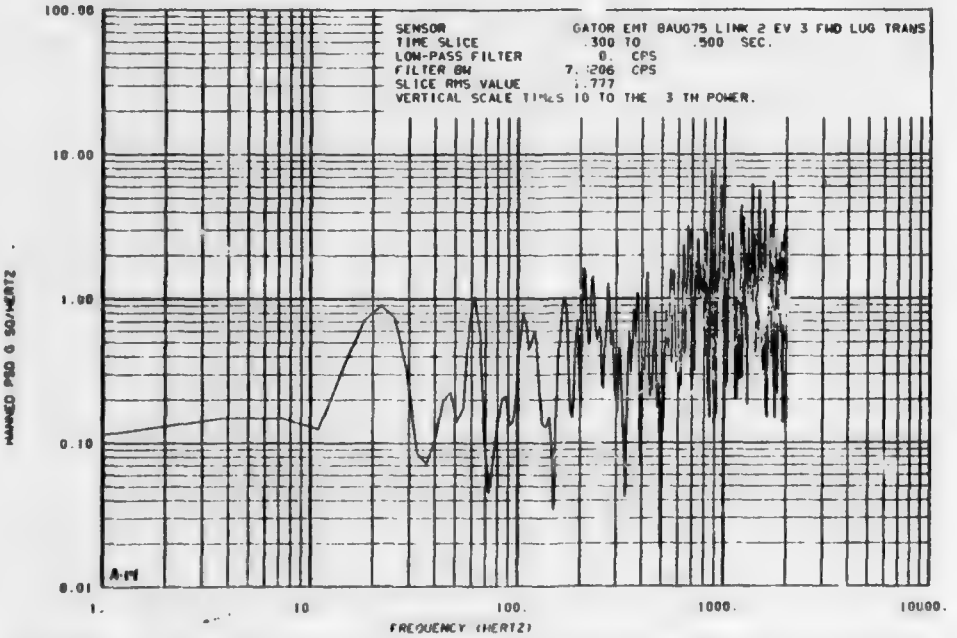

FIGURE A-14. PSD Plot Derived from Data Recorded During Flight at Maximum Speed at 5,000 Ft MSL.

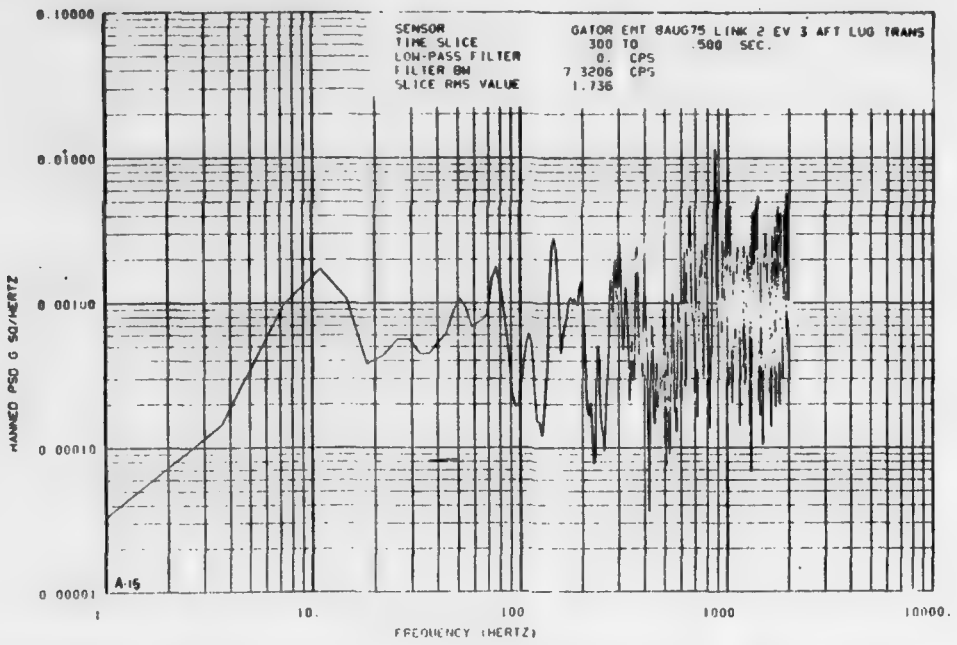

FIGURE A-15. PSD Plot Derived from Data Recorded During Flight at Maximum Speed at 5,000 Ft MSL.

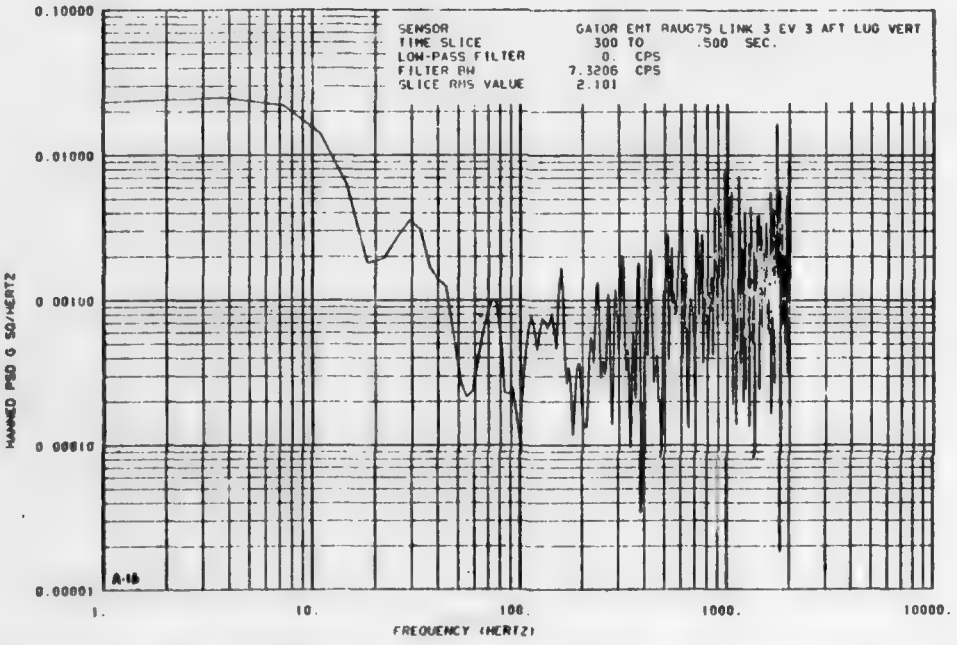

FIGURE A-16. PSD Plot Derived from Data Recorded During Flight at Maximum Speed at 5,000 Ft MSL.

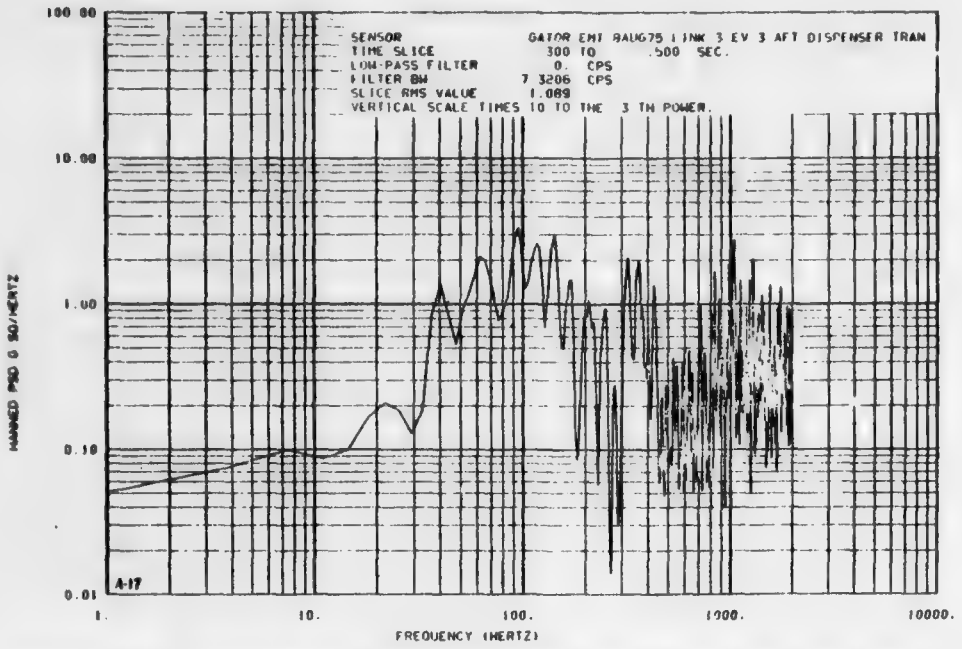

FIGURE A-17. PSD Plot Derived from Data Recorded During Flight at Maximum Speed at 5,000 Ft MSL.

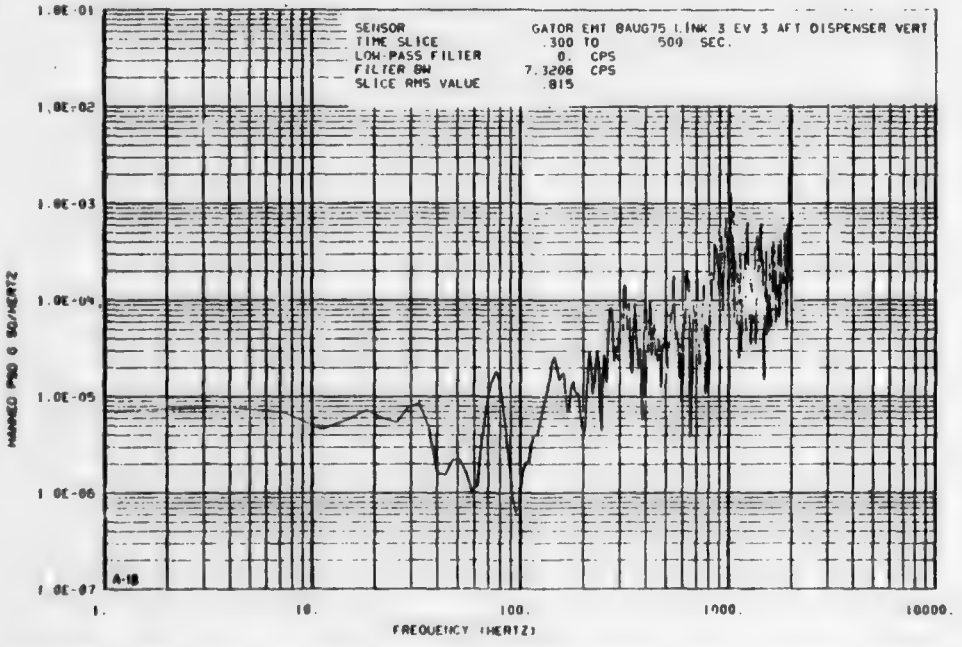

FIGURE A-18. PSD Plot Derived from Data Recorded During Flight at Maximum Speed at 5,000 Ft MSL.

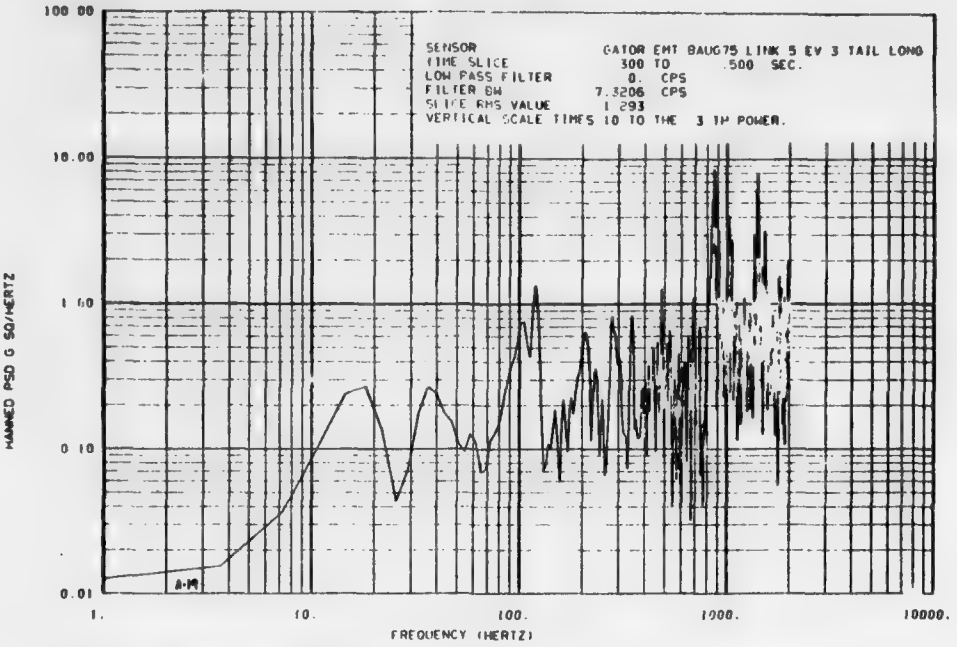

FIGURE A-19. PSD Plot Derived from Data Recorded During Flight at Maximum Speed at 5,000 Ft MSL.

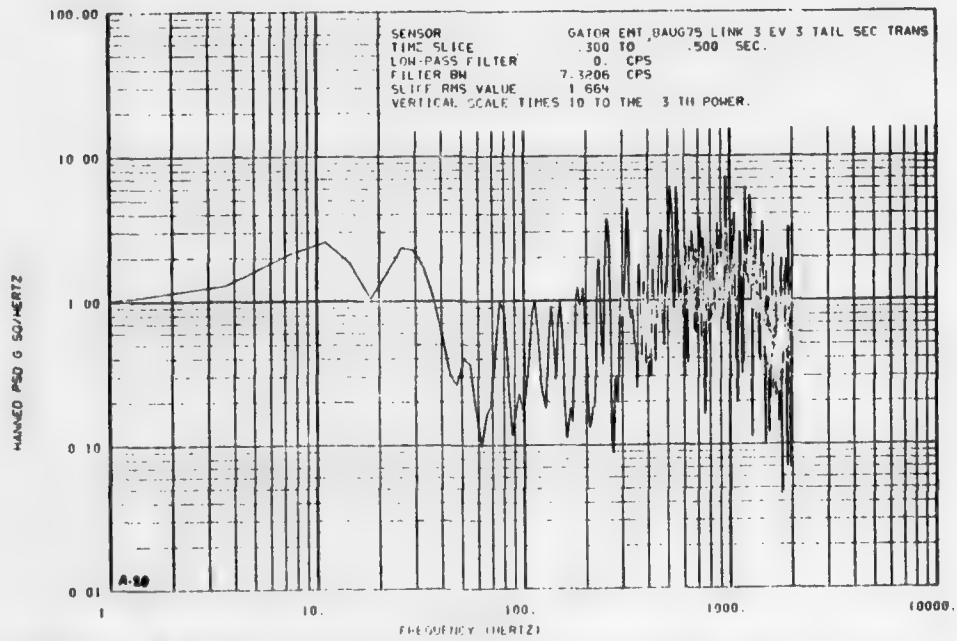

FIGURE A-20. PSD Plot Derived from Data Recorded During Flight at Maximum Speed at 5,000 Ft MSL.

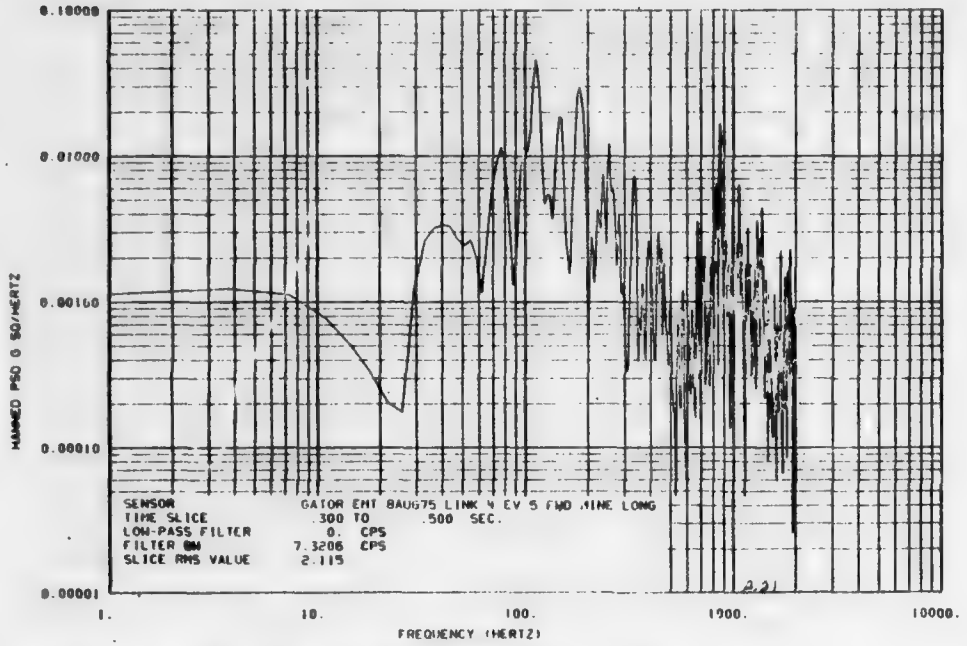

FIGURE A-21. PSD Plot Derived from Data Recorded During Flight at 250 Knots with 100% Power and Nozzle Deflected 81 Degrees.

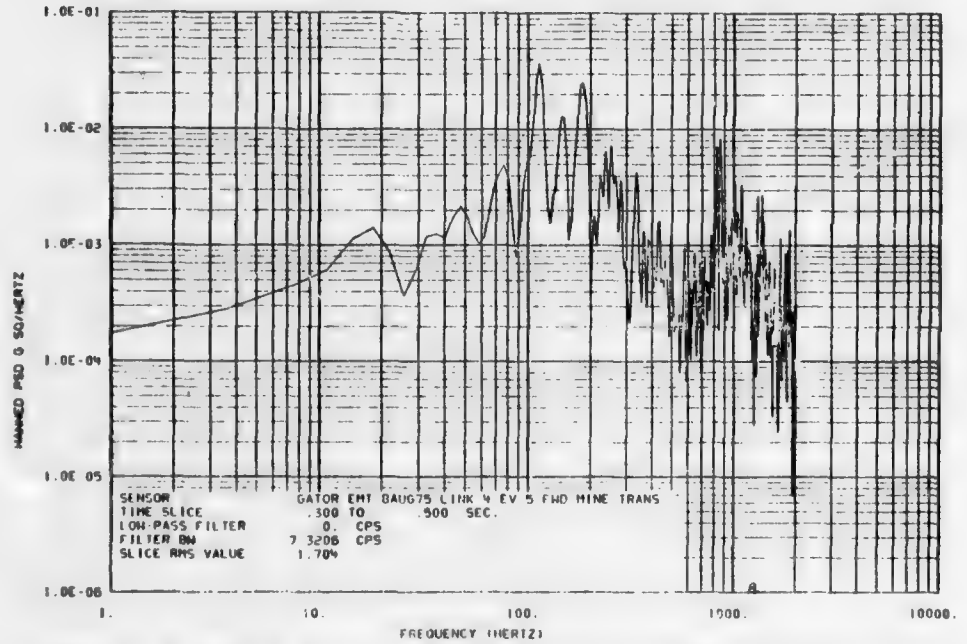

FIGURE A-22. PSD Plot Derived from Data Recorded During Flight at 250 Knots with 100% Power and Nozzle Deflected 81 Degrees.

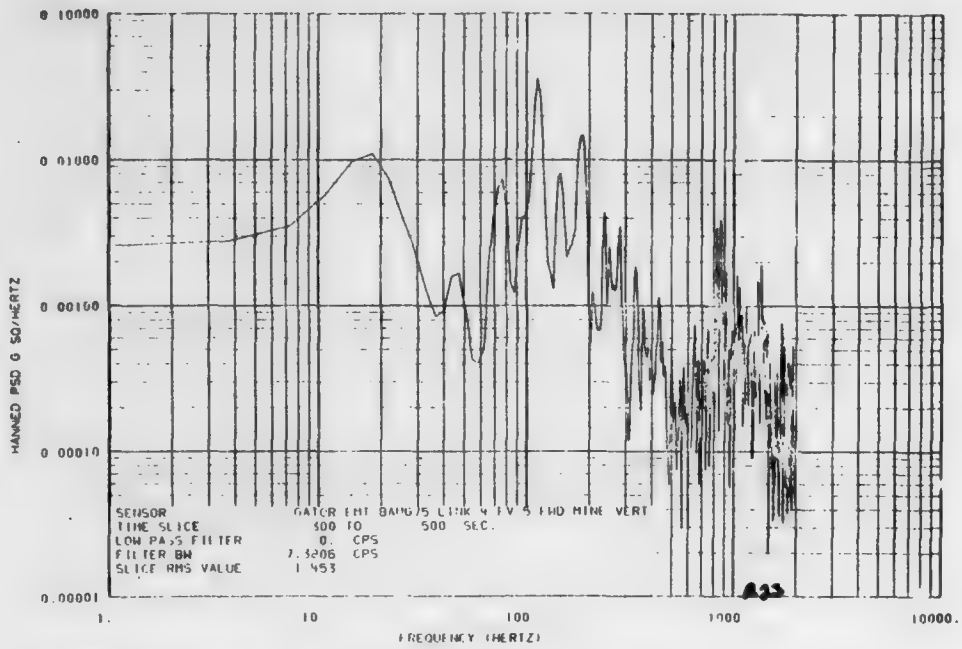

FIGURE A-23. PSD Plot Derived from Data Recorded During Flight at 250 Knots with 100% Power and Nozzle Deflected 81 Degrees.

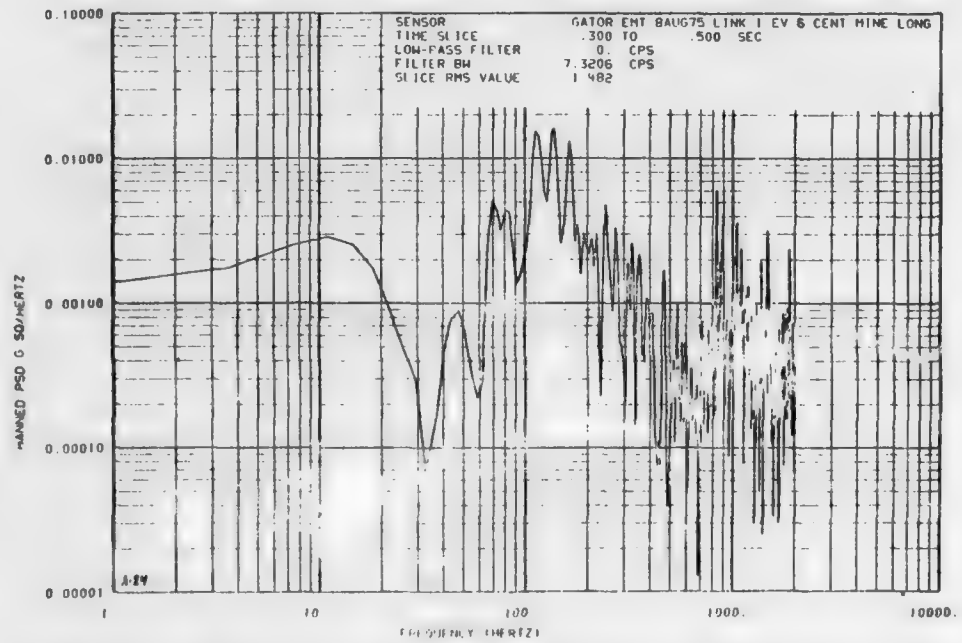

FIGURE A-24. PSD Plots Derived from Data Recorded During Flight at 250 Knots with 100% Power and Nozzle Deflected 98.5 Degrees.

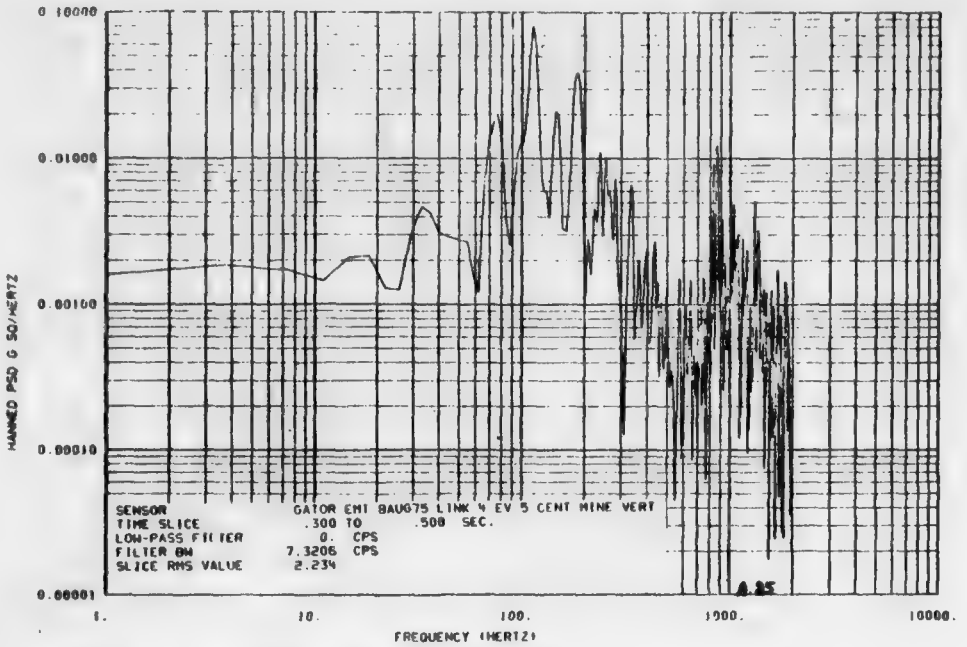

FIGURE A-25. PSD Plots Derived from Data Recorded During Flight at 250 Knots with 100% Power and Nozzle Deflected 81 Degrees.

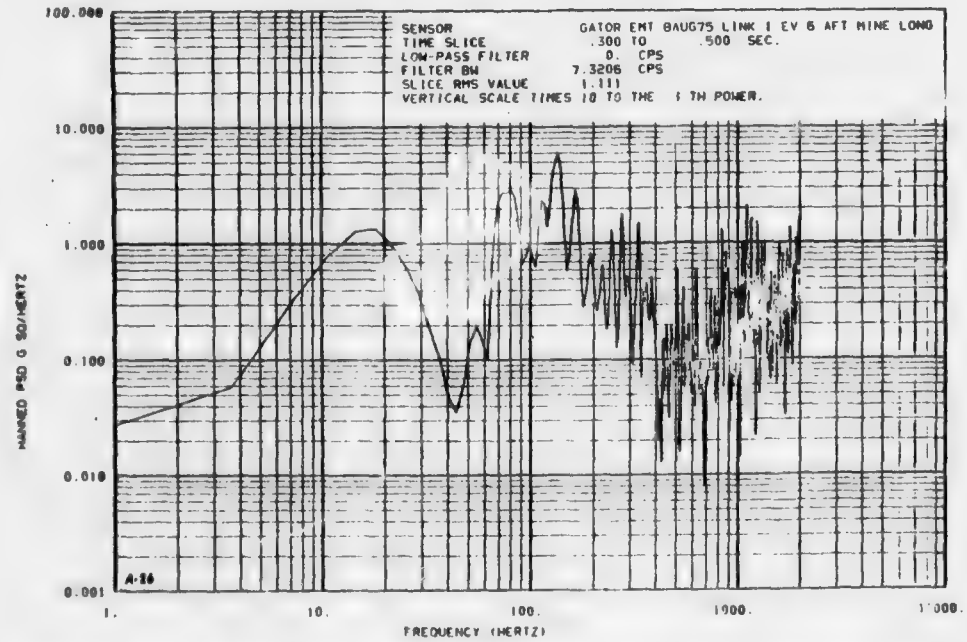

FIGURE A-26. PSD Plot Derived from Data Recorded During Flight at 250 Knots with 100% Power and Nozzle Deflected to 98.5 Degrees.

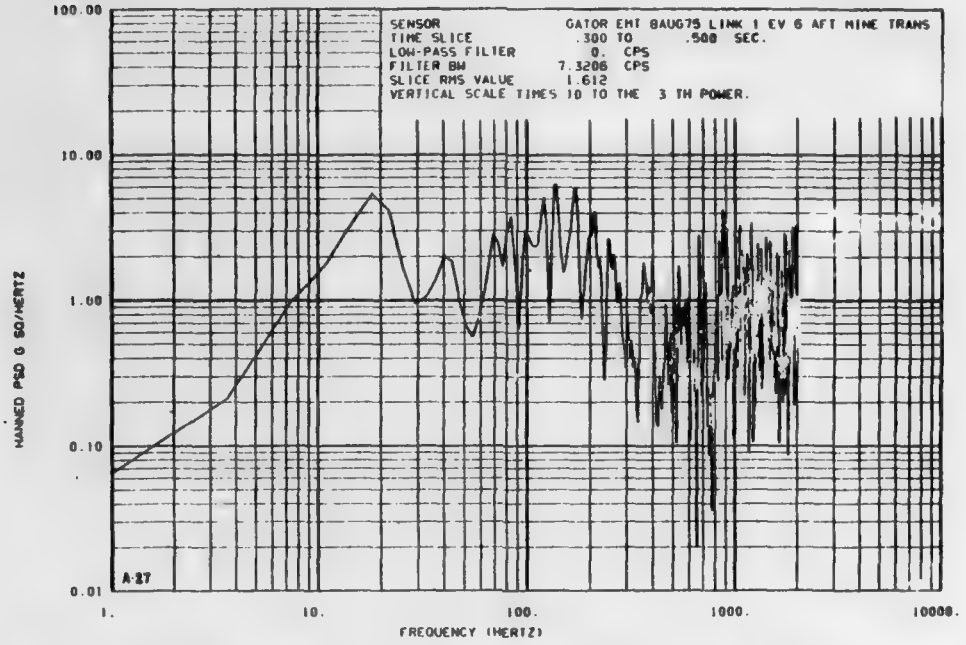

FIGURE A-27. PSD Plot Derived from Data Recorded During Flight at 250 Knots with 100% Power and Nozzle Deflected to 98.5 Degrees.

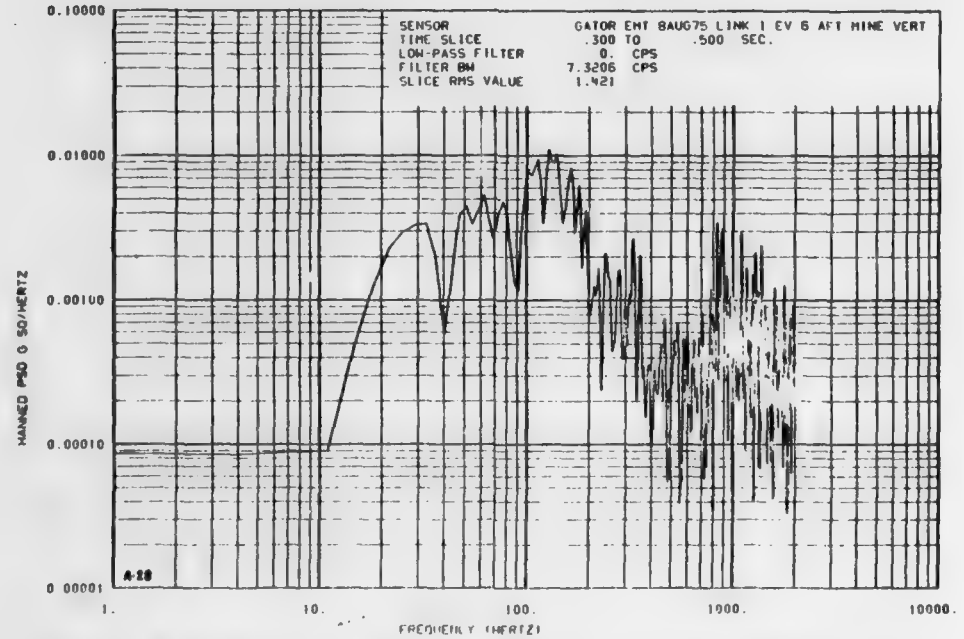

FIGURE A-28. PSD Plot Derived from Data Recorded During Flight at 250 Knots with 100% Power and Nozzle Deflected to 98.5 Degrees.

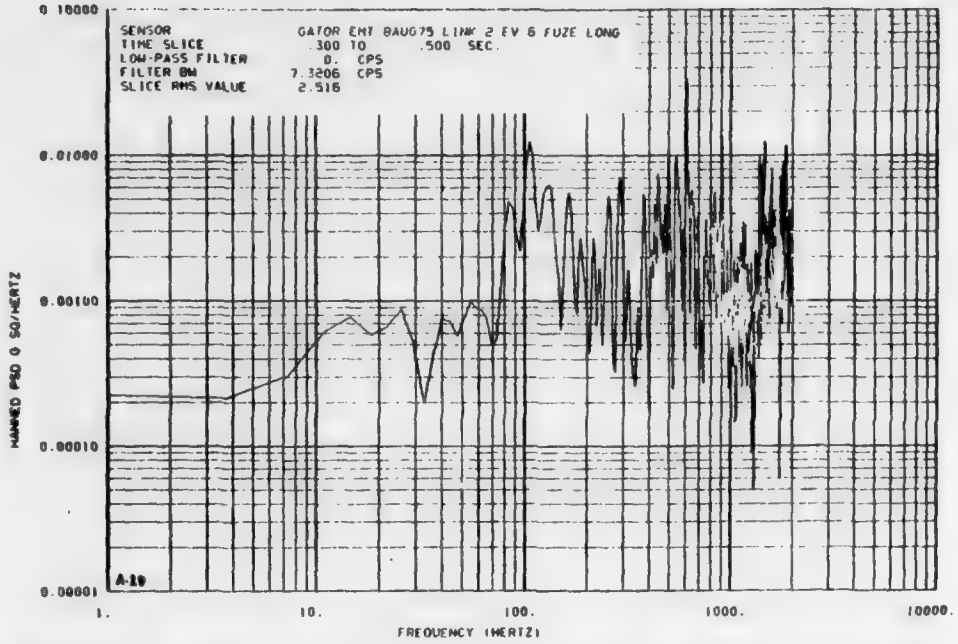

FIGURE A-29. PSD Plot Derived from Data Recorded During Flight at 250 Knots with 100% Power and Nozzle Deflected to 81 Degrees.

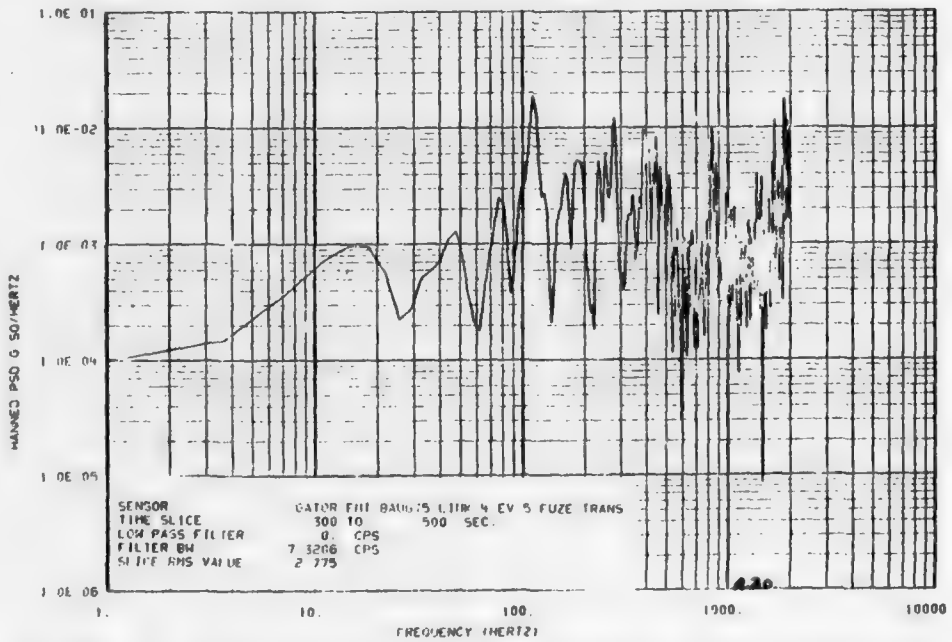

FIGURE A-30. PSD Plot Derived from Data Recorded During Flight at 250 Knots with 100% Power and Nozzle Deflected to 81 Degrees.

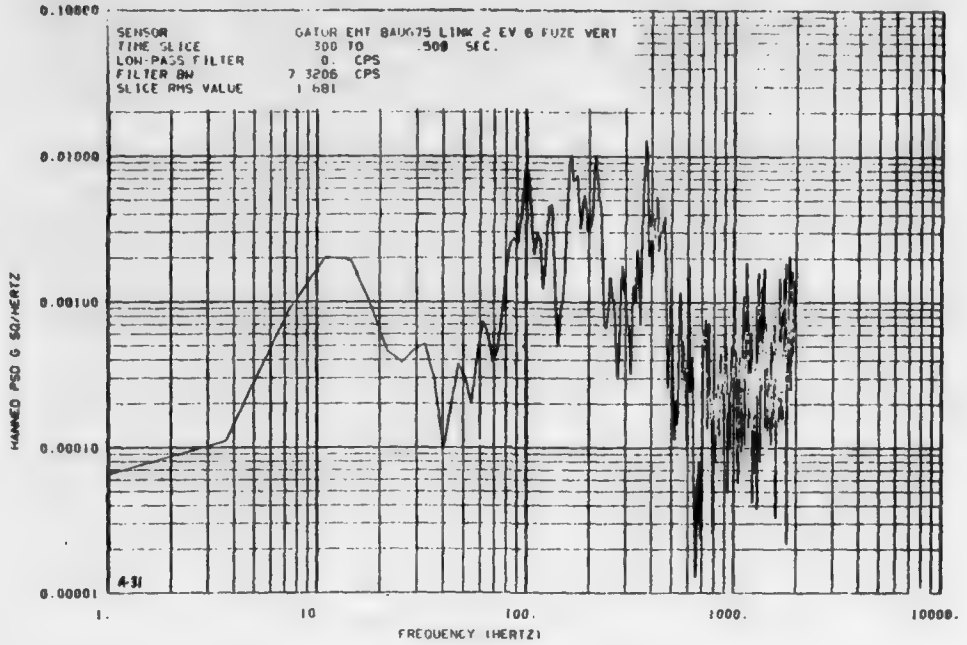

FIGURE A-31. PSD Plot Derived from Data Recorded During Flight at 250 Knots with 100% Power and Nozzle Deflected to 81 Degrees.

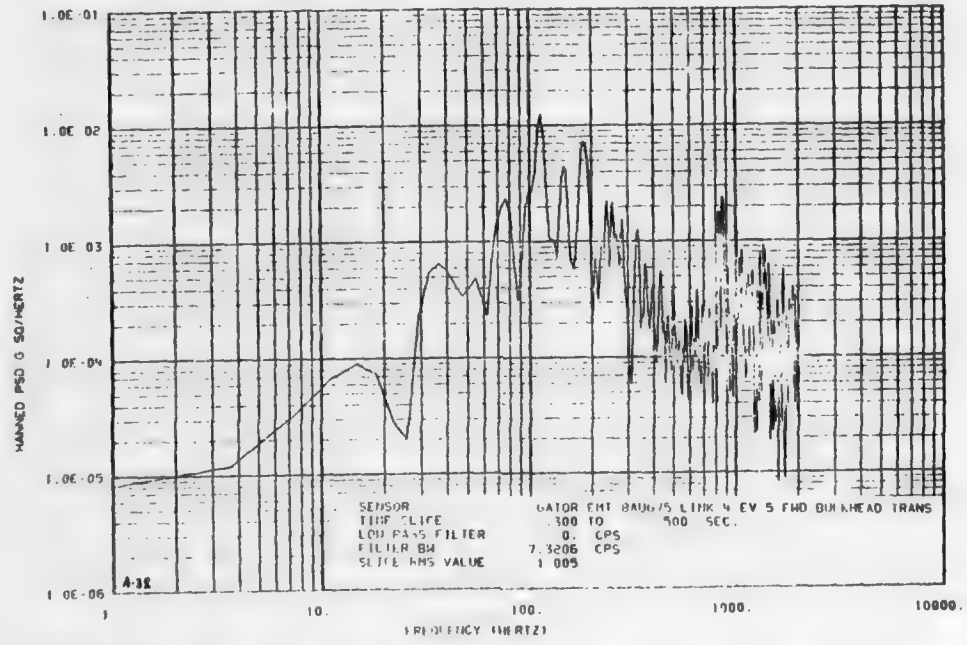

FIGURE A-32. PSD Plot Derived from Data Recorded During Flight at 250 Knots with 100% Power and Nozzle Deflected to 81 Degrees.

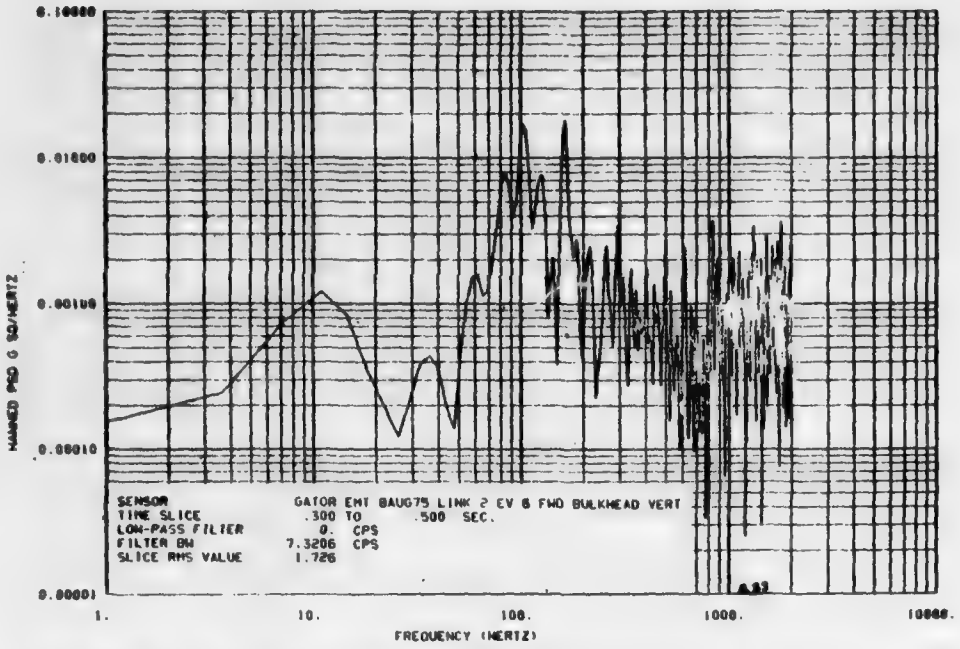

FIGURE A-33. PSD Plot Derived from Data Recorded During Flight at 250 Knots with 100% Power and Nozzle Deflected to 81 Degrees.

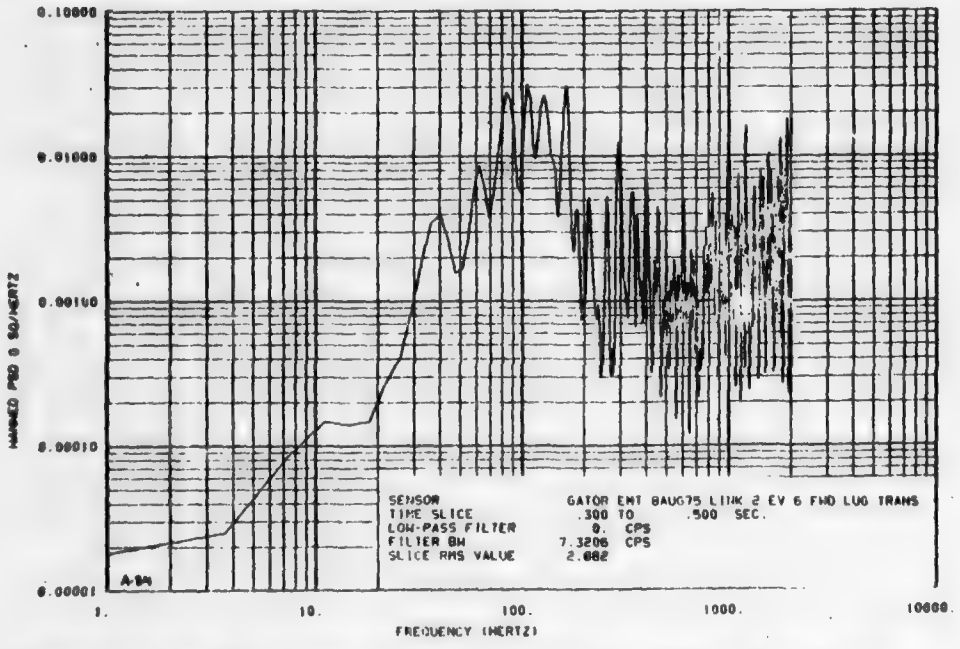

FIGURE A-34. PSD Plot Derived from Data Recorded During Flight at 250 Knots with 100% Power and Nozzle Deflected to 81 Degrees.

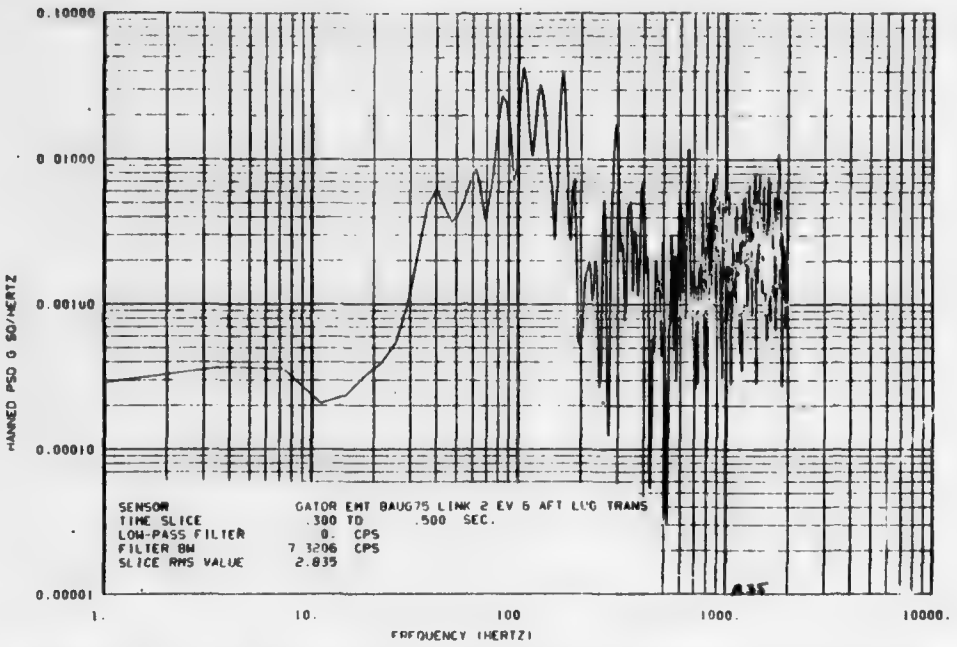

FIGURE A–35. PSD Plot Derived from Data Recorded During Flight at 250 Knots with 100% Power and Nozzle Deflected to 81 Degees.

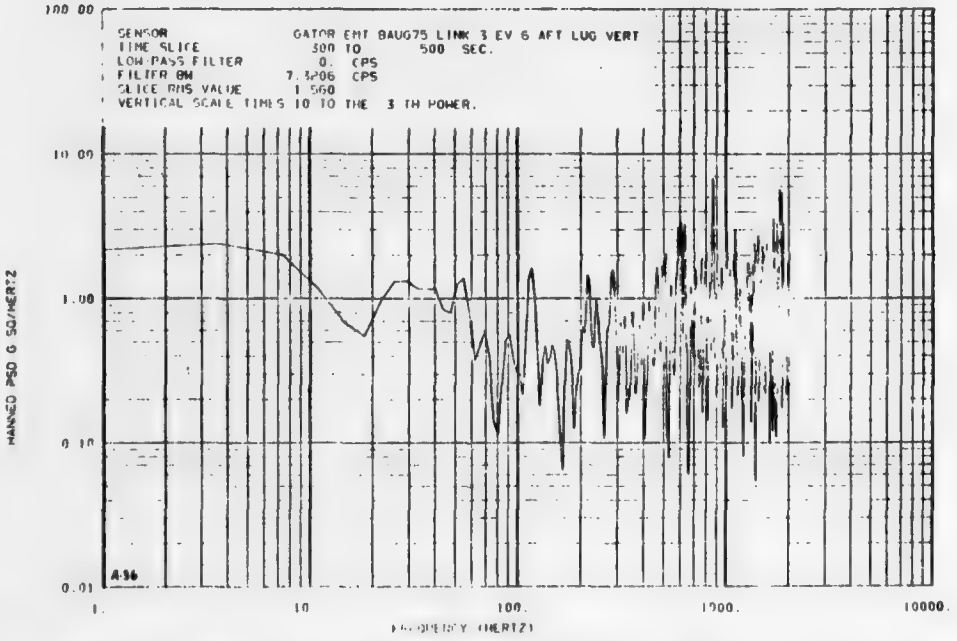

FIGURE A-36. PSD Plot Derived from Data Recorded During Flight at 250 Knots with 100% Power and Nozzle Deflected to 81 Degrees.

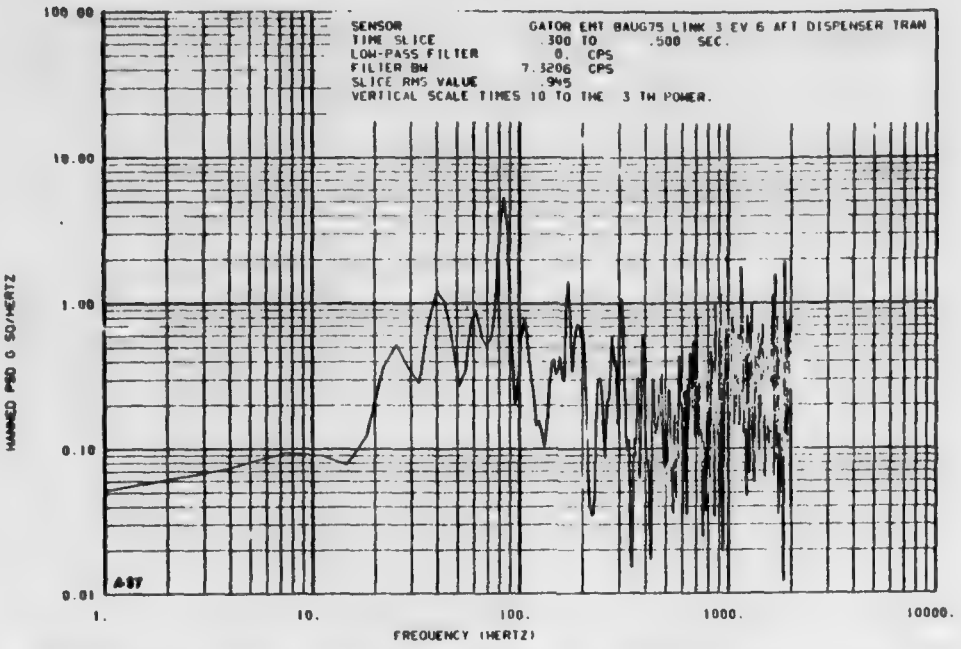

FIGURE A-37. PSD Plot Derived from Data Recorded During Flight at 250 Knots with 100% Power and Nozzle Deflected to 81 Degrees.

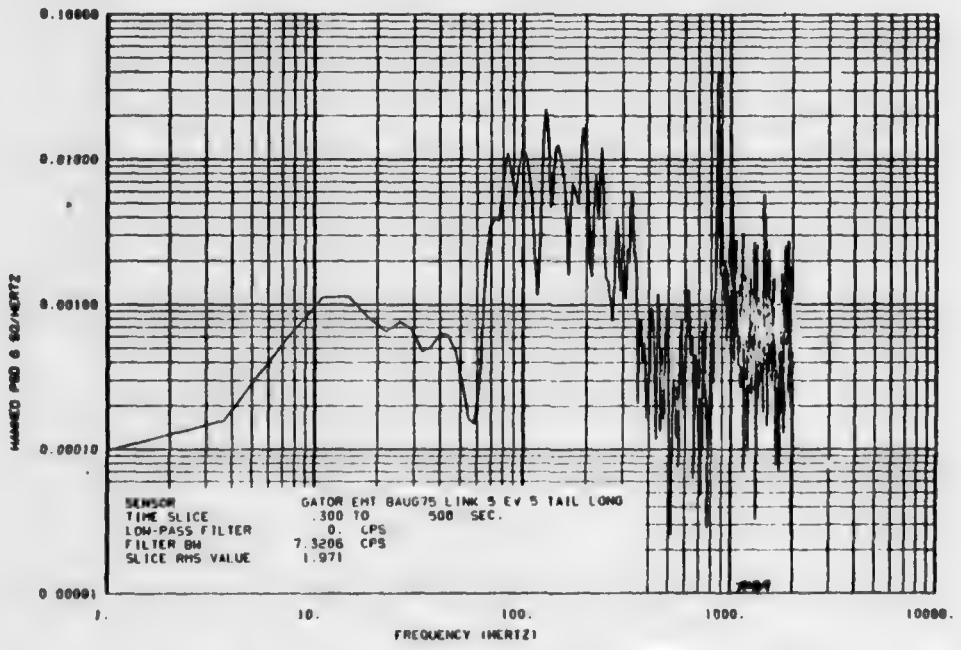

FIGURE A-38. PSD Plot Derived from Data Recorded During Flight at 250 Knots with 100% Power and Nozzle Deflected to 81 Degrees.

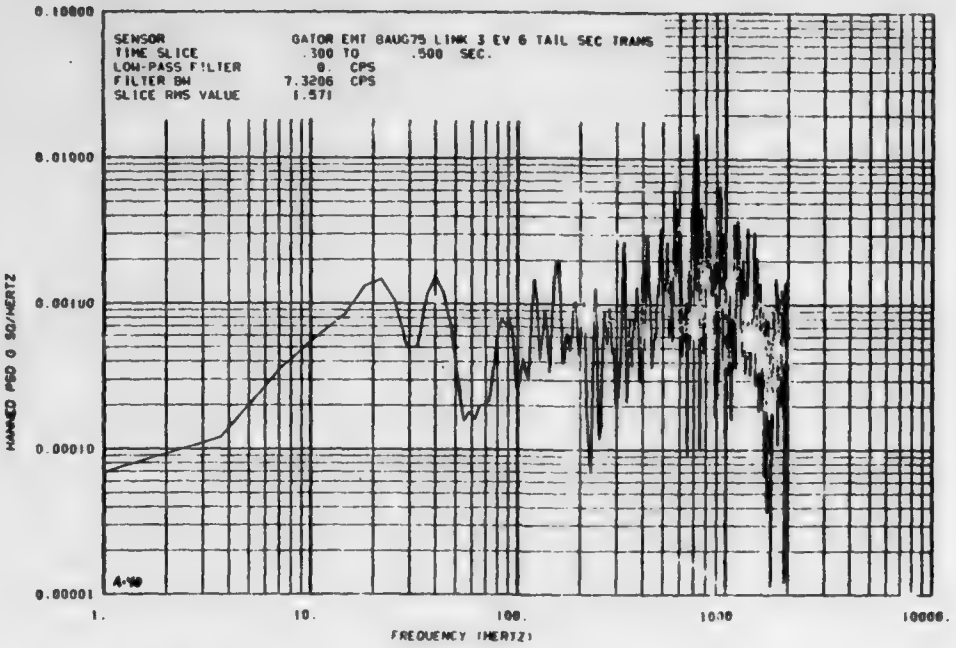

FIGURE A-39. PSD Plot Derived from Data Recorded During Flight at 250 Knots with 100% Power and Nozzle Deflected to 81 Degrees.

Appendix B

Acceleration PSD Plots:
Captive Flight Tests During Hover
(Figure B-1 through B-15)
and
Rolling Vertical Landing
(Figure B-16 through B-20)

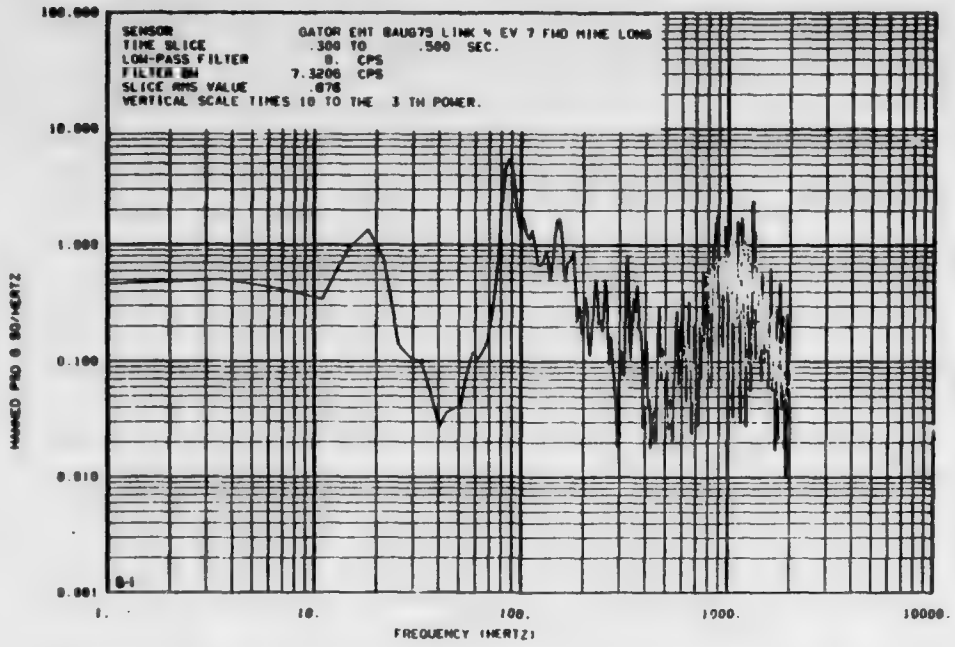

FIGURE B-1. PSD Plot Derived from Data Recorded During Hover Landing.

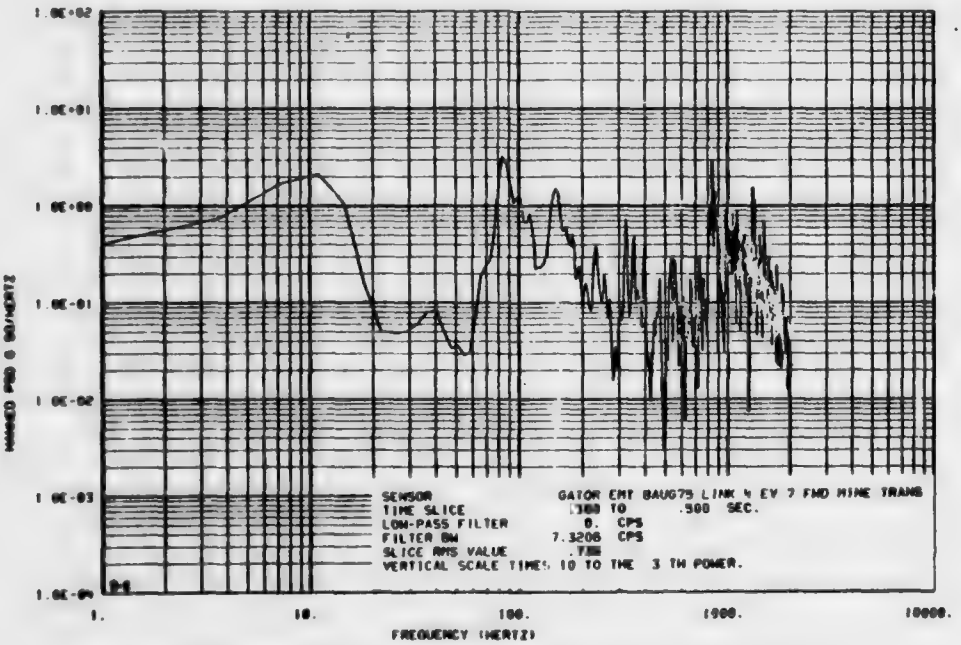

FIGURE B-2. PSD Plot Derived from Data Recorded During Hover Landing.

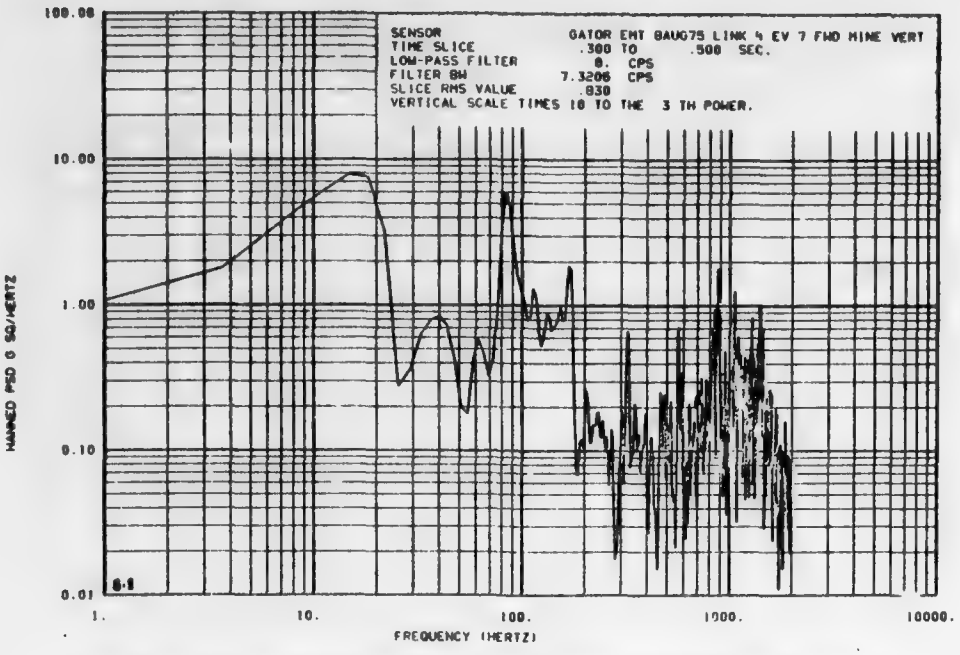

FIGURE B-3. PSD Plot Derived from Data Recorded During Hover Landing.

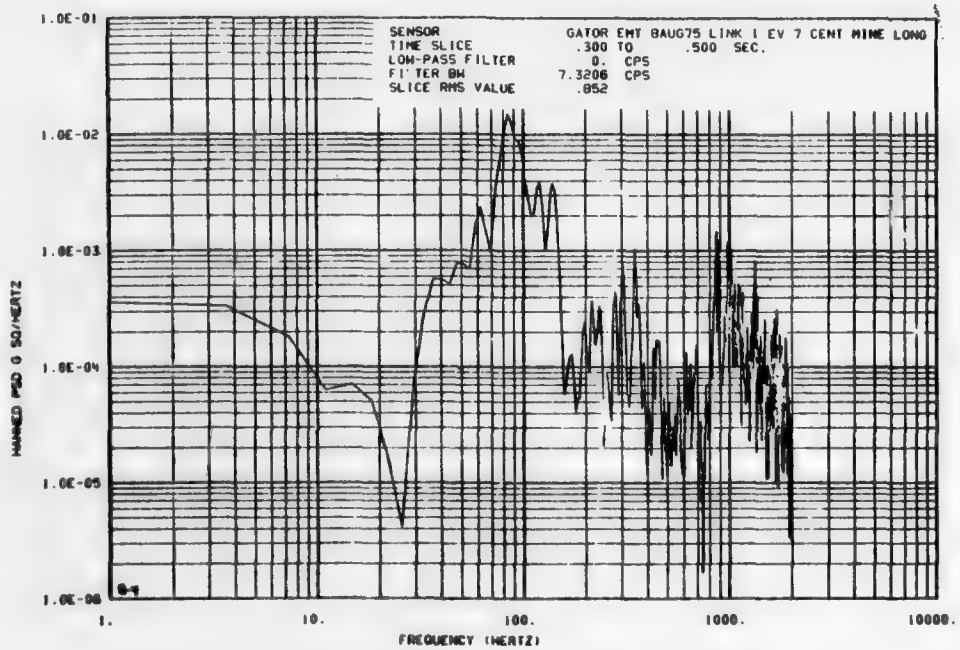

FIGURE B-4. PSD Plot Derived from Data Recorded During Hover Landing.

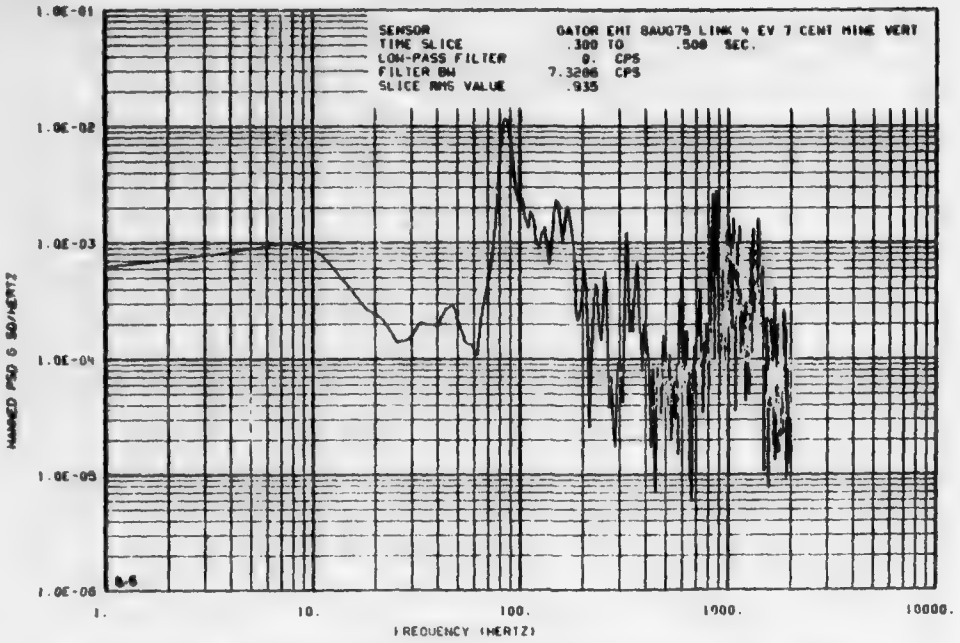

FIGURE B-5. PSD Plot Derived from Data Recorded During Hover Landing.

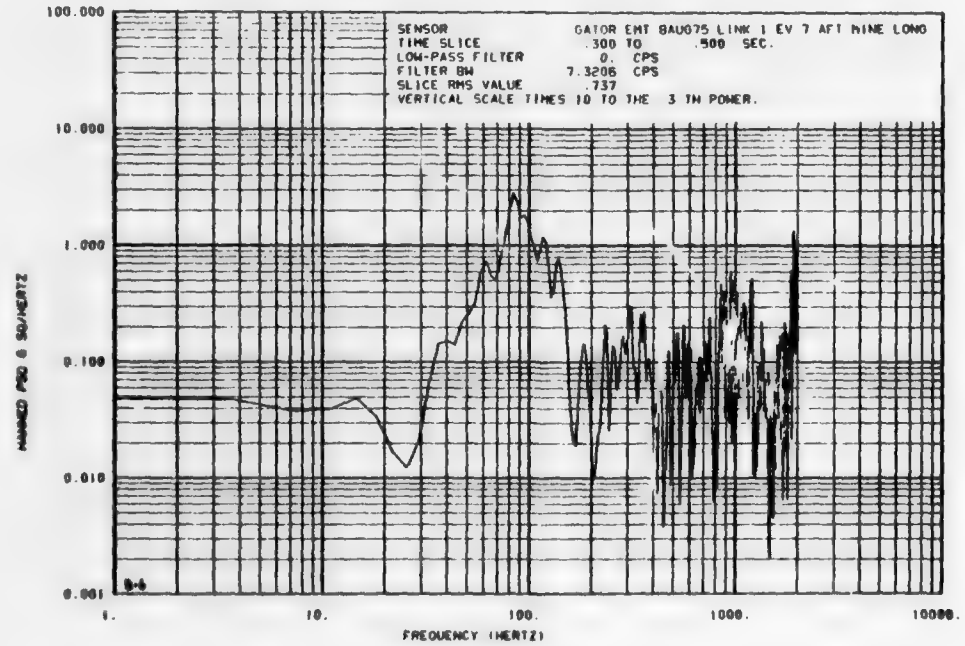

FIGURE B-6. PSD Plot Derived from Data Recorded During Hover Landing.

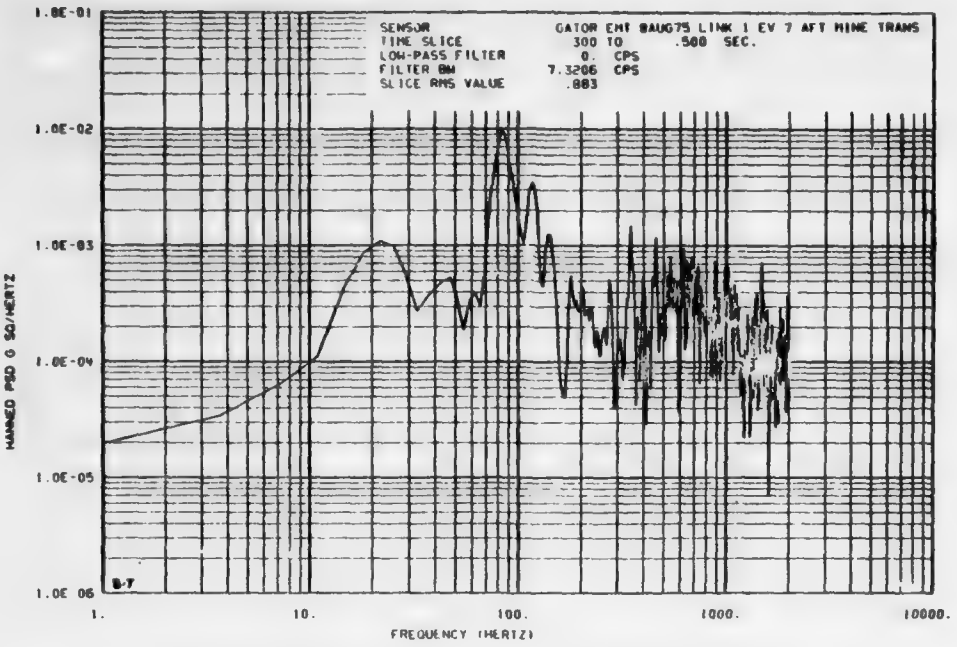

FIGURE B-7. PSD Plot Derived from Data Recorded During Hover Landing.

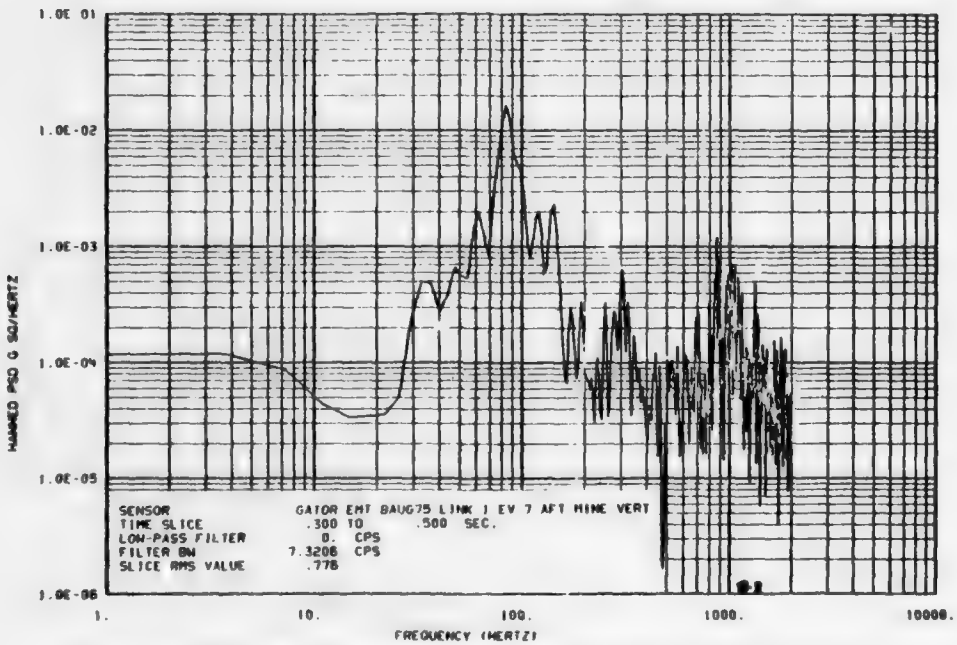

FIGURE B-8. PSD Plot Derived from Data Recorded During Hover Landing.

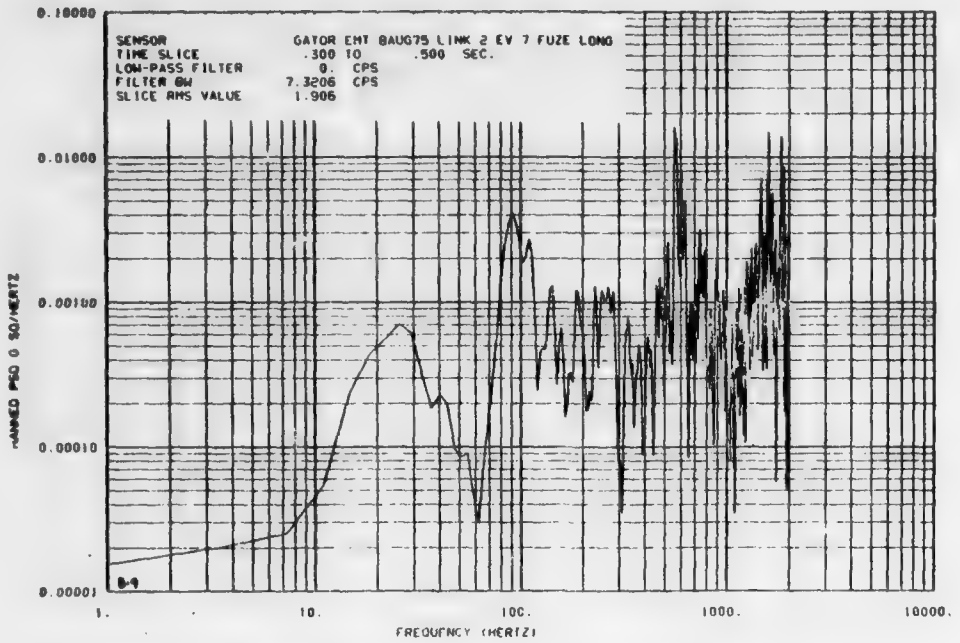

FIGURE B-9. PSD Plot Derived from Data Recorded During Hover Landing.

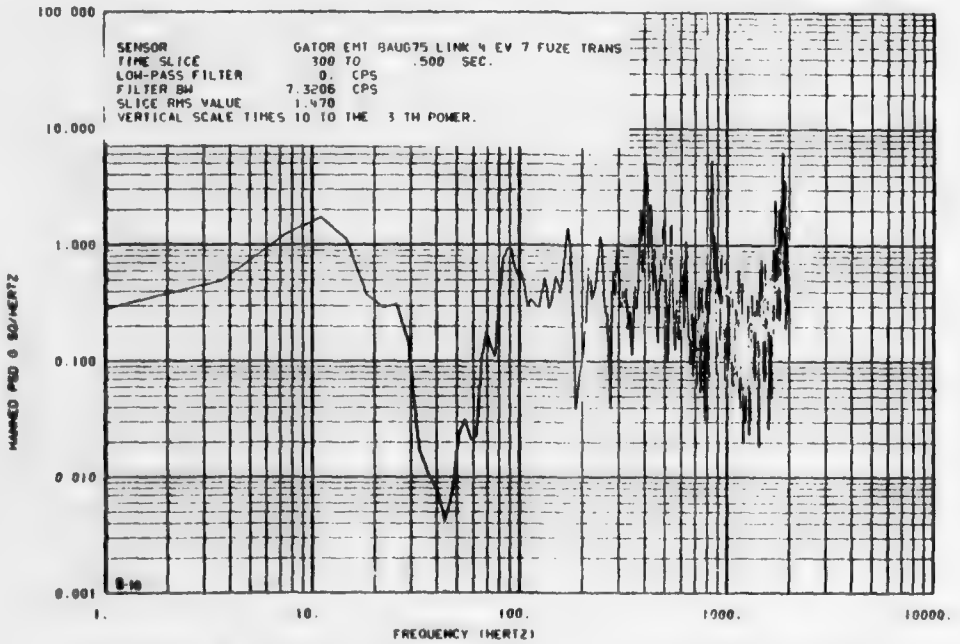

FIGURE B-10. PSD Plot Derived from Data Recorded During Hover Landing.

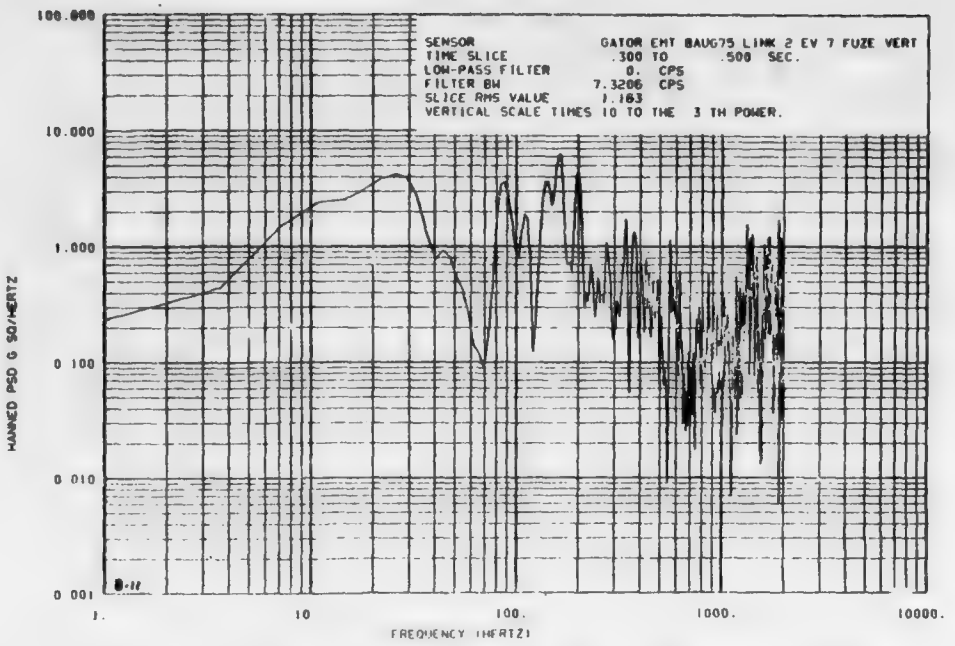

FIGURE B-11. PSD Plot Derived from Data Recorded During Hover Landing.

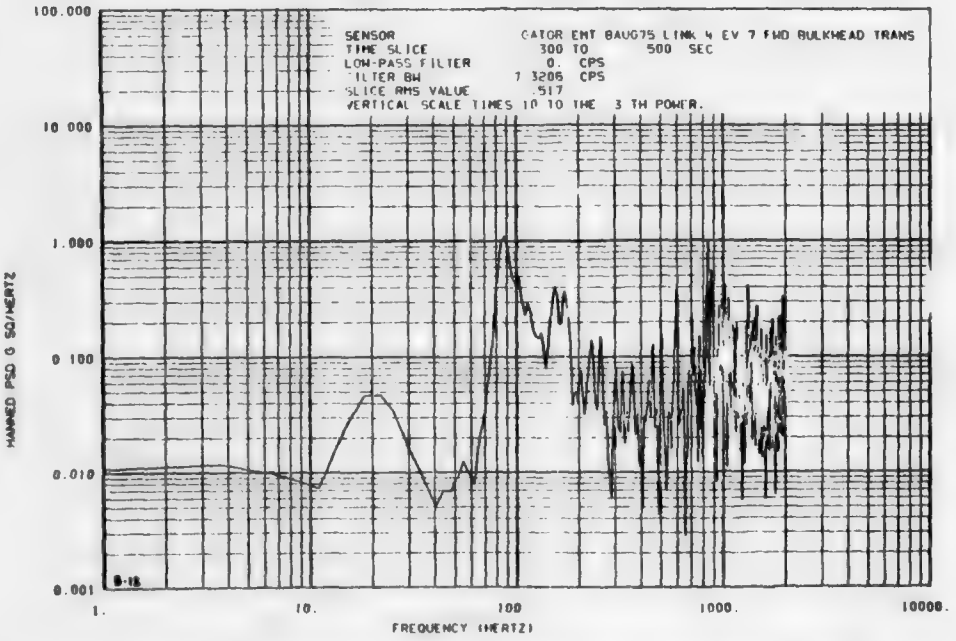

FIGURE B-12. PSD Plot Derived from Data Recorded During Hover Landing.

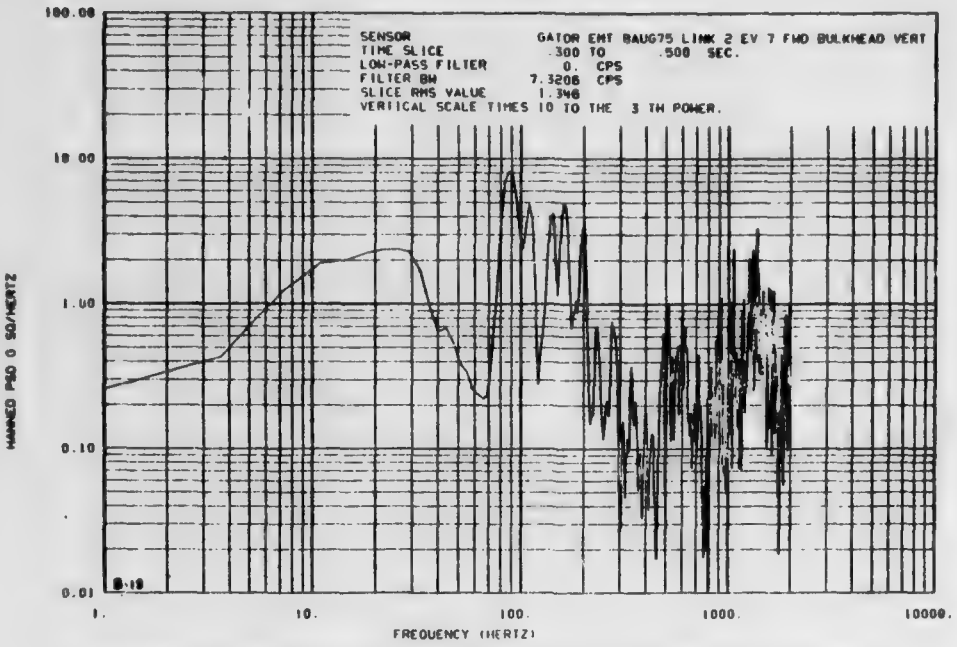

FIGURE B-13. PSD Plot Derived from Data Recorded During Hover Landing.

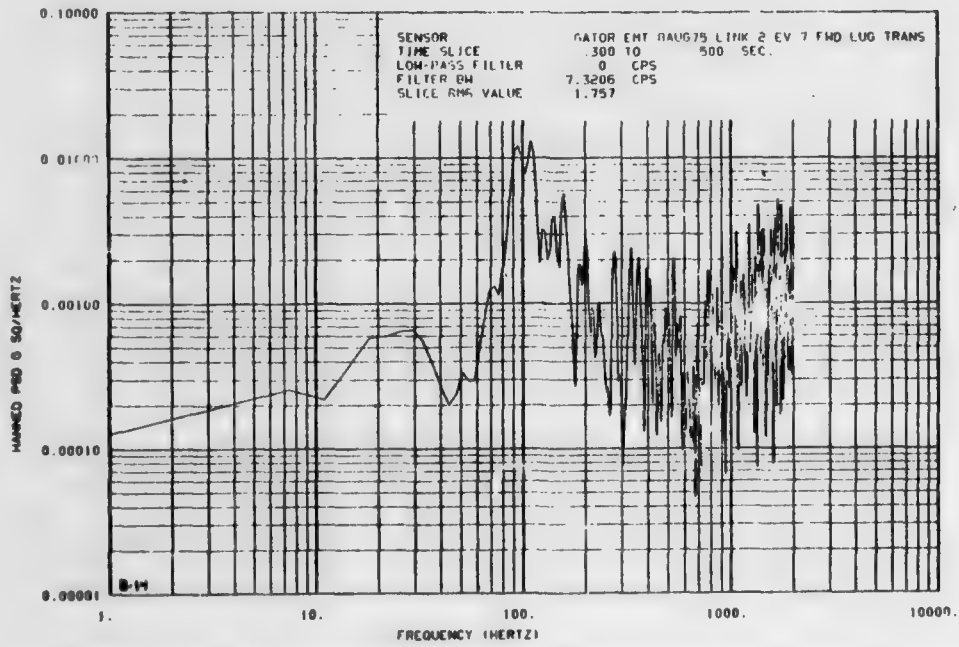

FIGURE B-14. PSD Plot Derived from Data Recorded During Hover Landing.

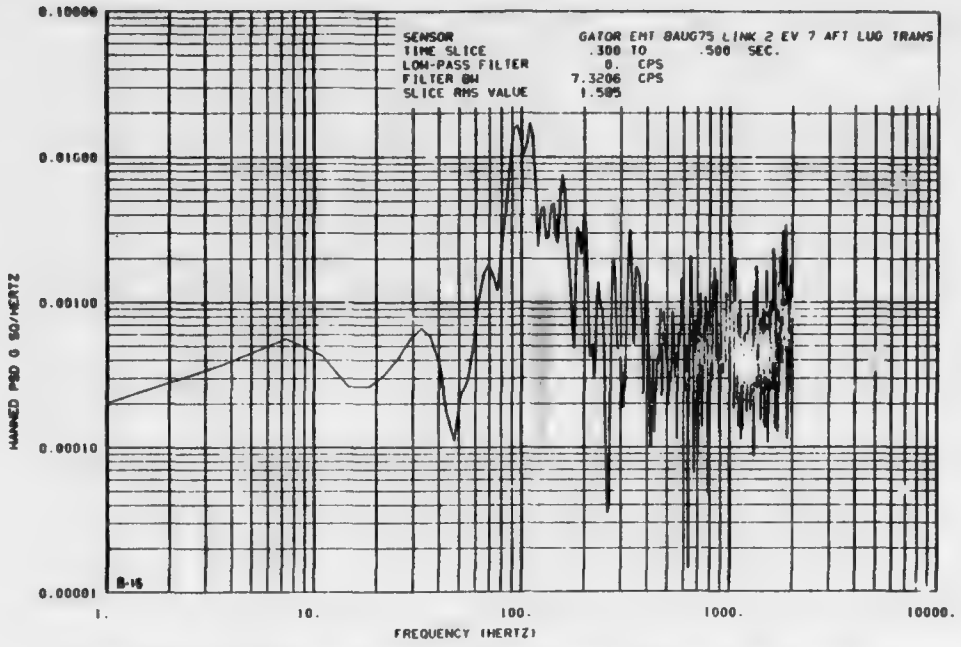

FIGURE B-15. PSD Plot Derived from Data Recorded During Hover Landing.

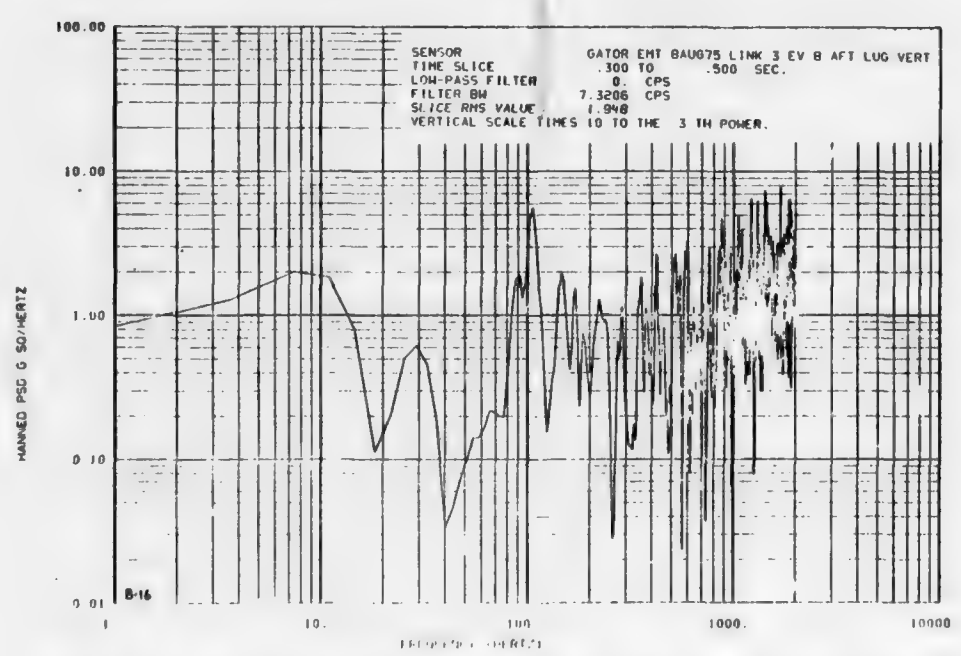

FIGURE B-16. PSD Plot Derived from Data Recorded During Rolling Vertical Landing.

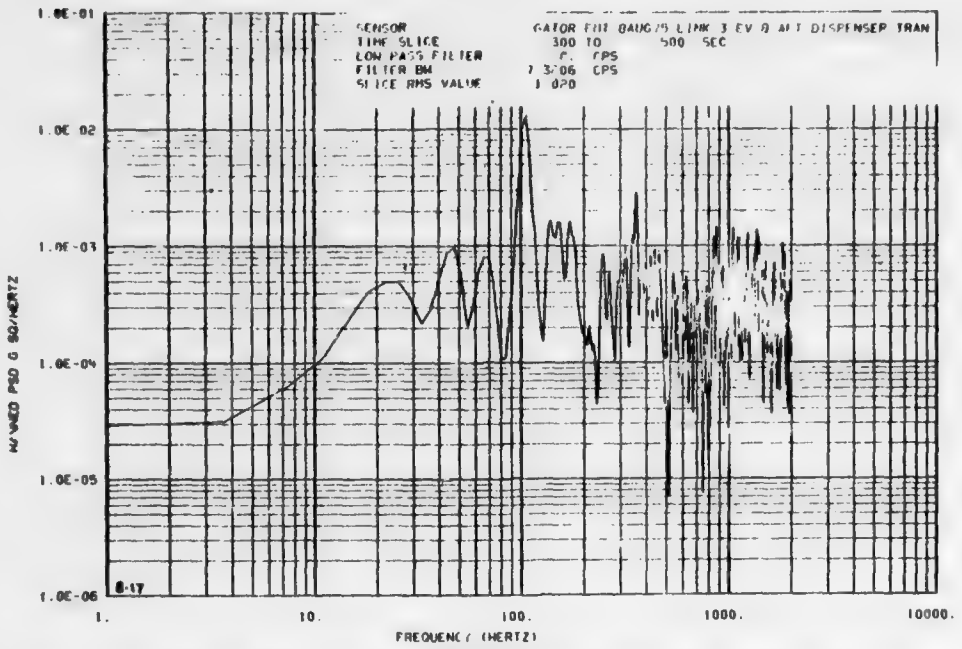

FIGURE B-17. PSD Plot Derived from Data Recorded During Rolling Vertical Landing.

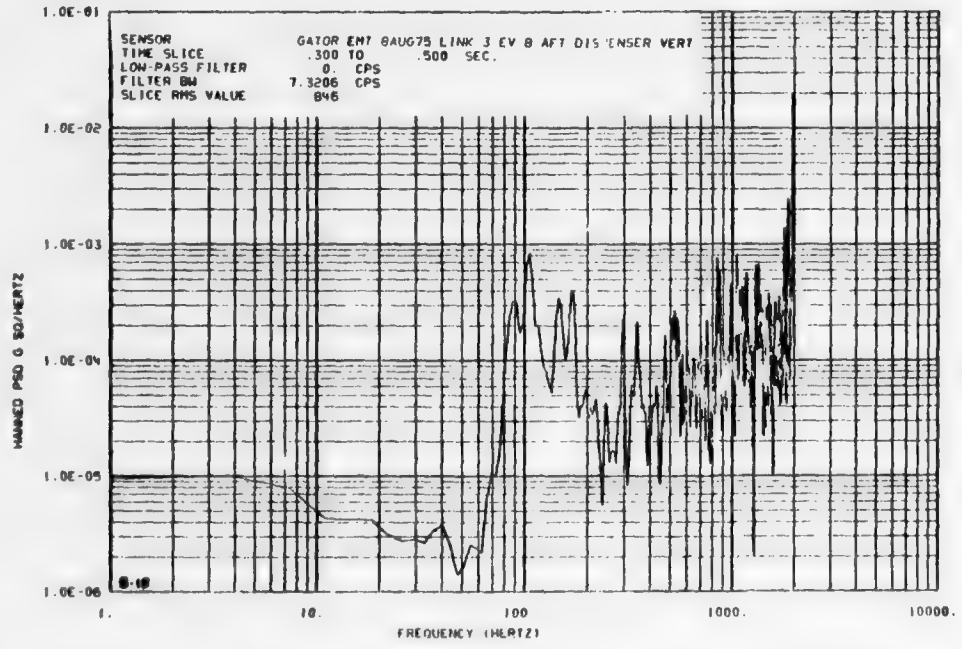

FIGURE B-18. PSD Plot Derived from Data Recorded During Rolling Vertical Landing.

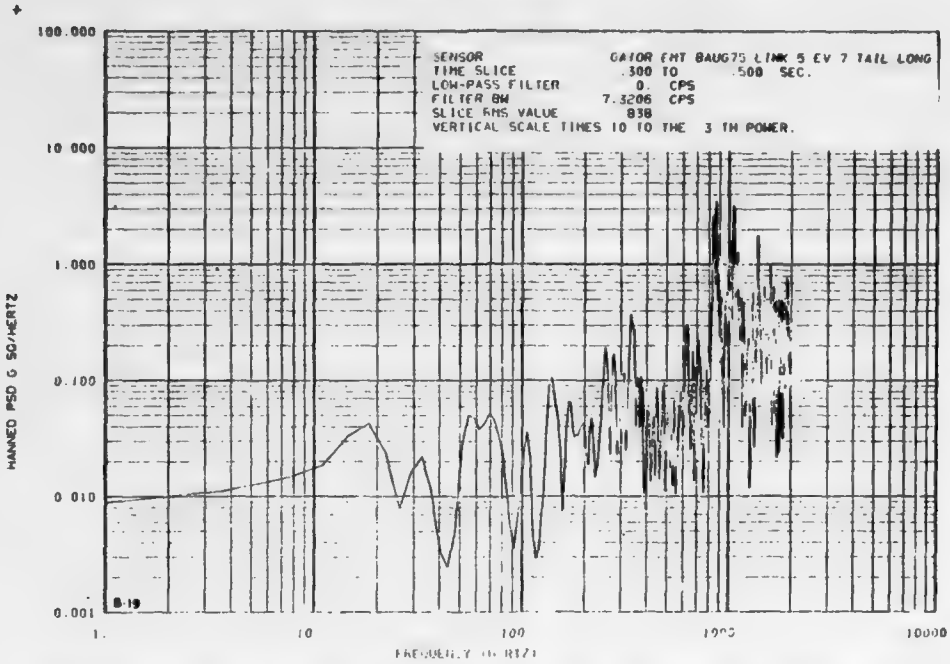

FIGURE B-19. PSD Plot Derived from Data Recorded During Rolling Vertical Landing.

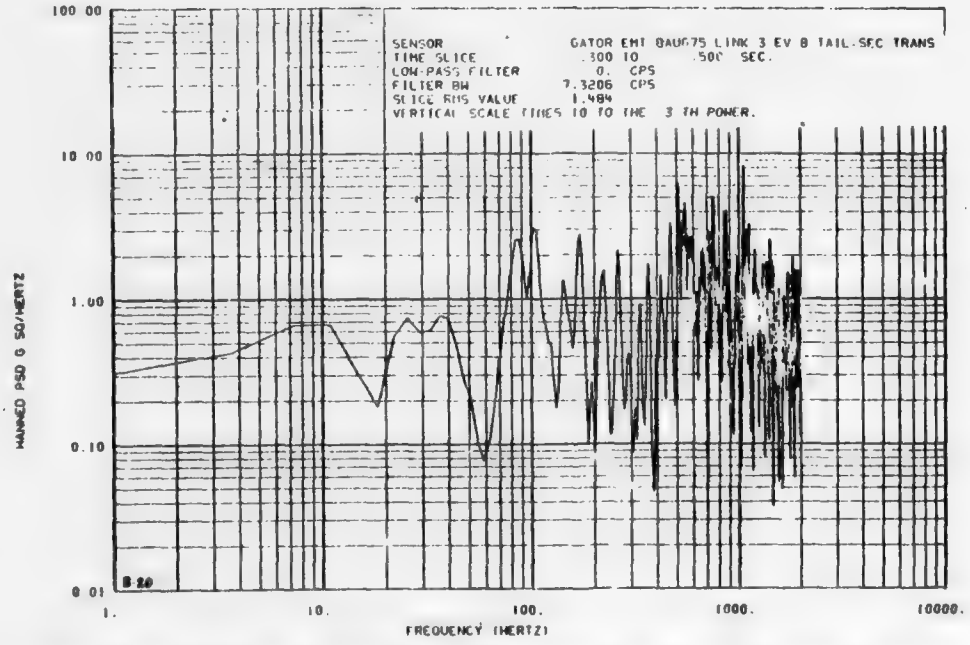

FIGURE B-20. PSD Plot Derived from Data Recorded During Rolling Vertical Landing.

Appendix C

Acoustic RMS Sound Pressure Level
Time Histories
(Figures C-1 through C-15)
and
PSD Plots
(Figures C-16 through C-30)

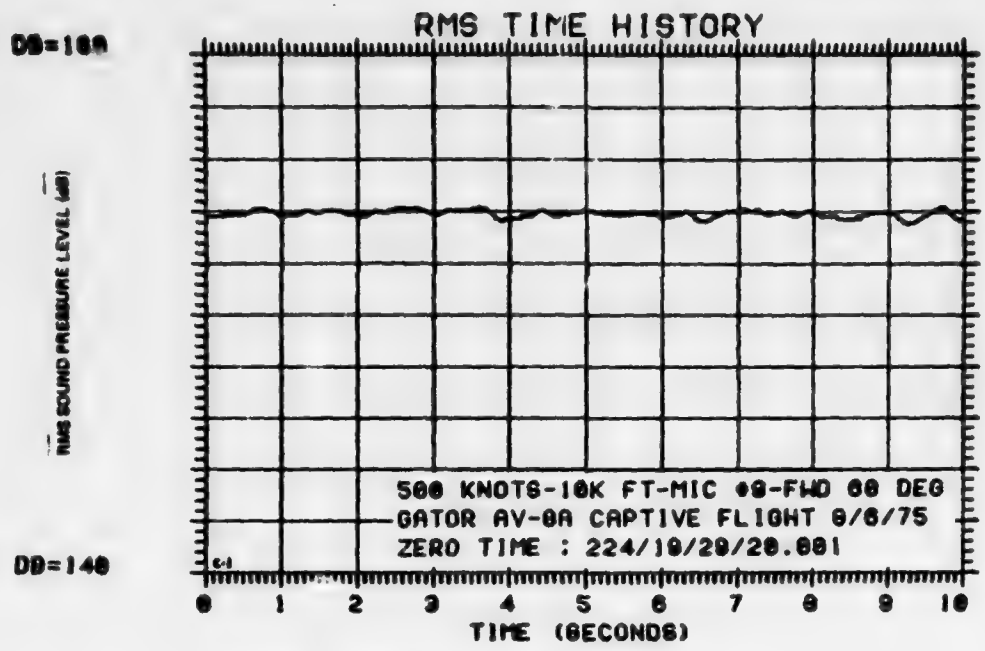

FIGURE C-1. RMS Sound Pressure Levels Time History.

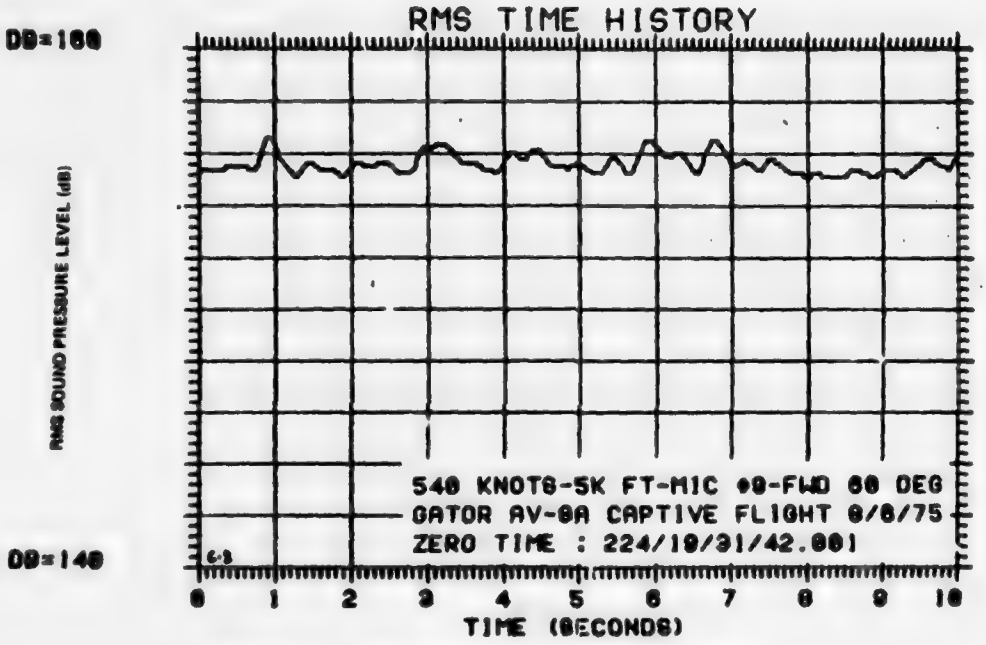

FIGURE C-2. RMS Sound Pressure Levels Time History.

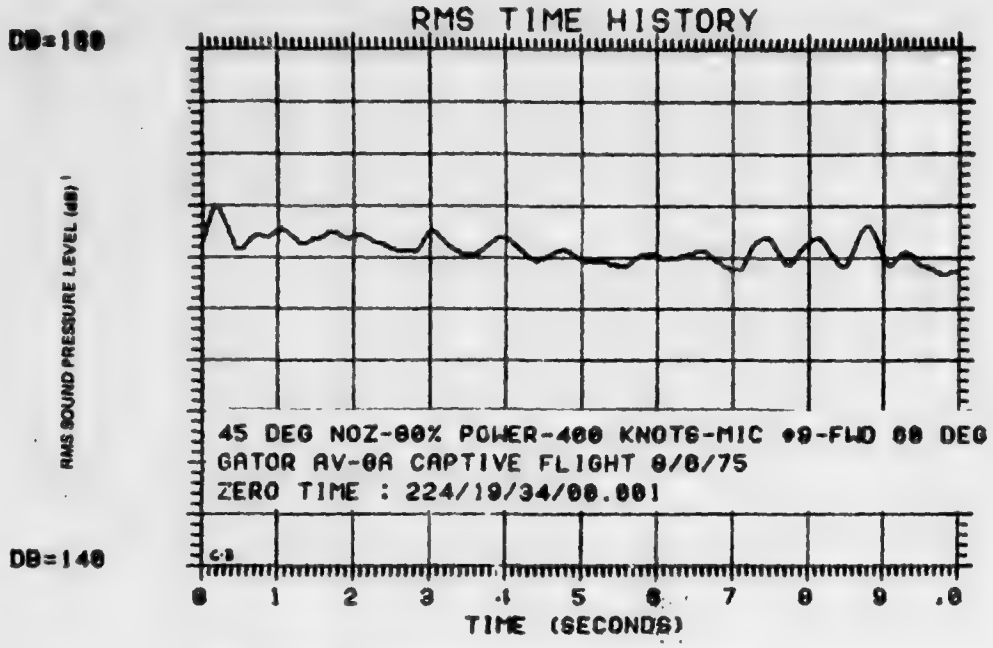

FIGURE C-3. RMS Sound Pressure Levels Time History.

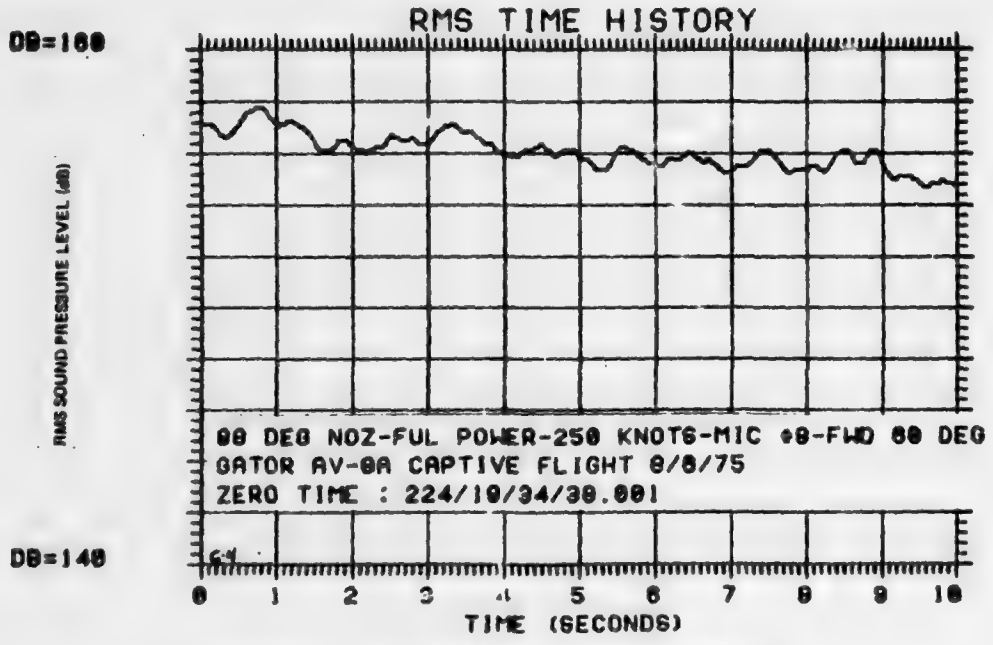

FIGURE C-4. RMS Sound Pressure Levels Time History.

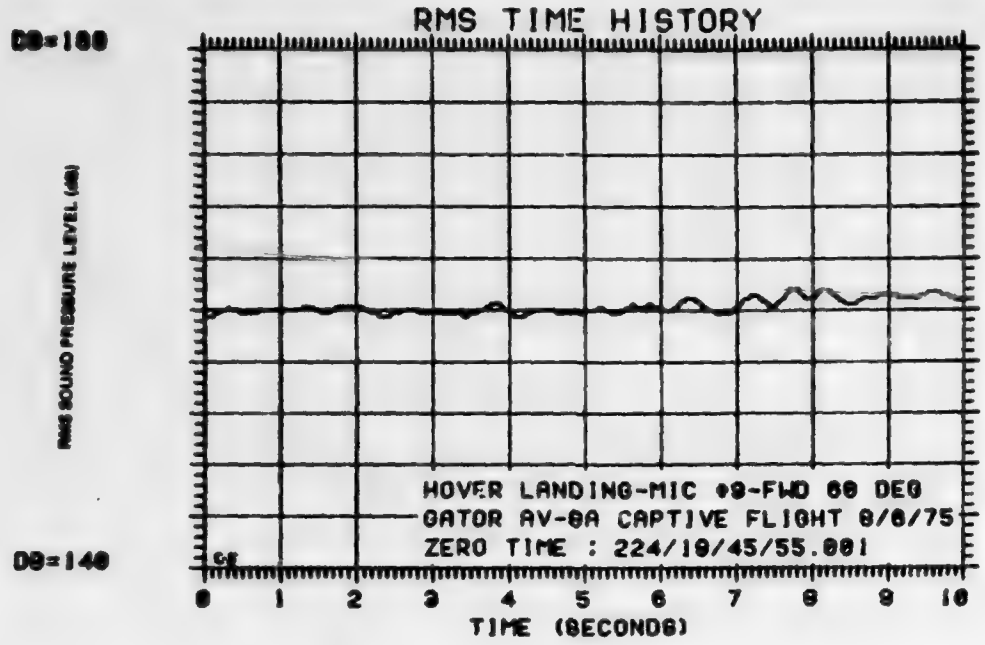

FIGURE C-5. RMS Sound Pressure Levels Time History.

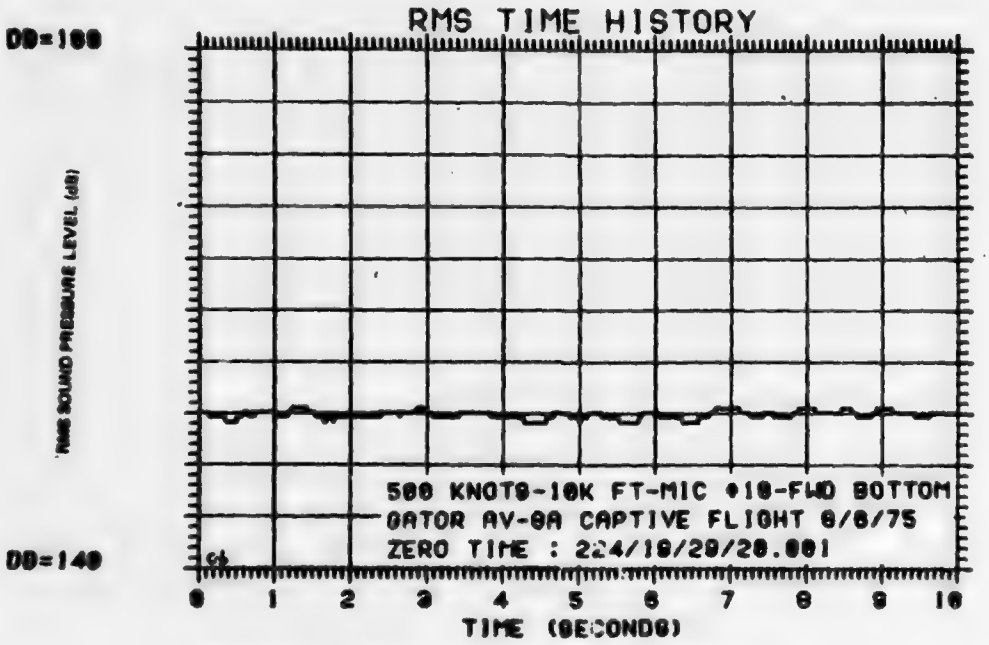

FIGURE C-6. RMS Sound Pressure Levels Time History.

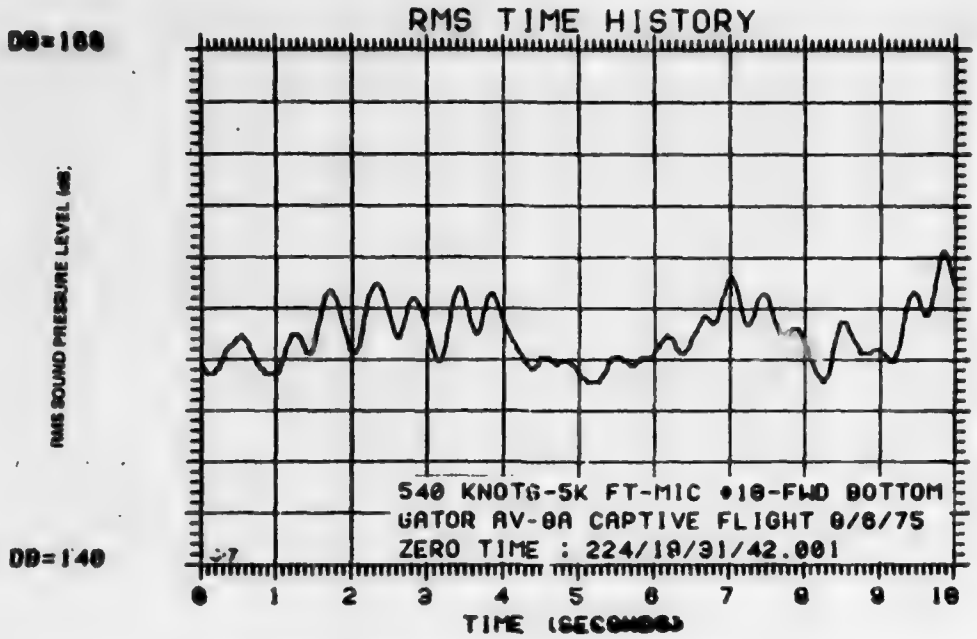

FIGURE C-7. RMS Sound Pressure Levels Time History.

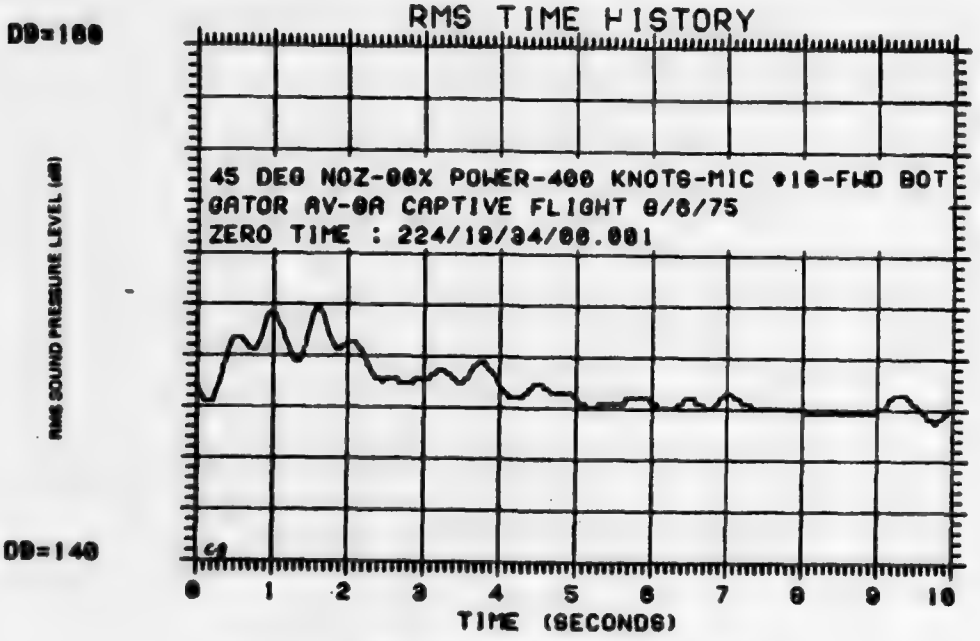

FIGURE C-8. RMS Sound Pressure Levels Time History.

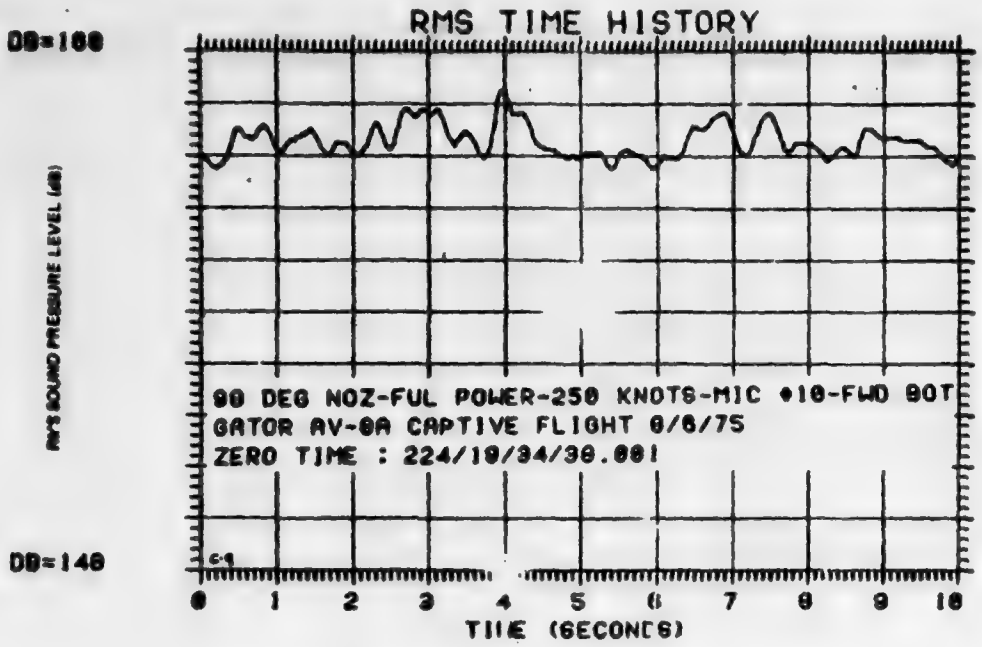

FIGURE C-9. RMS Sound Pressure Levels Time History.

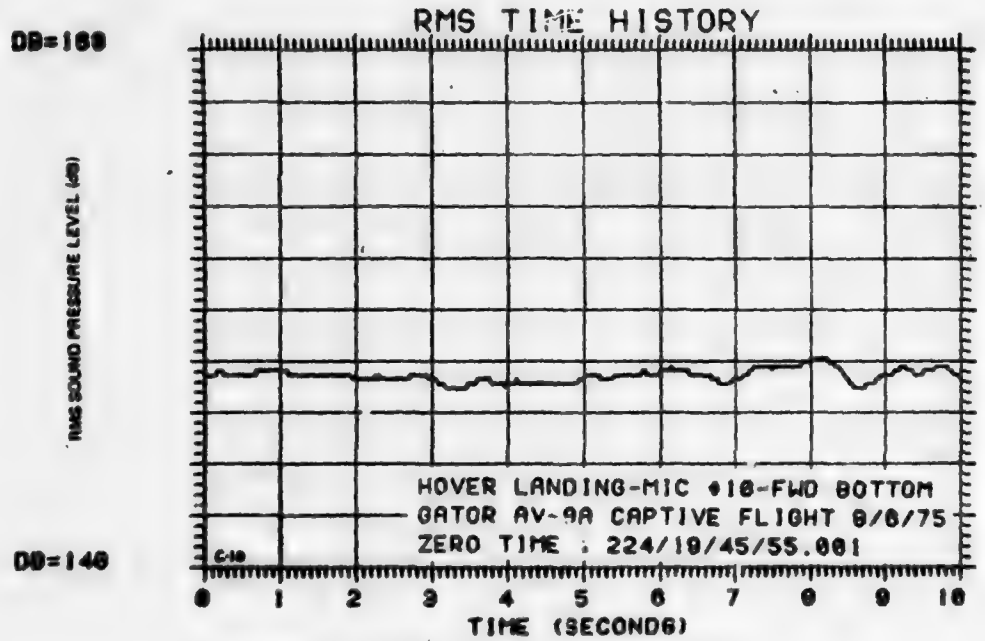

FIGURE C-10. RMS Sound Pressure Levels Time History.

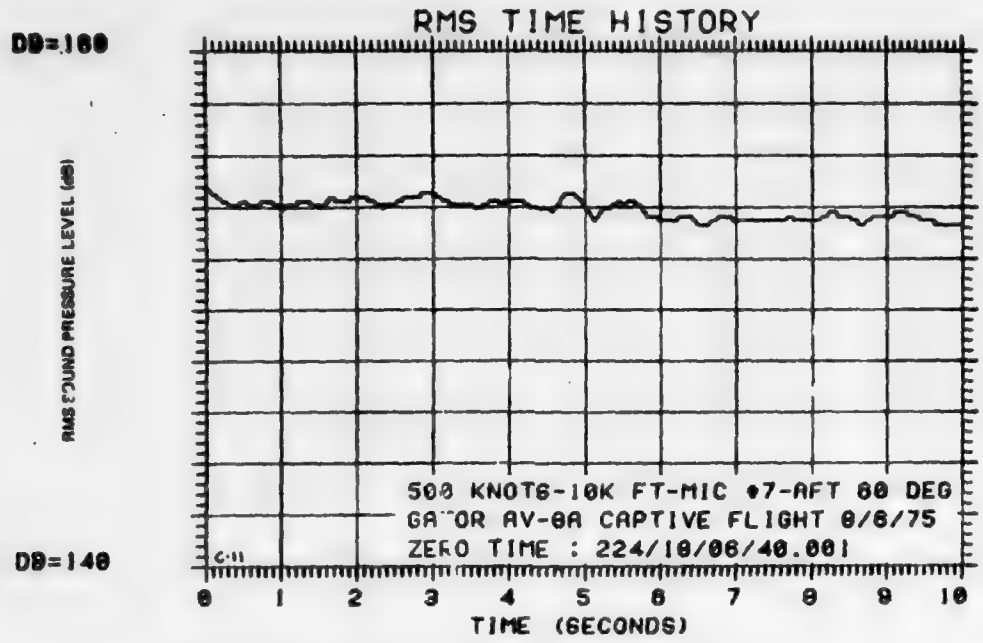

FIGURE C-11. RMS Sound Pressure Levels Time History.

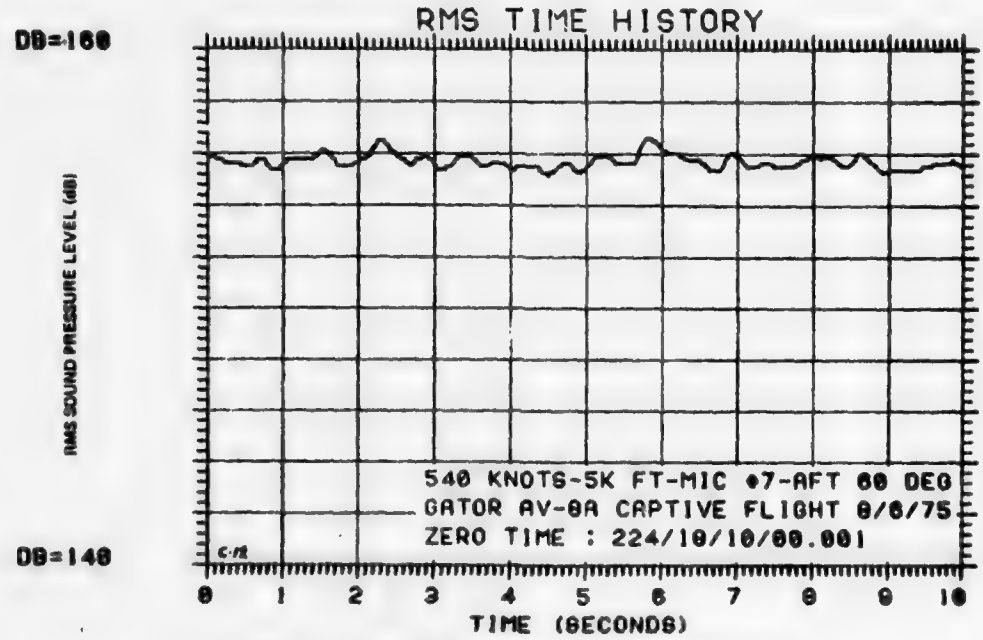

FIGURE C-12. RMS Sound Pressure Levels Time History.

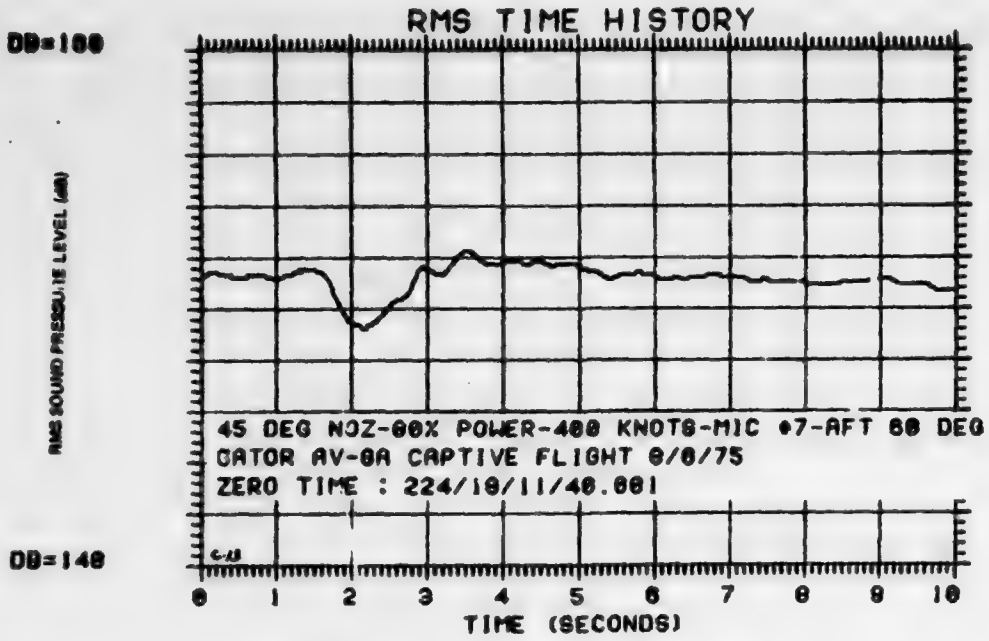

FIGURE C-13. RMS Sound Pressure Levels Time History.

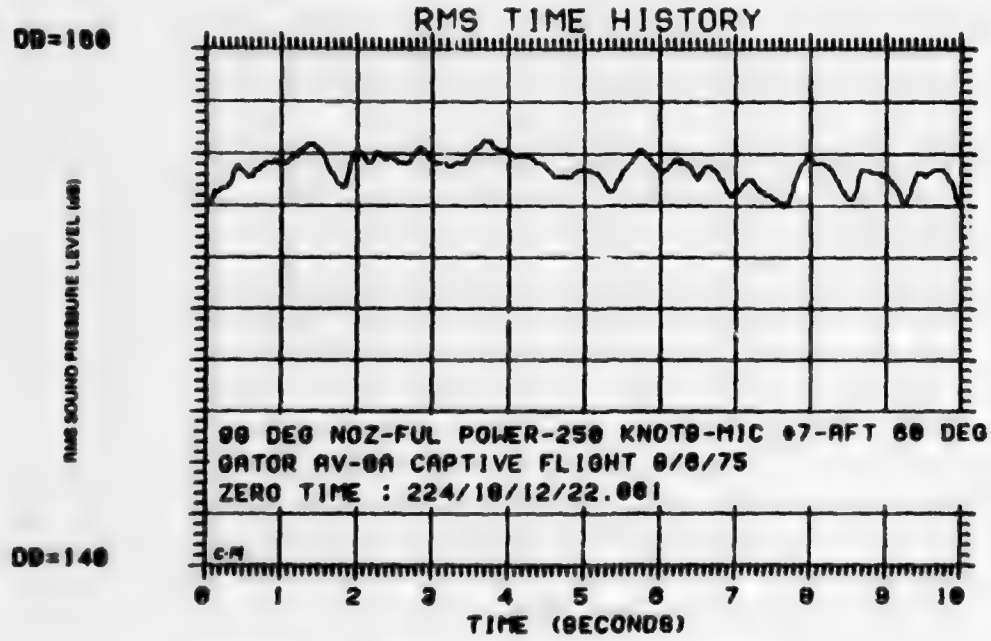

FIGURE C-14. RMS Sound Pressure Levels Time History.

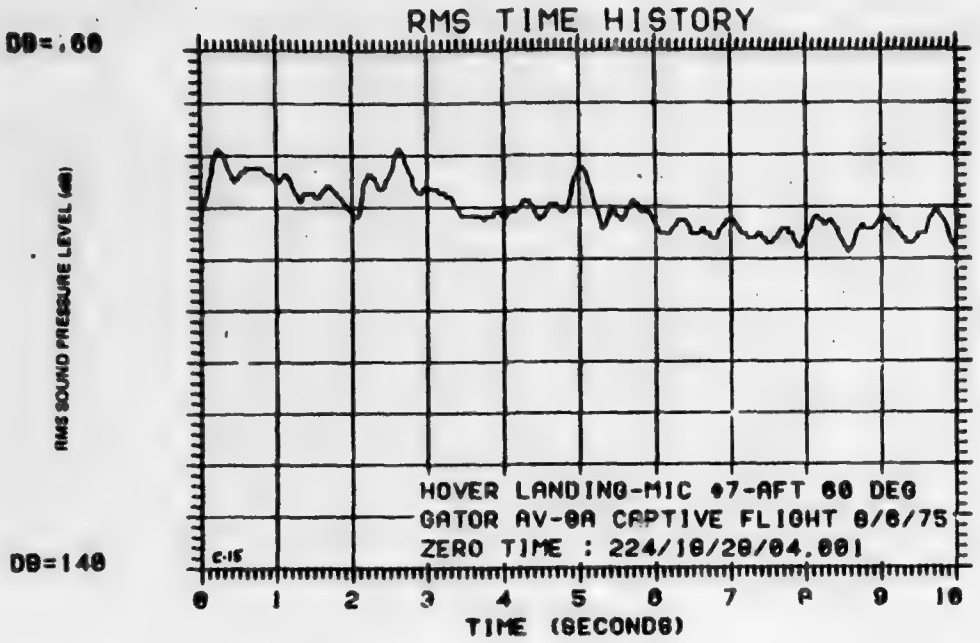

FIGURE C-15. RMS Sound Pressure Levels Time History.

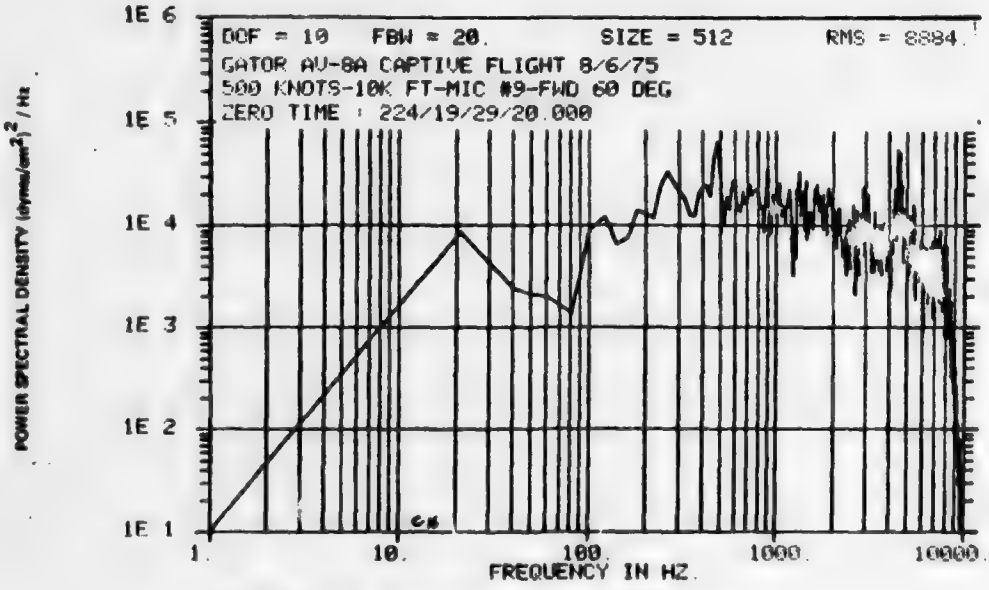

FIGURE C-16. Power Spectral Density vs. Frequency.

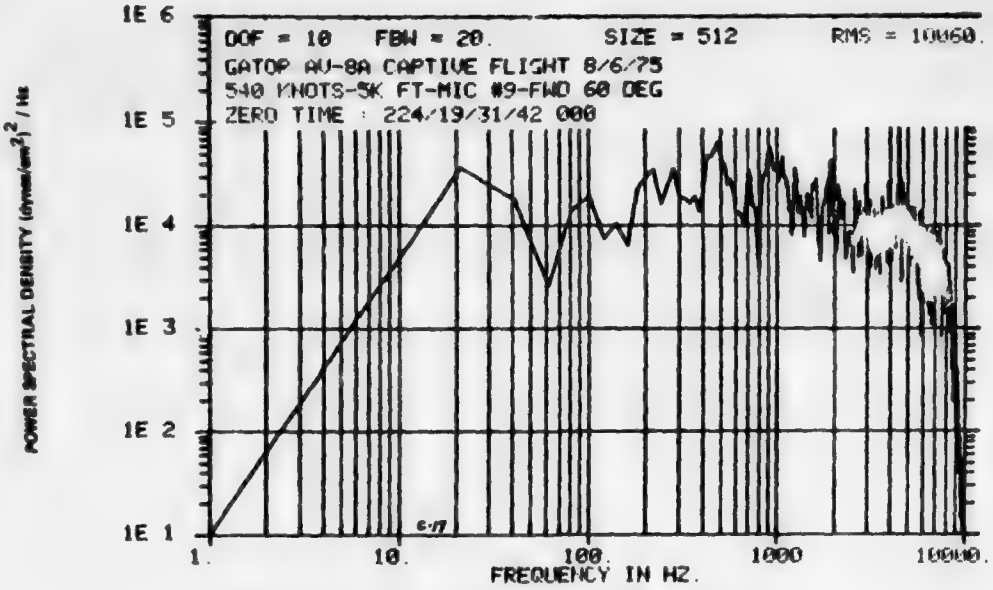

FIGURE C-17. Power Spectral Density vs. Frequency.

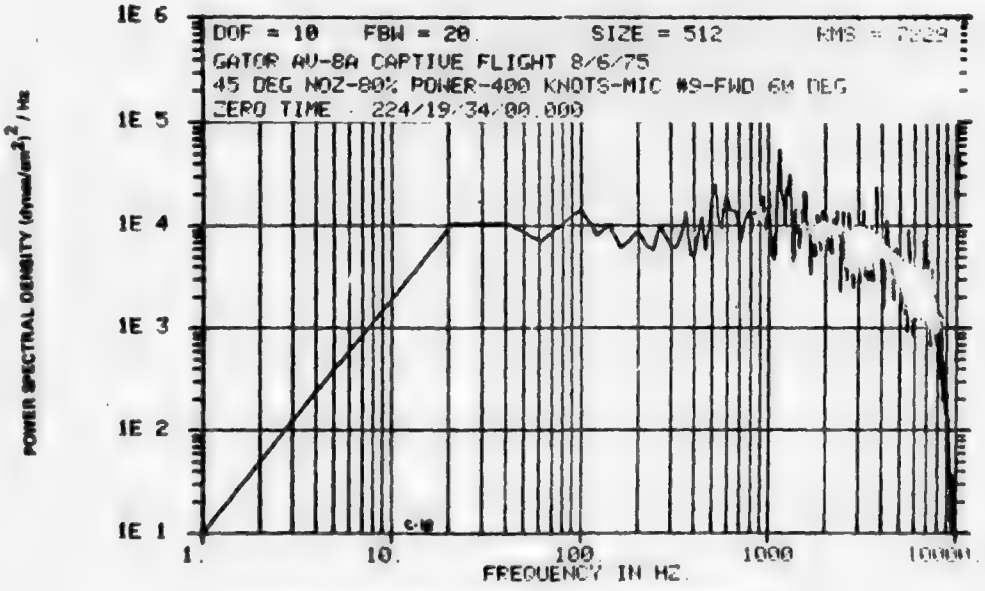

FIGURE C-18. Power Spectral Density vs. Frequency.

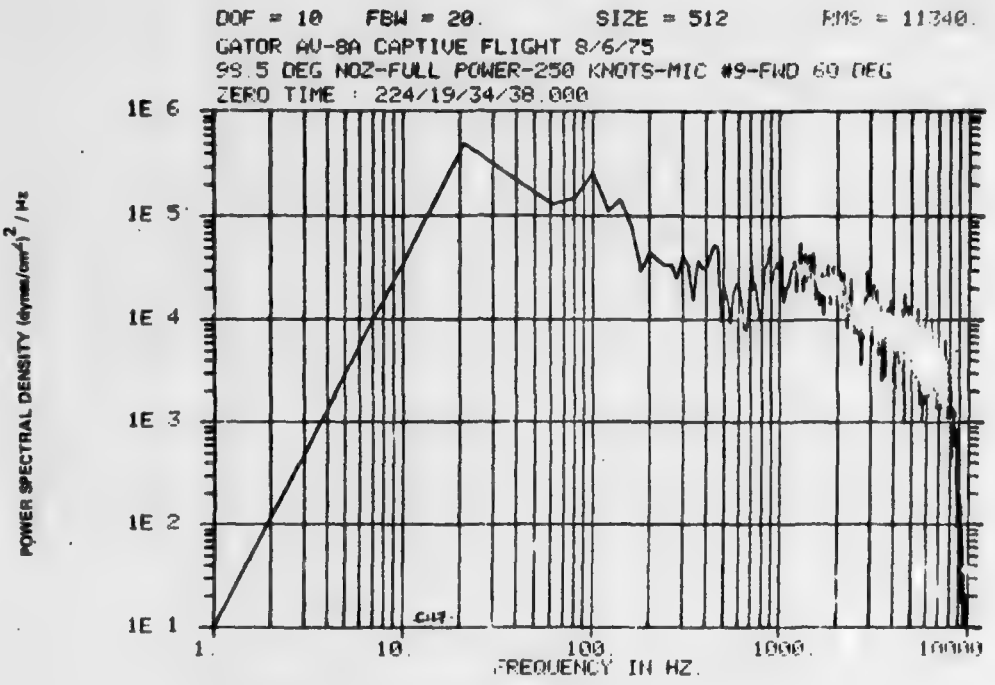

FIGURE C-19. Power Spectral Density vs. Frequency.

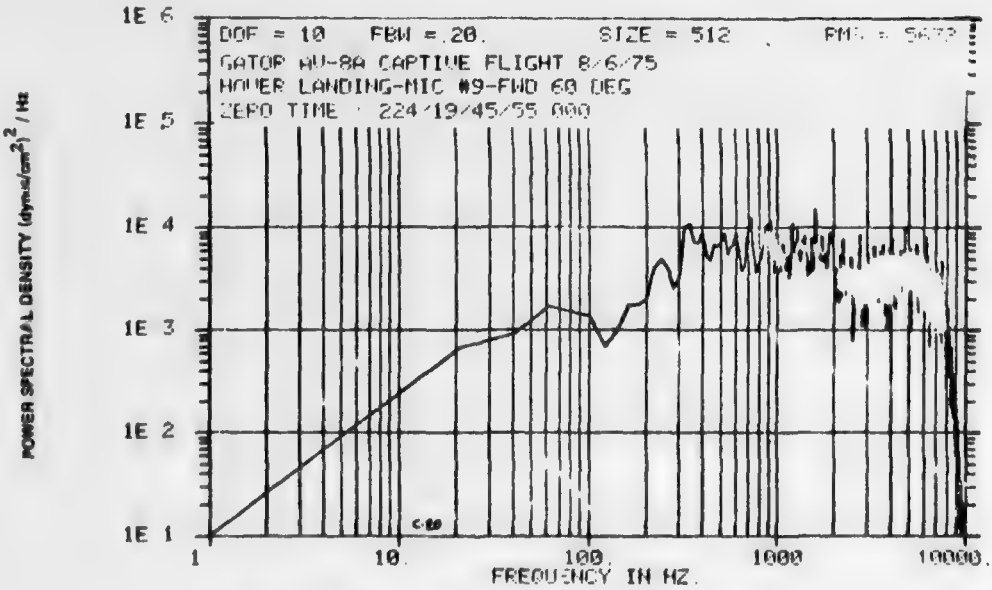

FIGURE C-20. Power Spectral Density vs. Frequency.

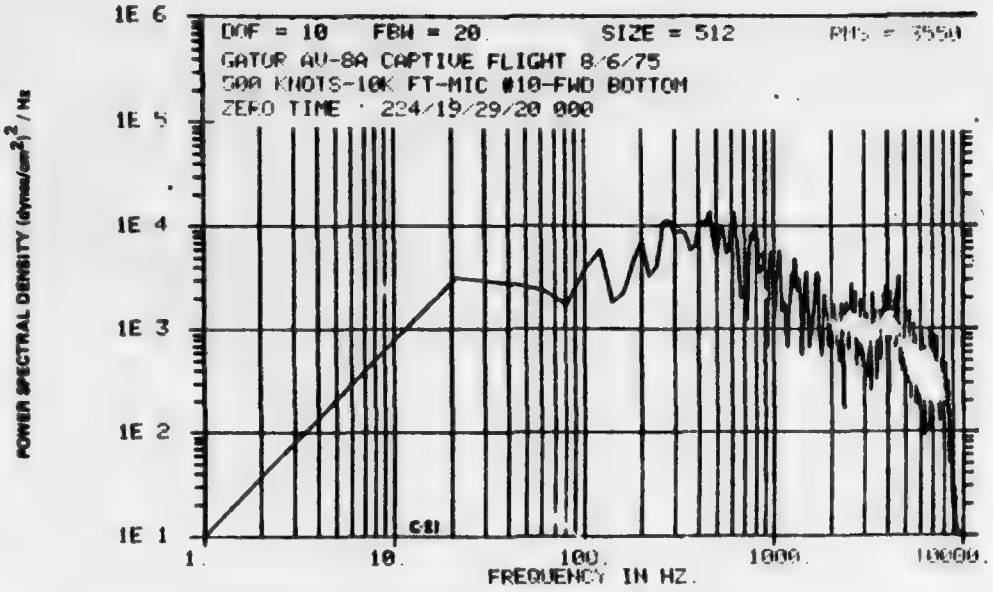

FIGURE C-21. Power Spectral Density vs. Frequency.

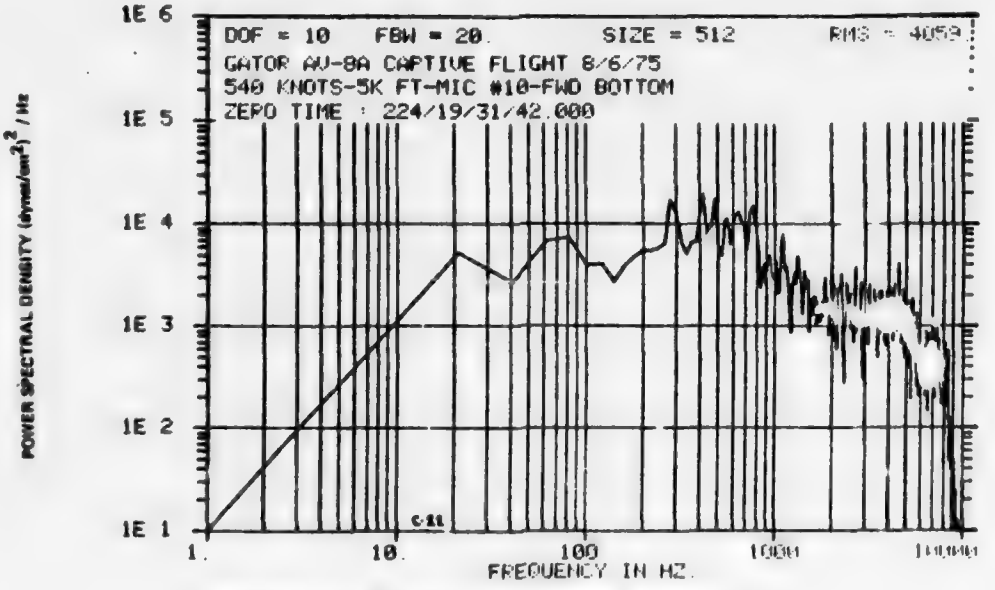

FIGURE C-22. Power Spectral Density vs. Frequency.

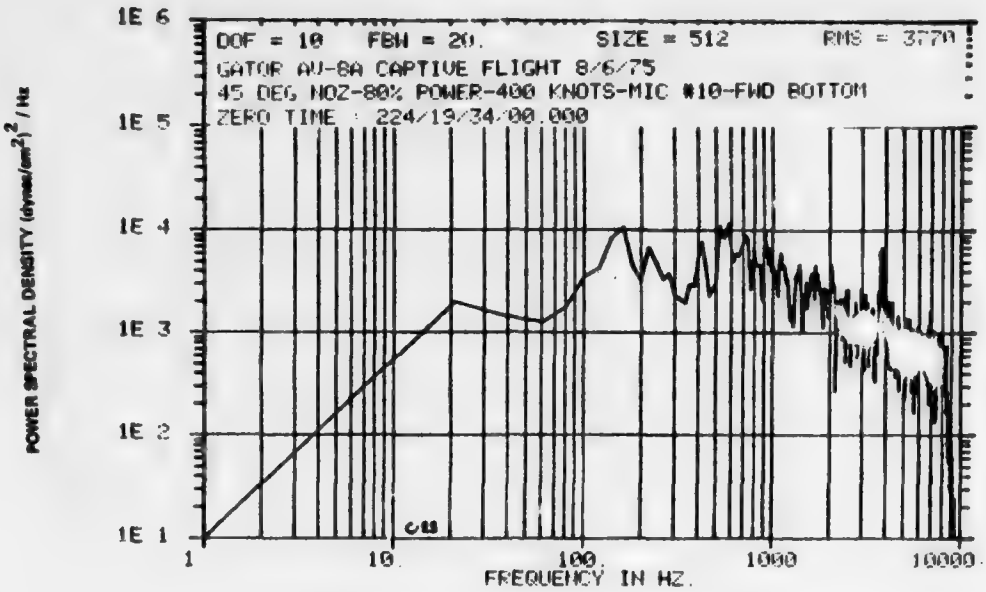

FIGURE C-23. Power Spectral Density vs. Frequency.

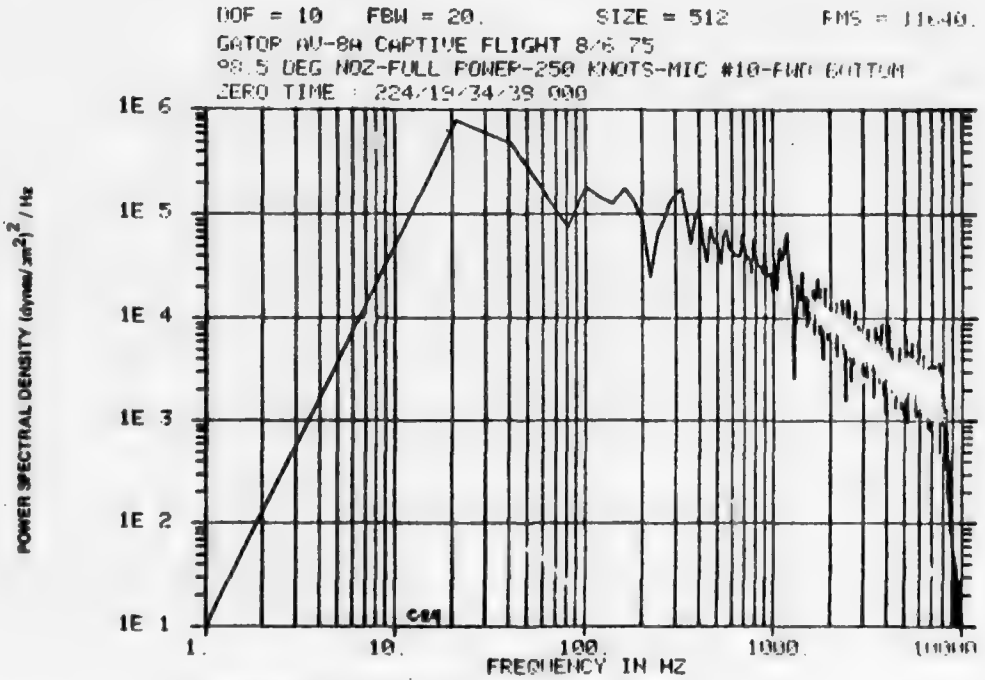

FIGURE C-24. Power Spectral Density vs. Frequency.

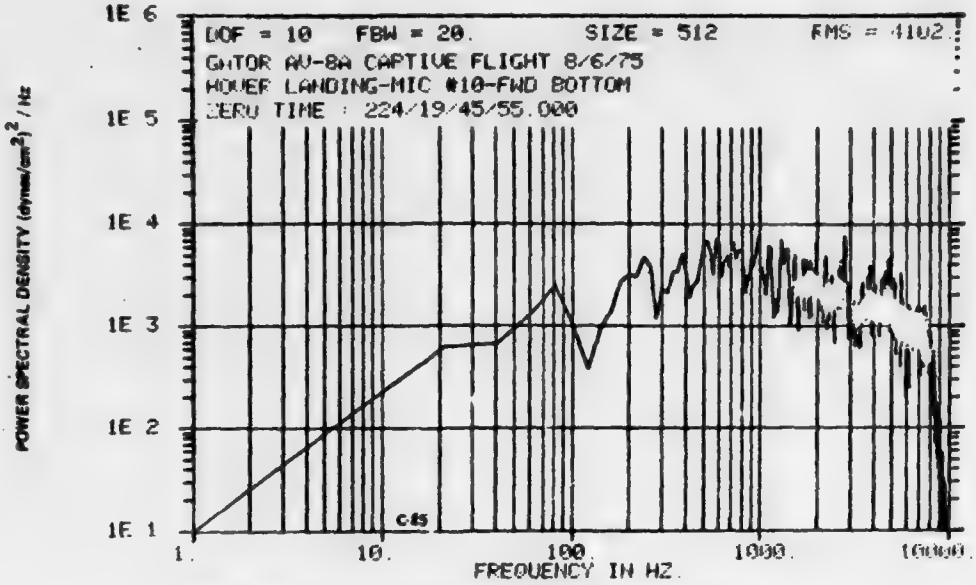

FIGURE C-25. Power Spectral Density vs. Frequency.

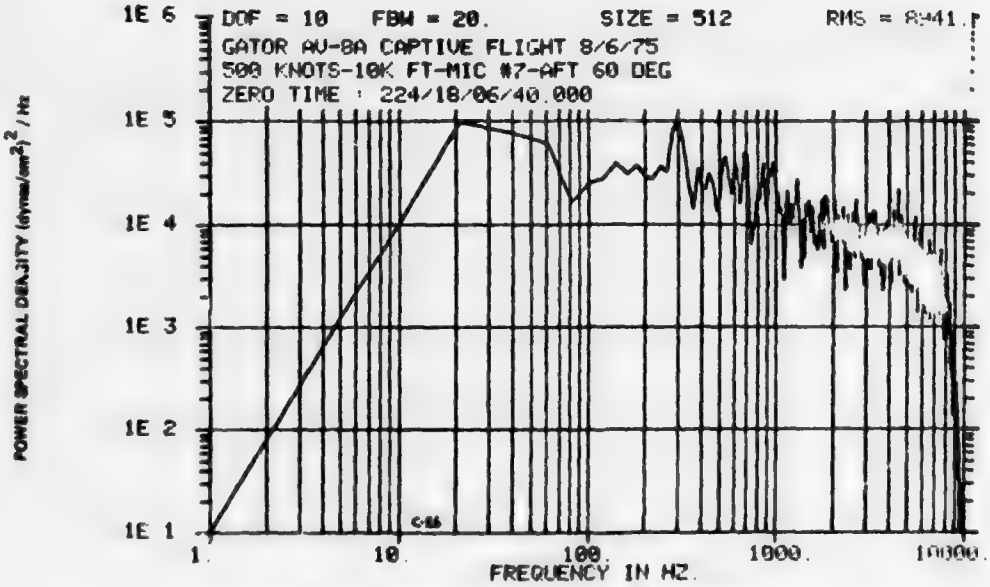

FIGURE C-26. Power Spectral Density vs. Frequency.

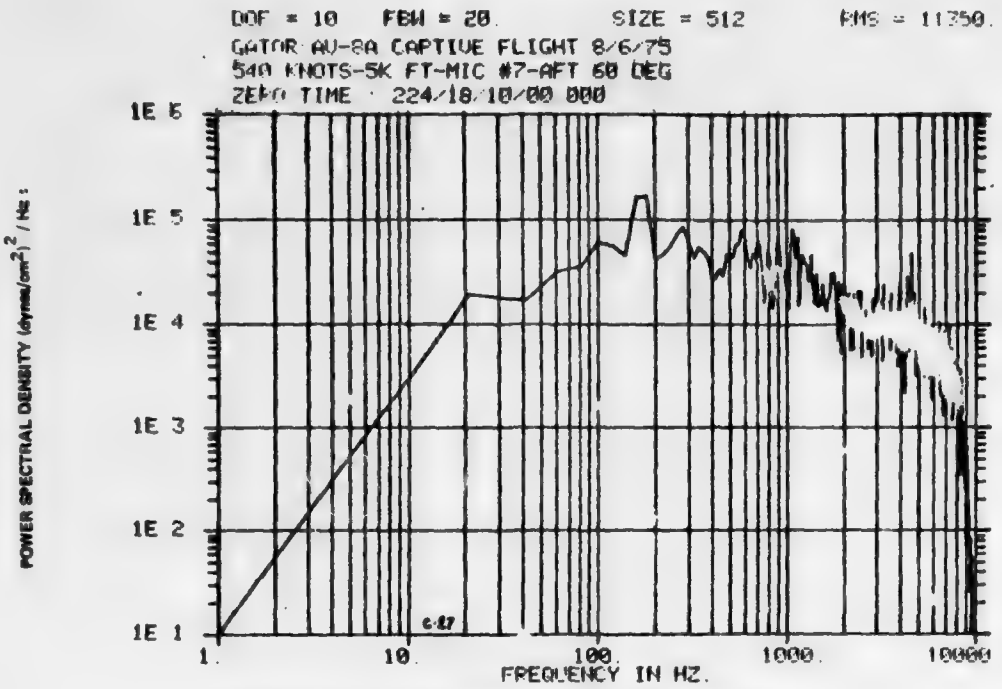

FIGURE C-27. Power Spectral Density vs. Frequency.

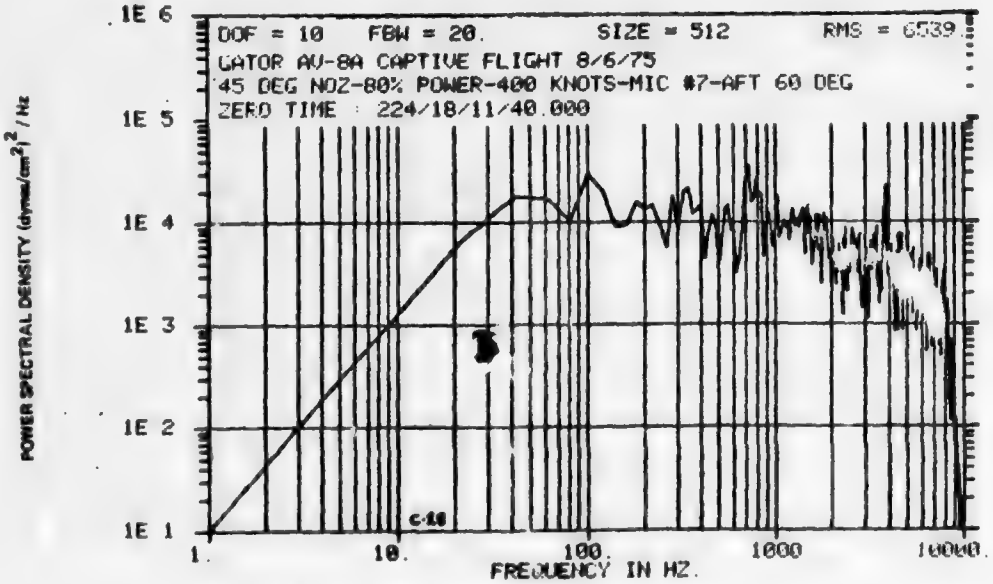

FIGURE C-28. Power Spectral Density vs. Frequency.

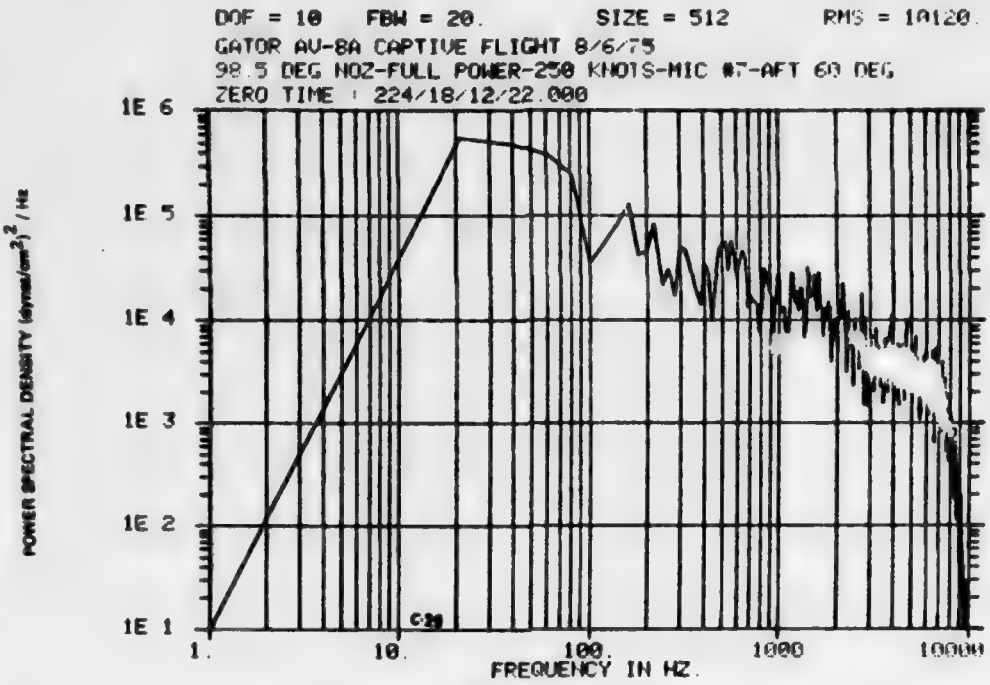

FIGURE C-29. Power Spectral Density vs. Frequency.

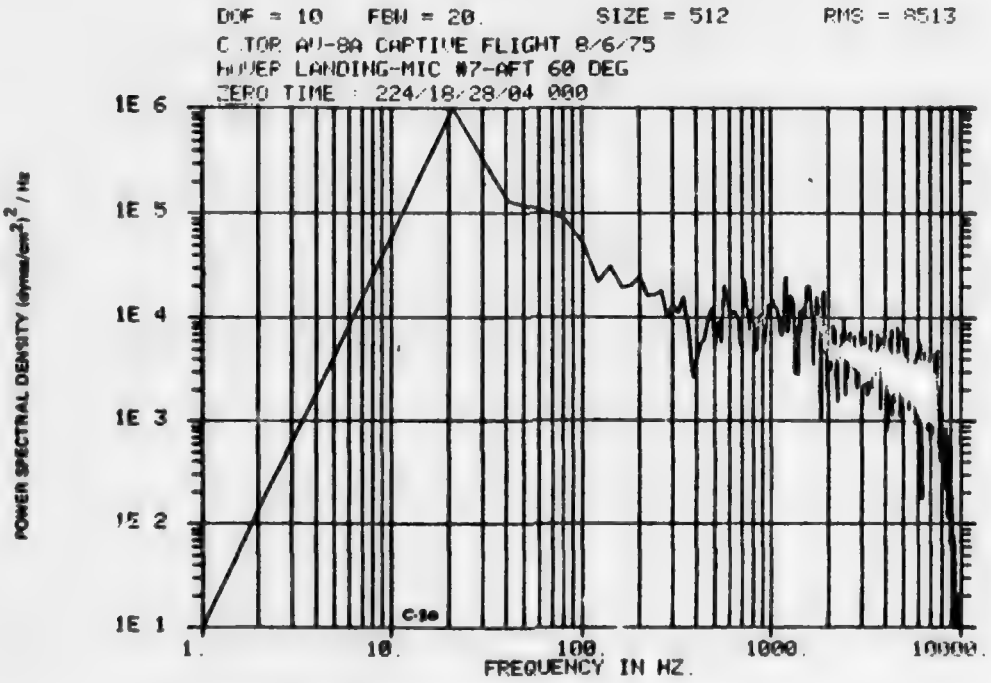

FIGURE C-30. Power Spectral Density vs. Frequency.

Appendix D

Acceleration PSD Plots:
Laboratory Tests
(Transverse Axis: Figures D-1 through D-18)
(Vertical Axis: Figures D-19 through D-38)

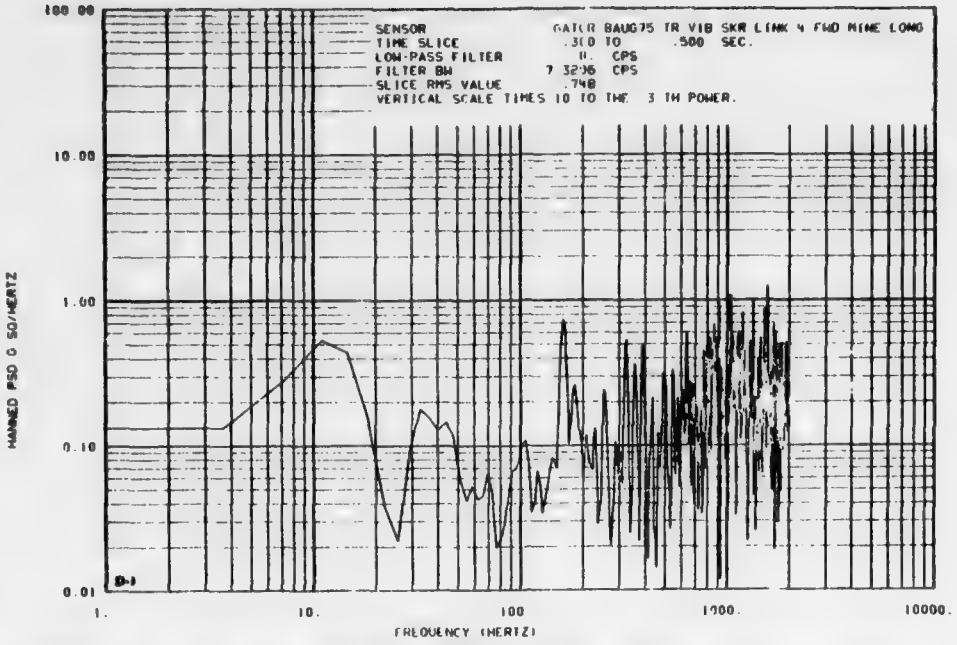

FIGURE D-1. PSD Plots Derived from Data Recorded During Laboratory Vibration Tests in the Transverse Axis of the Weapon.

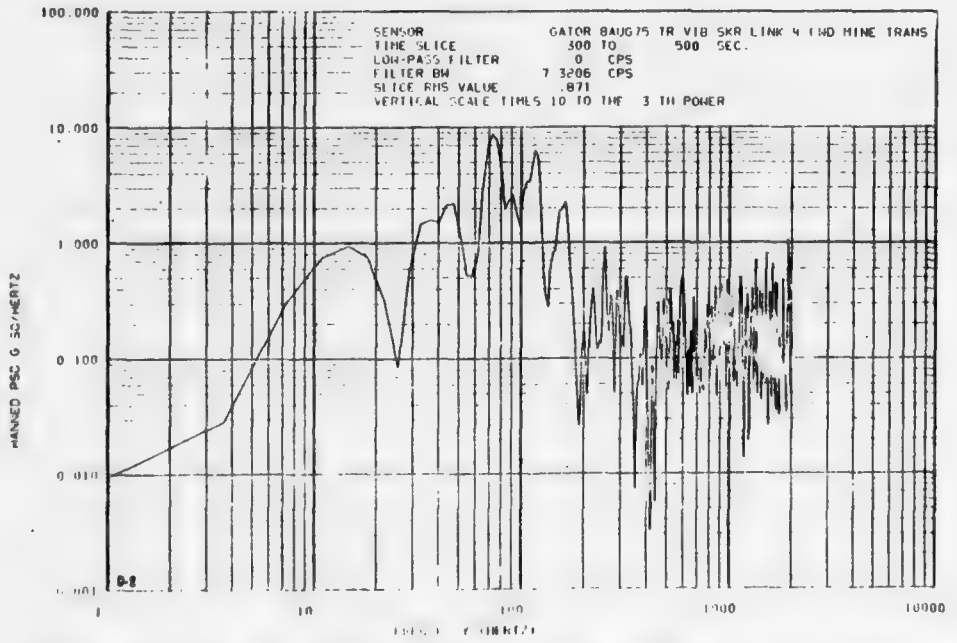

FIGURE D-2. PSD Plots Derived from Data Recorded During Laboratory Vibration Tests in the Transverse Axis of the Weapon.

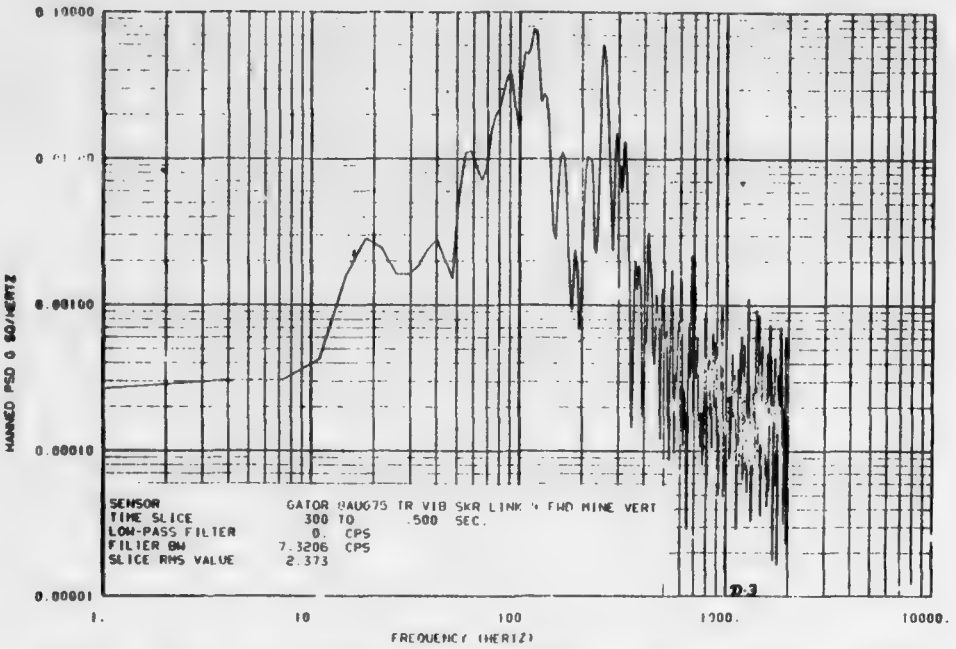

FIGURE D-3. PSD Plots Derived from Data Recorded During Laboratory Vibration Tests in the Transverse Axis of the Weapon.

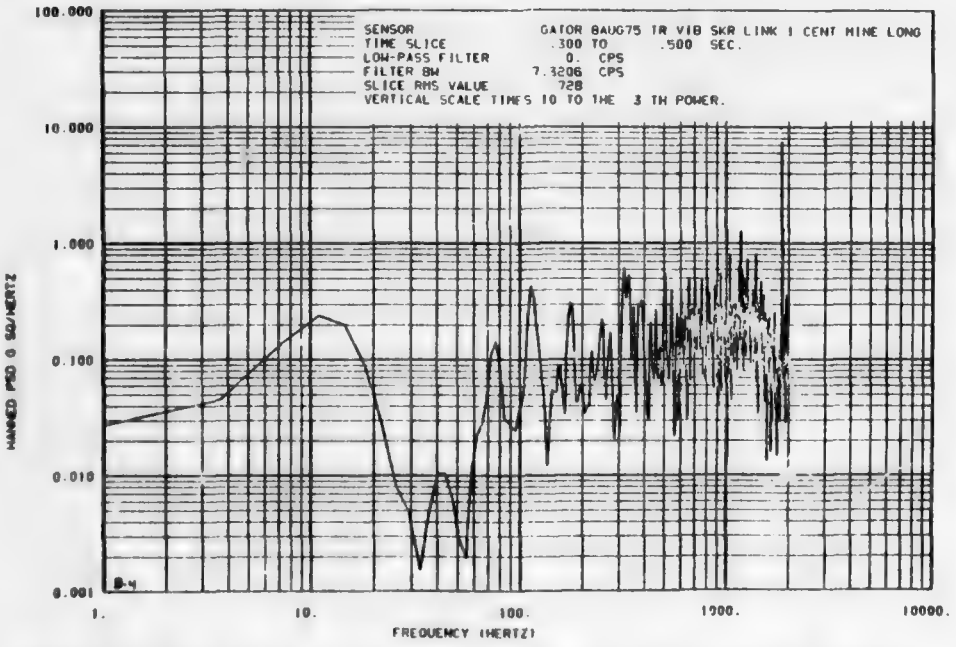

FIGURE D-4. PSD Plots Derived from Data Recorded During Laboratory Vibration Tests in the Transverse Axis of the Weapon.

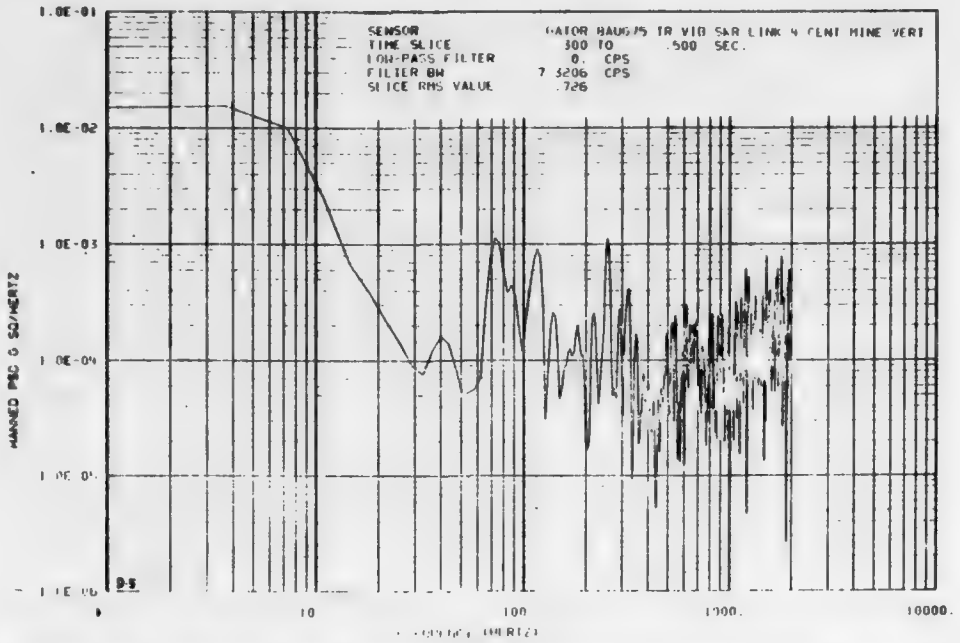

FIGURE D-5. PSD Plot Plots Derived from Data Recorded During Laboratory Vibration Tests in the Transverse Axis of the Weapon.

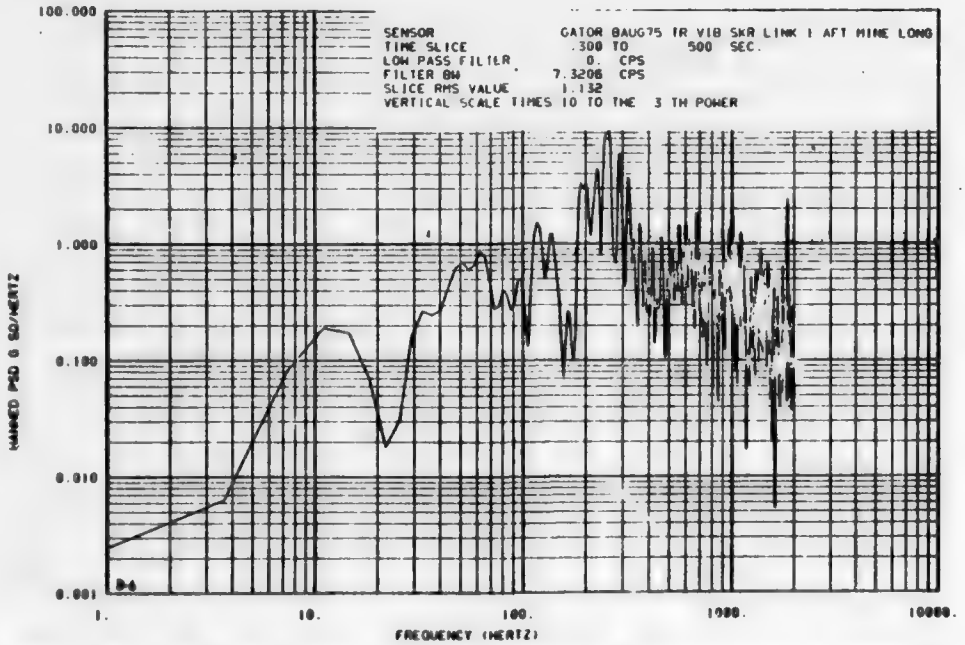

FIGURE D-6. PSD Plots Derived from Data Recorded During Laboratory Vibration Tests in the Transverse Axis of the Weapon.

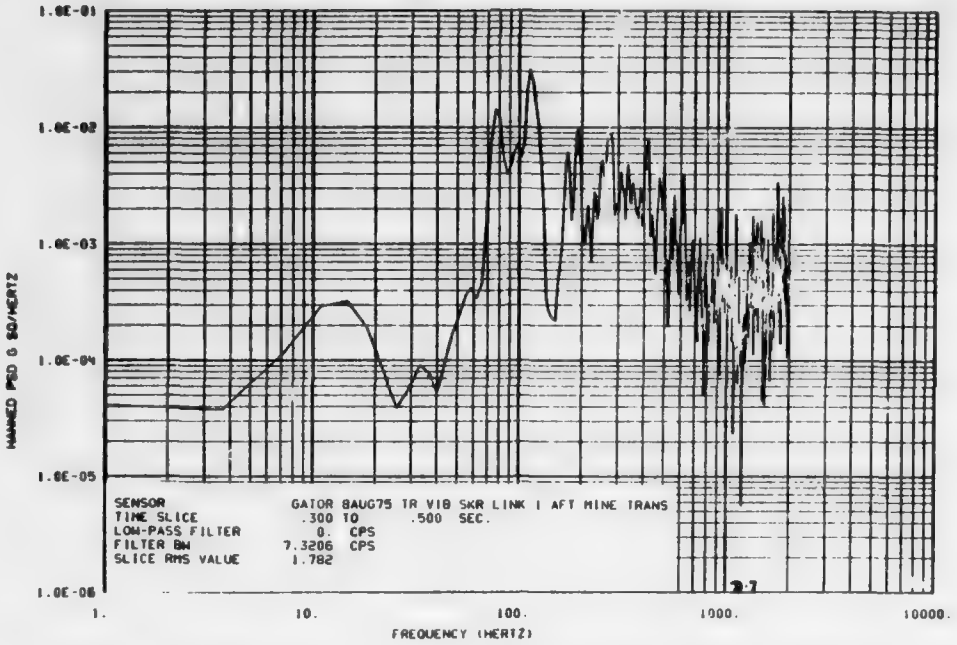

FIGURE D-7. PSD Plots Derived from Data Recorded During Laboratory Vibration Tests in the Transverse Axis of the Weapon.

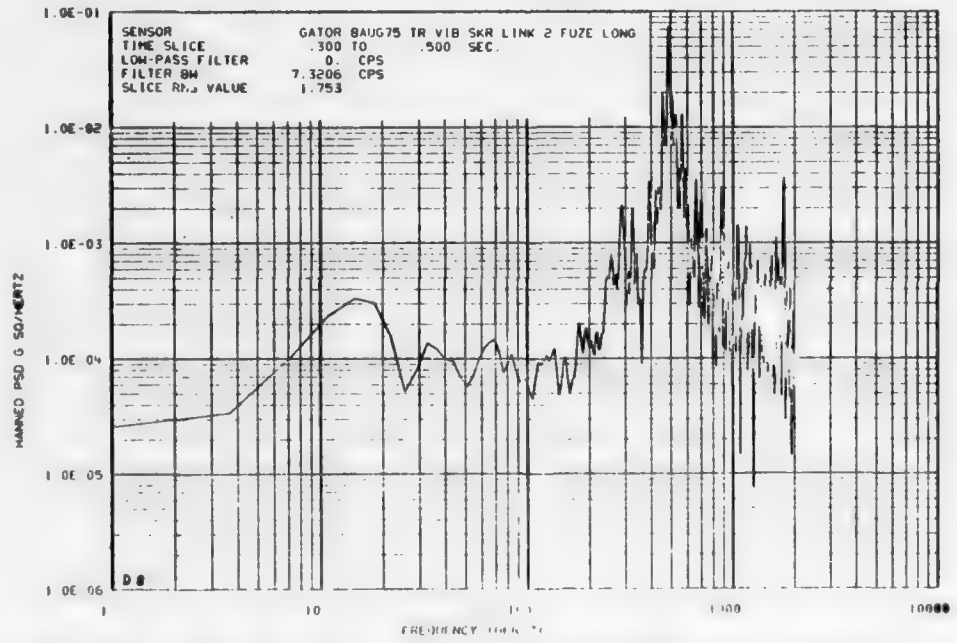

FIGURE D-8. PSD Plots Derived from Data Recorded During Laboratory Vibration Tests in the Transverse Axis of the Weapon.

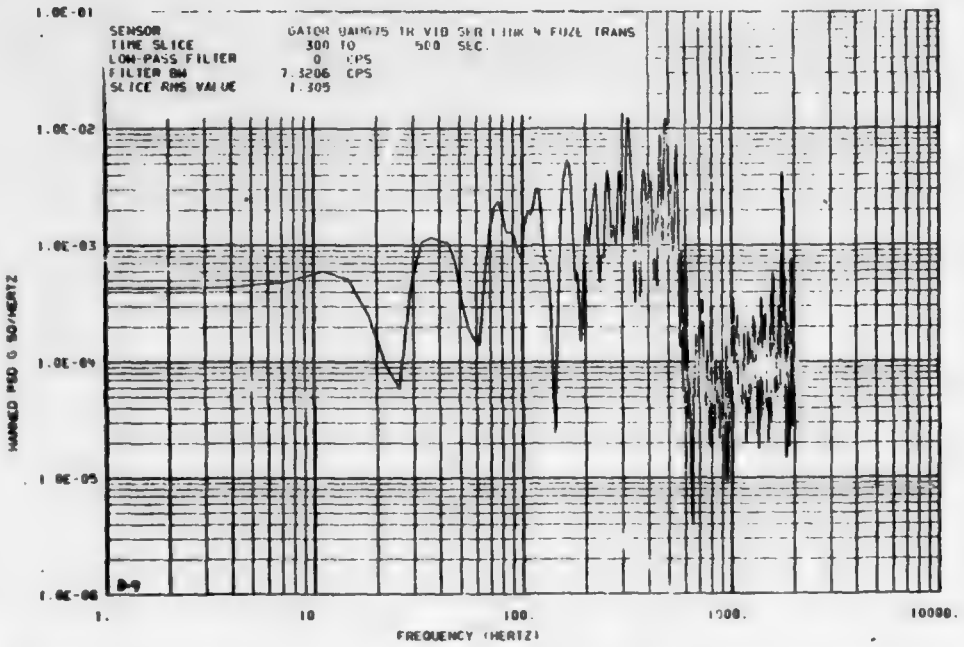

FIGURE D-9. PSD Plots Derived from Data Recorded During Laboratory Vibration Tests in the Transverse Axis of the Weapon.

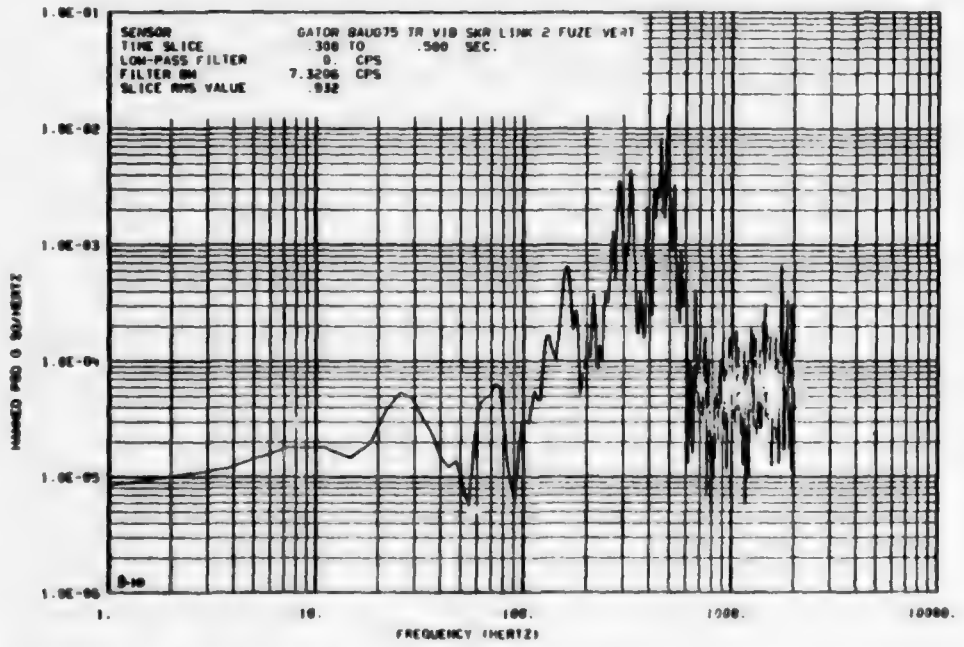

FIGURE D-10. PSD Plots Derived from Data Recorded During Laboratory Vibration Tests in the Transverse Axis of the Weapon.

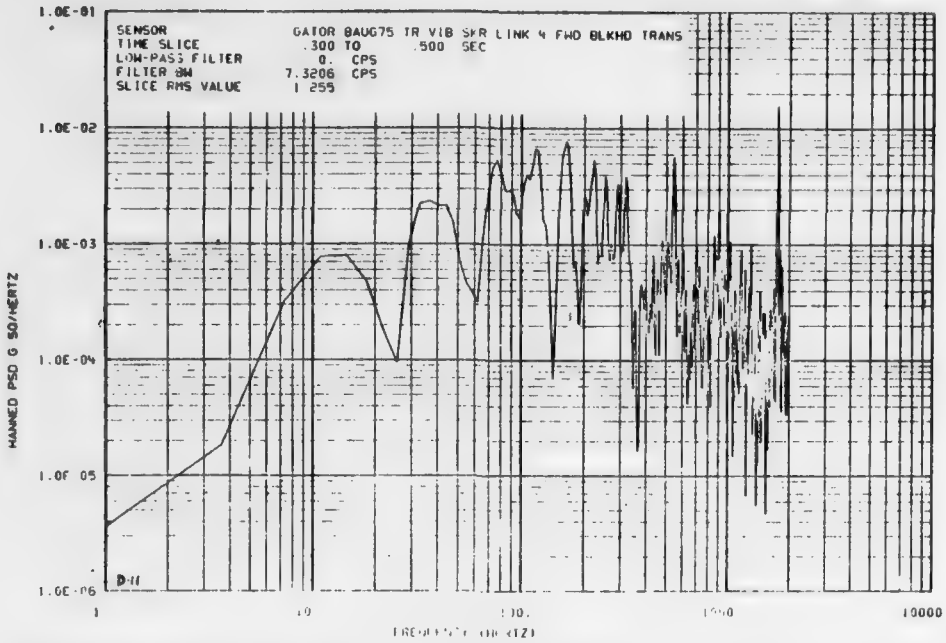

FIGURE D-11. PSD Plots Derived from Data Recorded During Laboratory Vibration Tests in the Transverse Axis of the Weapon.

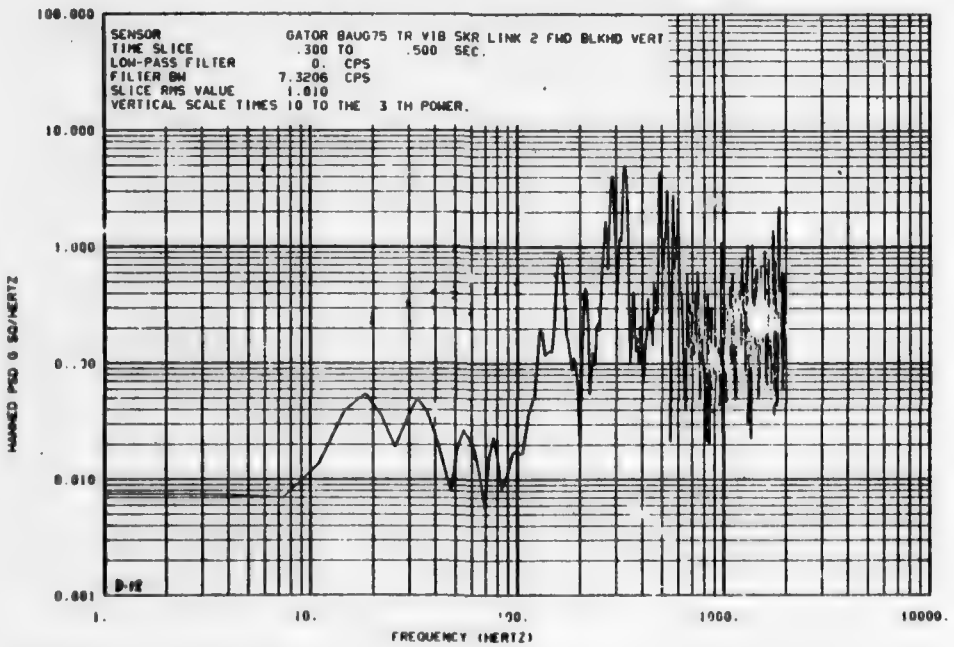

FIGURE D-12. PSD Plots Derived from Data Recorded During Laboratory Vibration Tests in the Transverse Axis of the Weapon.

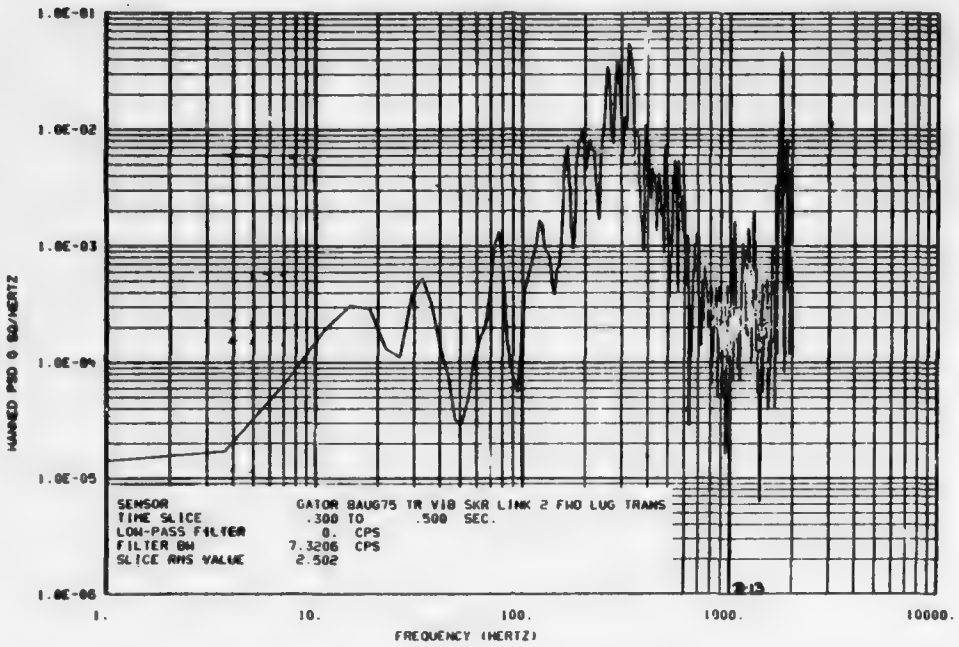

FIGURE D-13. PSD Plots Derived from Data Recorded During Laboratory Vibration Tests in the Transverse Axis of the Weapon.

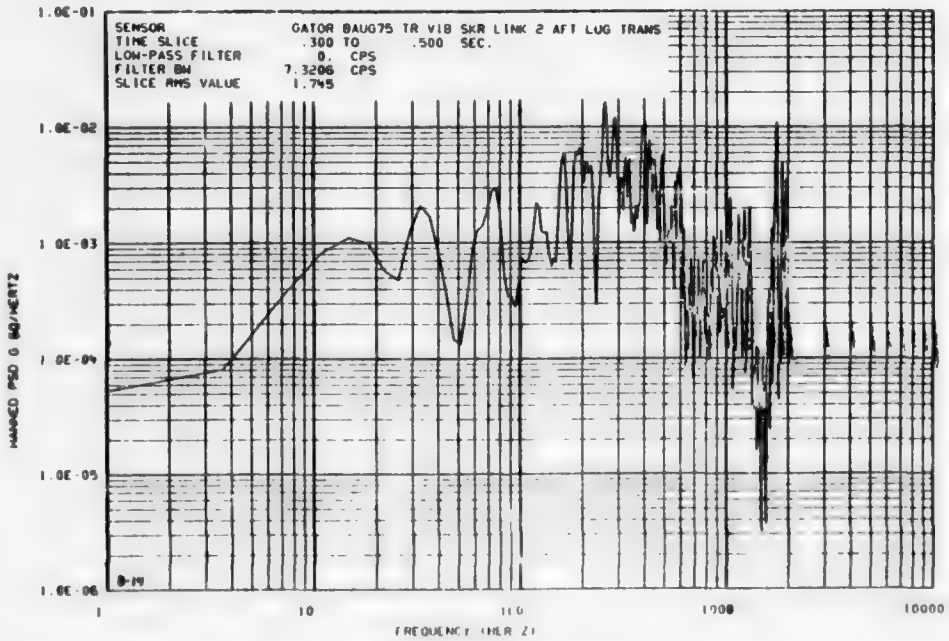

FIGURE D-14. PSD Plots Derived from Data Recorded During Laboratory Vibration Tests in the Transverse Axis of the Weapon.

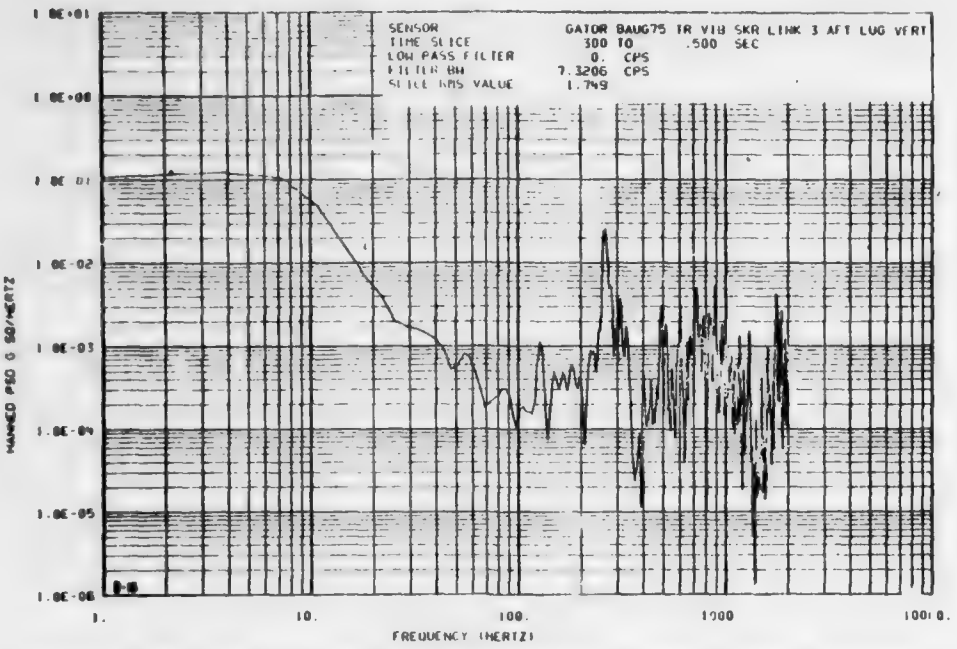

FIGURE D-15. PSD Plots Derived from Data Recorded During Laboratory Vibration Tests in the Transverse Axis of the Weapon.

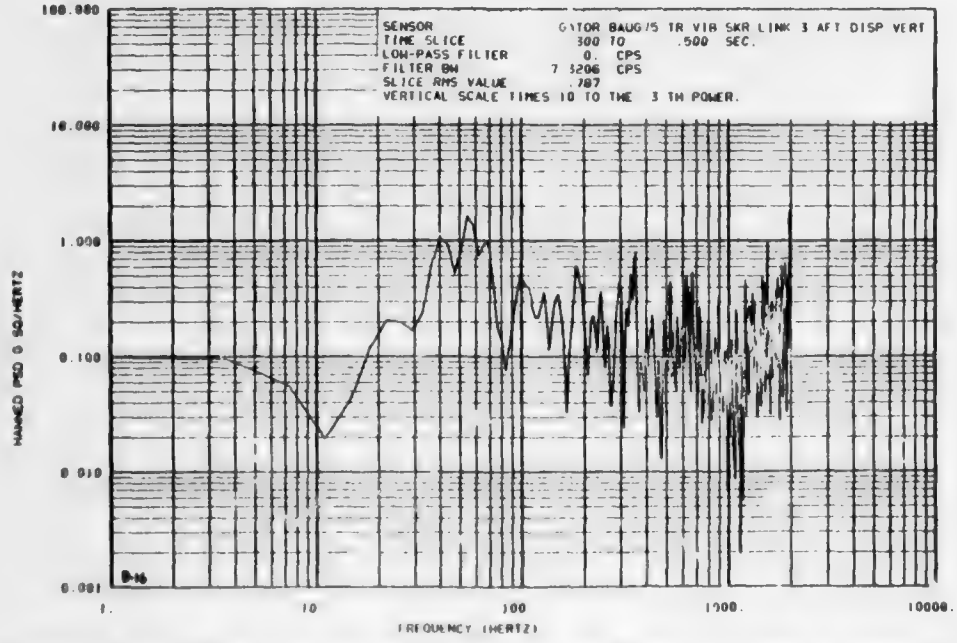

FIGURE D-16. PSD Plots Derived from Data Recorded During Laboratory Vibration Tests in the Transverse Axis of the Weapon.

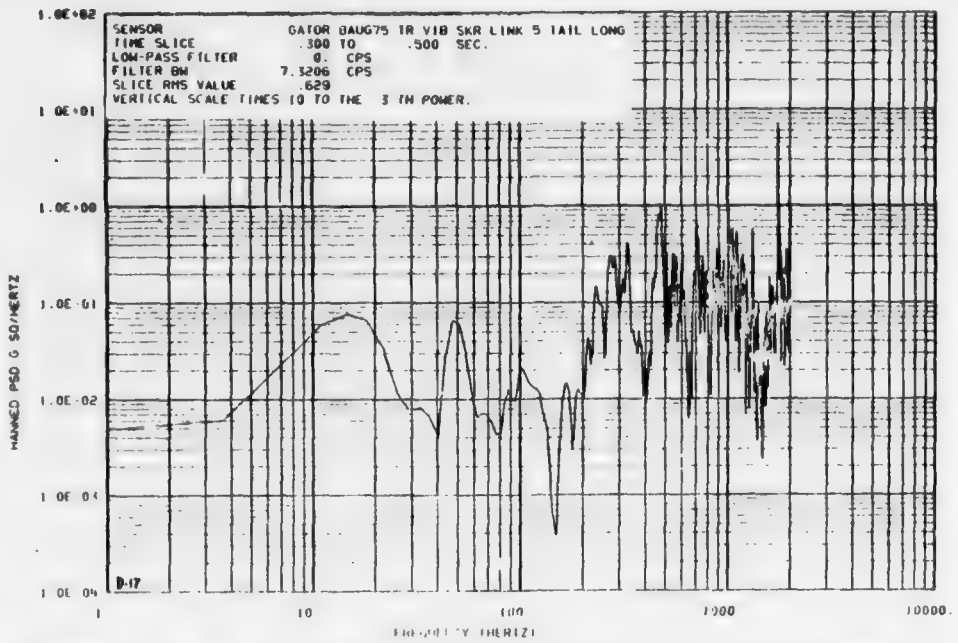

FIGURE D-17. PSD Plots Derived from Data Recorded During Laboratory Vibration Tests in the Transverse Axis of the Weapon.

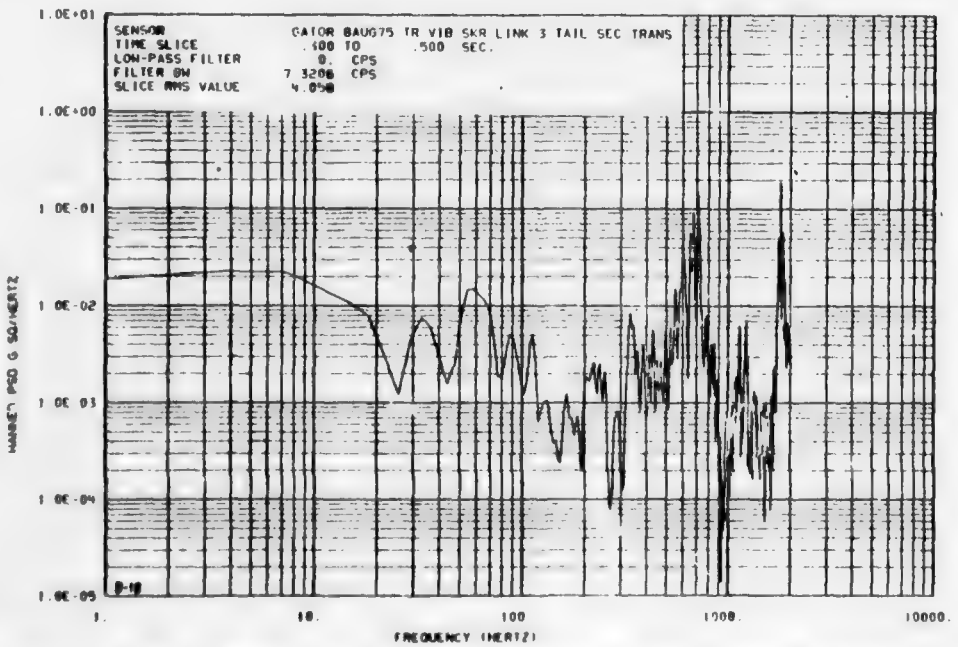

FIGURE D-18. PSD Plots Derived from Data Recorded During Laboratory Vibration Tests in the Transverse Axis of the Weapon.

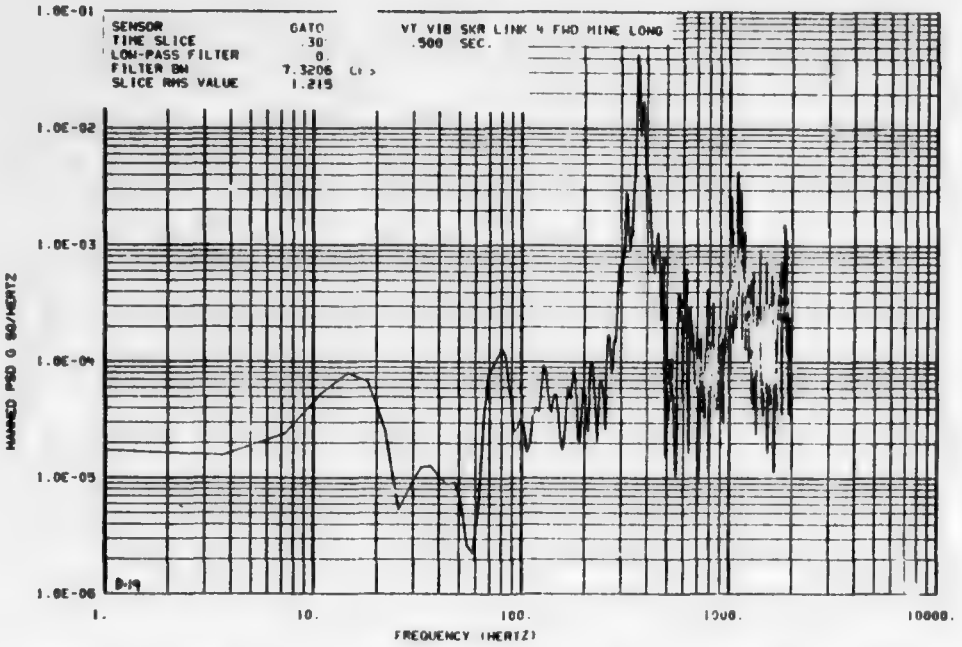

FIGURE D-19. PSD Plot Derived from Data Recorded During Laboratory Vibration Tests in the Vertical Axis of the Weapon.

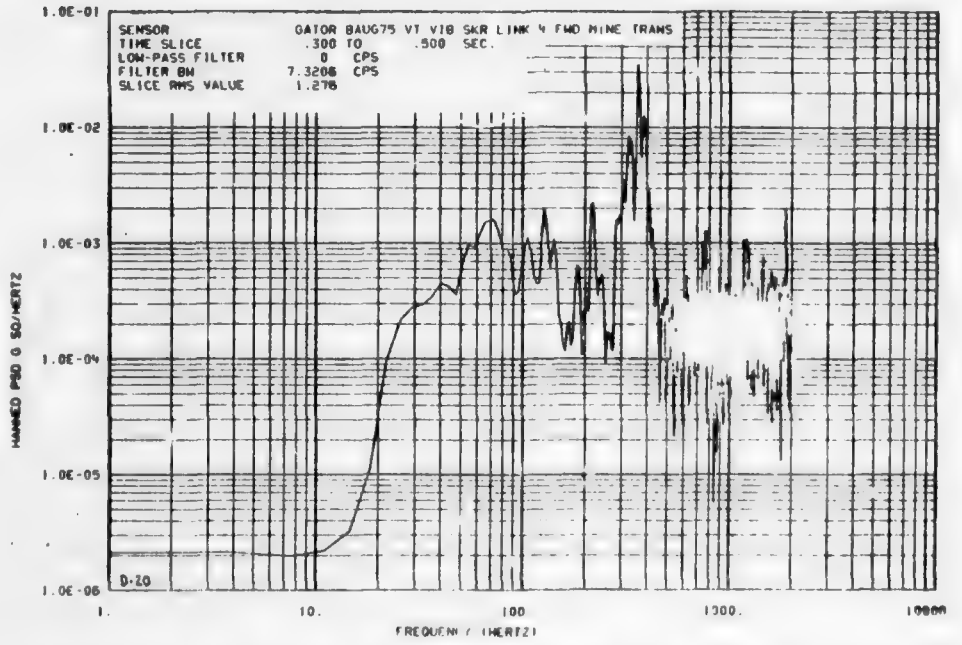

FIGURE D-20. PSD Plot Derived from Data Recorded During Laboratory Vibration Tests in the Vertical Axis of the Weapon.

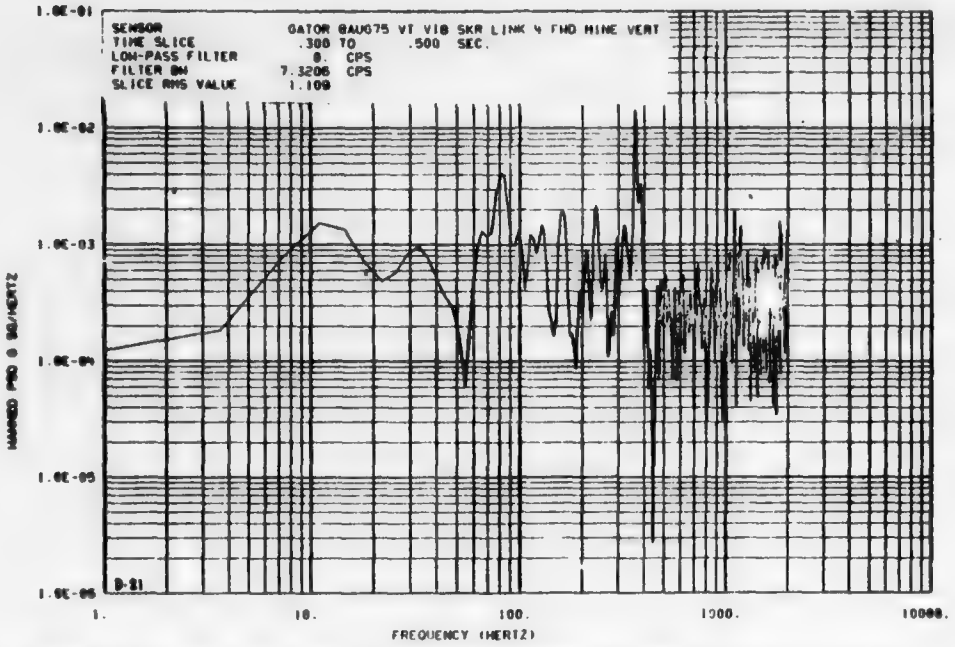

FIGURE D-21. PSD Plot Derived from Data Recorded During Laboratory Vibration Tests in the Vertical Axis of the Weapon.

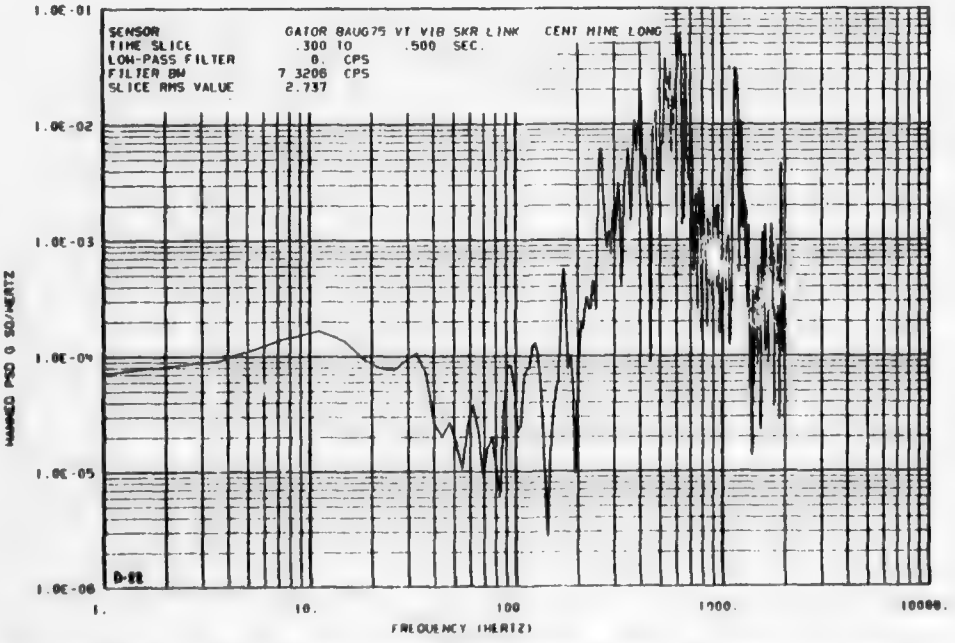

FIGURE D-22. PSD Plot Derived from Data Recorded During Laboratory Vibration Tests in the Vertical Axis of the Weapon.

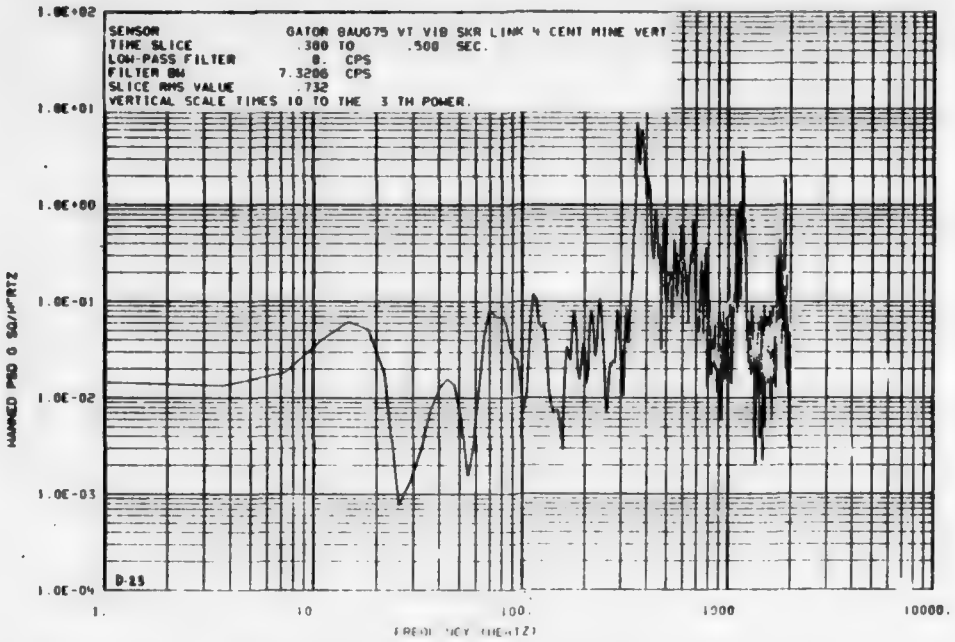

FIGURE D-23. PSD Plot Derived from Data Recorded During Laboratory Vibration Tests in the Vertical Axis of the Weapon.

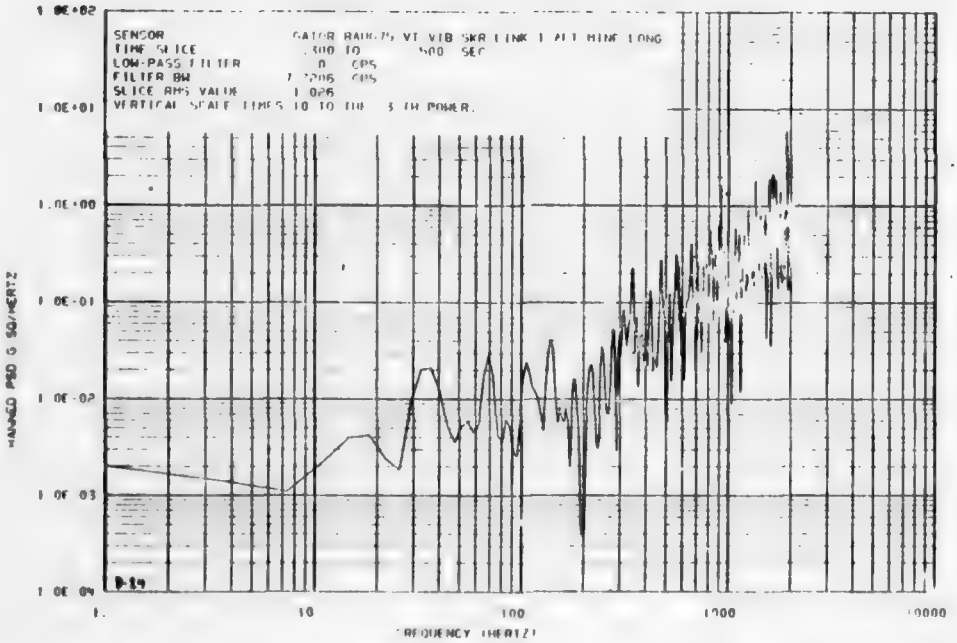

FIGURE D-24. PSD Plot Derived from Data Recorded During Laboratory Vibration Tests in the Vertical Axis of the Weapon.

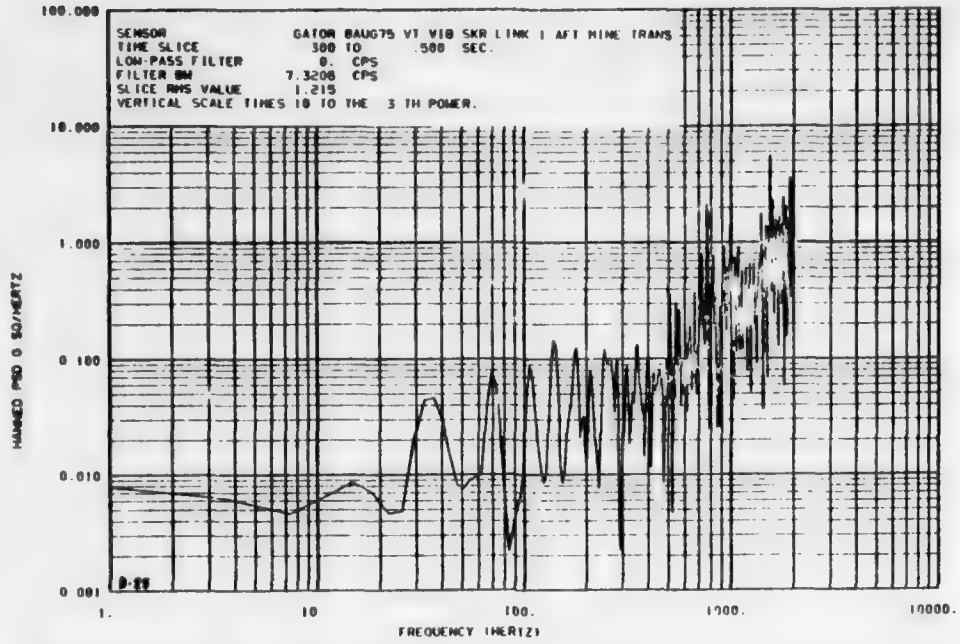

FIGURE D-25. PSD Plot Derived from Data Recorded During Laboratory Vibration Tests in the Vertical Axis of the Weapon.

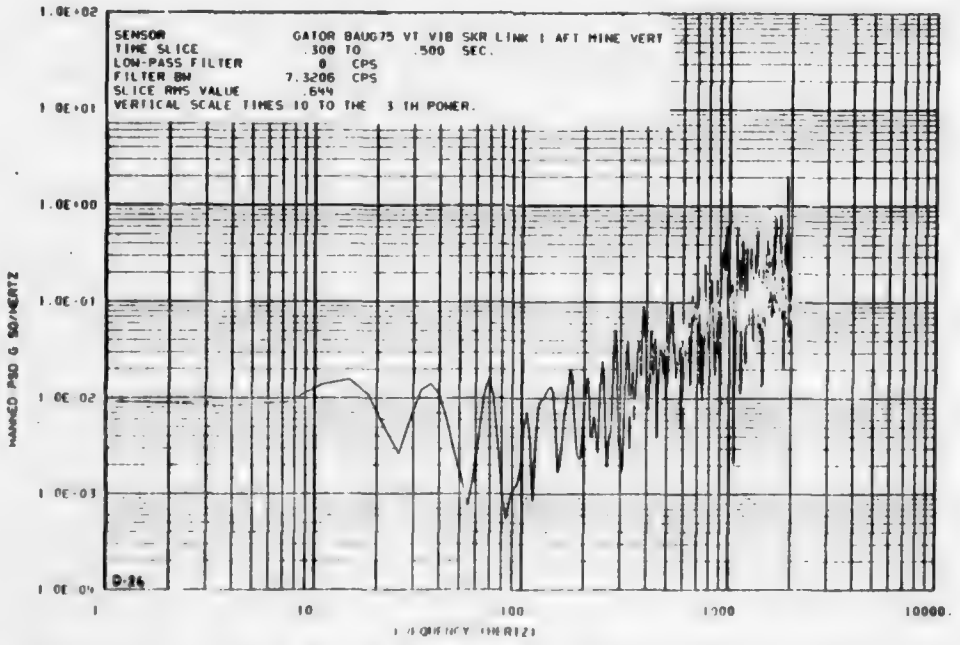

FIGURE D-26. PSD Plot Derived from Data Recorded During Laboratory Vibration Tests in the Vertical Axis of the Weapon.

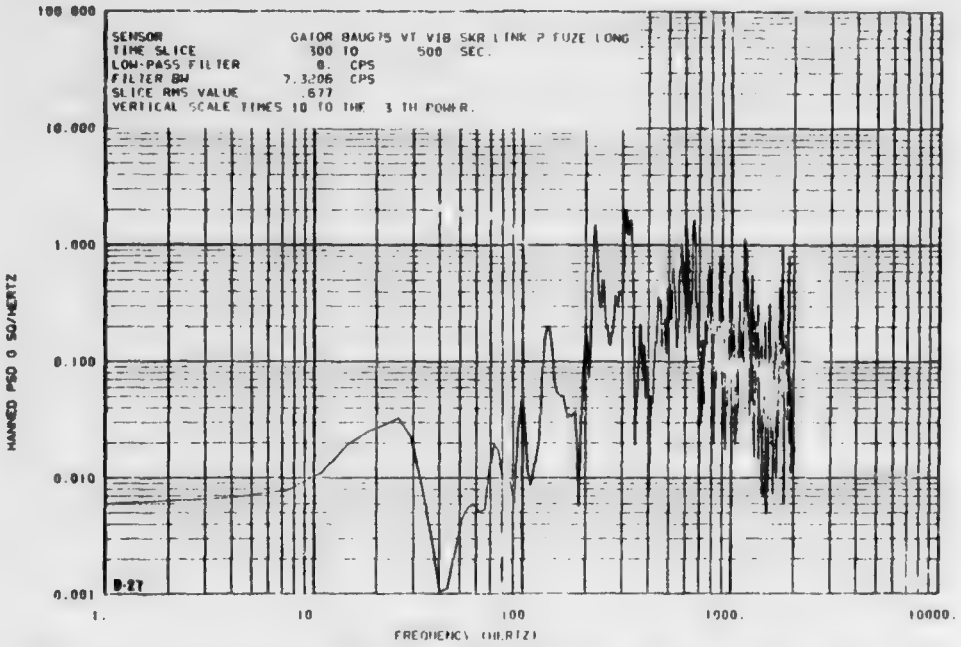

FIGURE D-27. PSD Plot Derived from Data Recorded During Laboratory Vibration Tests in the Vertical Axis of the Weapon.

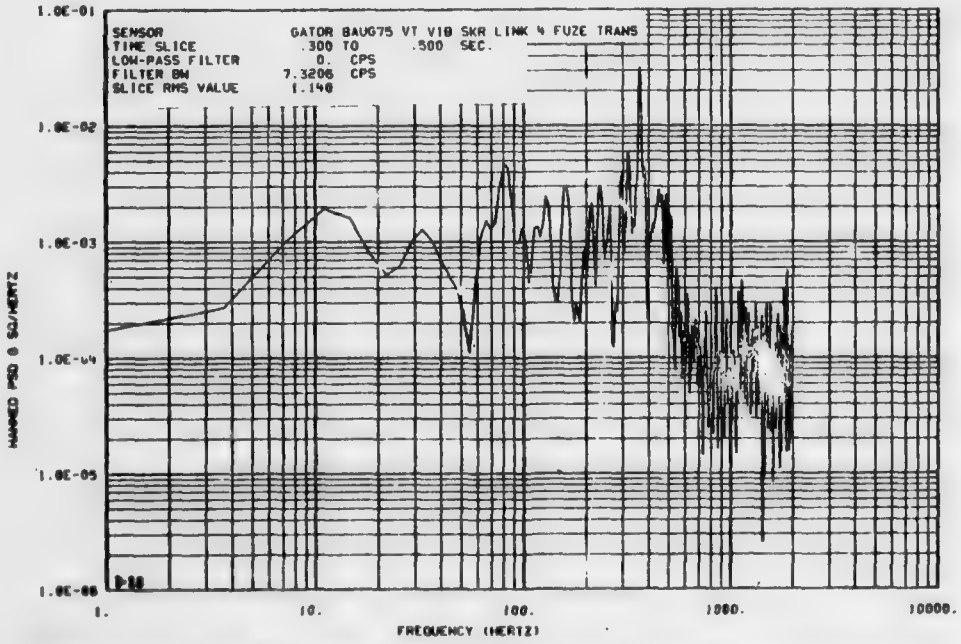

FIGURE D-28. PSD Plot Derived from Data Recorded During Laboratory Vibration Tests in the Vertical Axis of the Weapon.

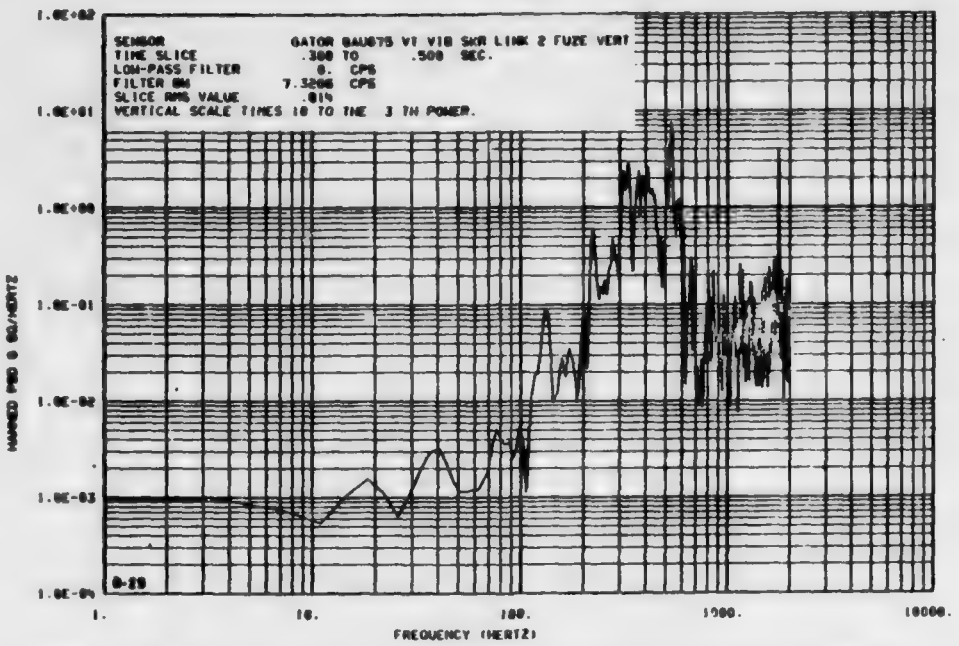

FIGURE D-29. PSD Plot Derived from Data Recorded During Laboratory Vibration Tests in the Vertical Axis of the Weapon.

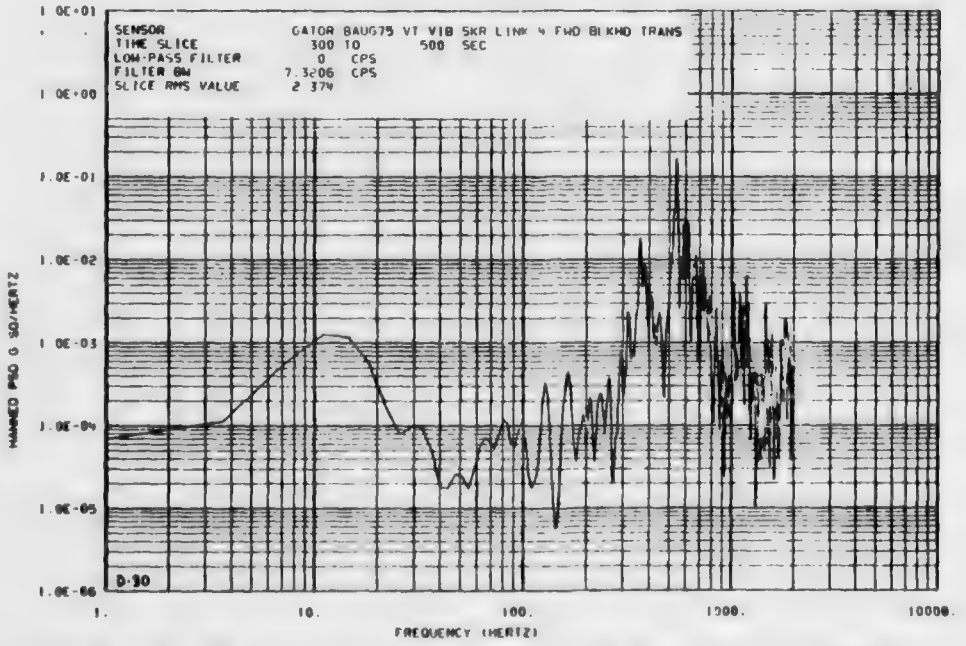

FIGURE D-30. PSD Plot Derived from Data Recorded During Laboratory Vibration Tests in the Vertical Axis of the Weapon.

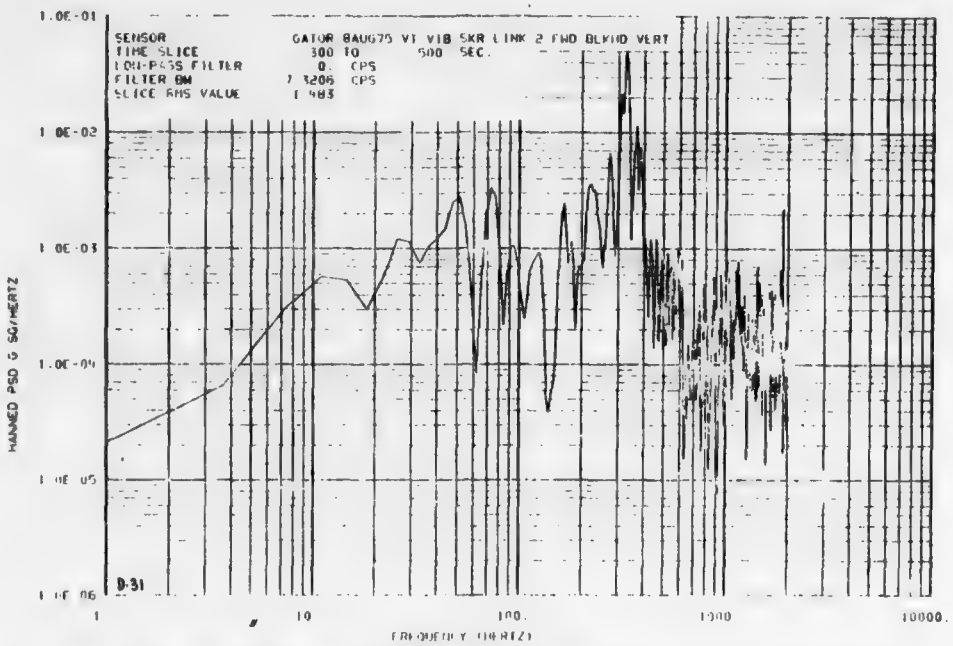

FIGURE D-31. PSD Plot Derived from Data Recorded During Laboratory Vibration Tests in the Vertical Axis of the Weapon.

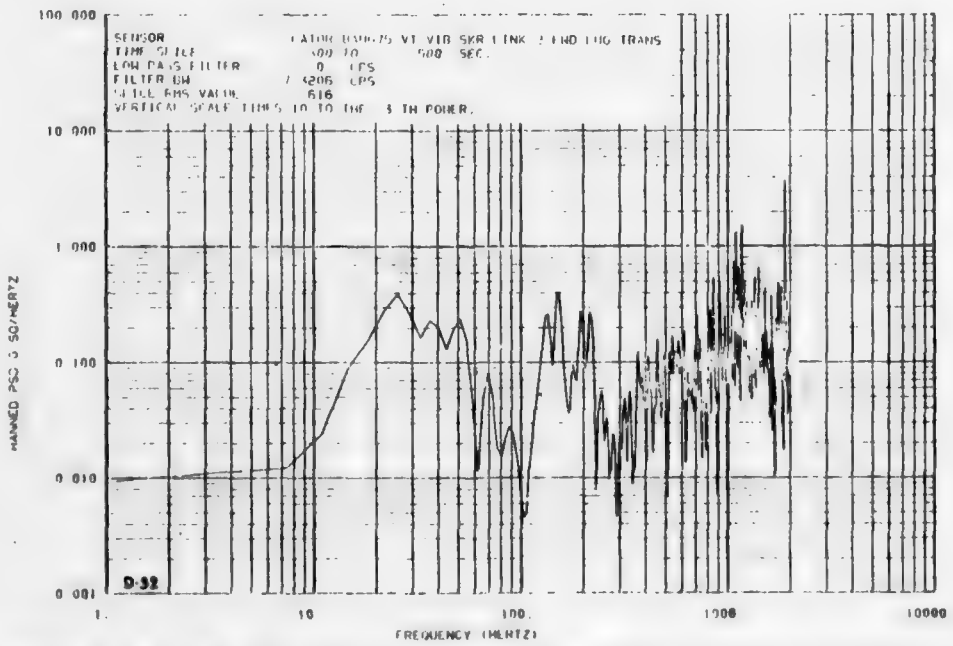

FIGURE D-32. PSD Plot Derived from Data Recorded During Laboratory Vibration Tests in the Vertical Axis of the Weapon.

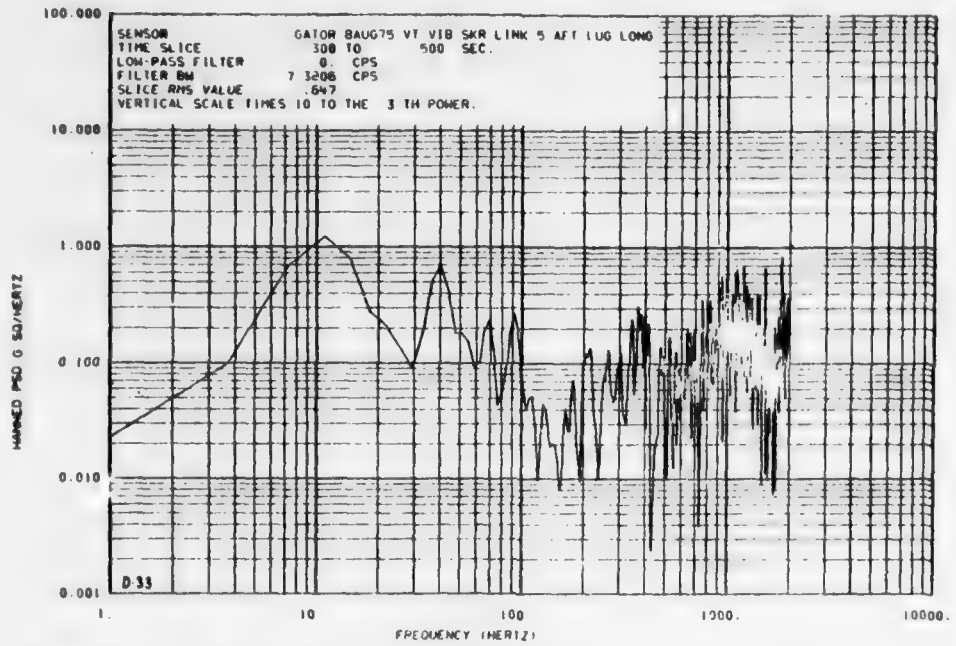

FIGURE D-33. PSD Plot Derived from Data Recorded During Laboratory Vibration Tests in the Vertical Axis of the Weapon.

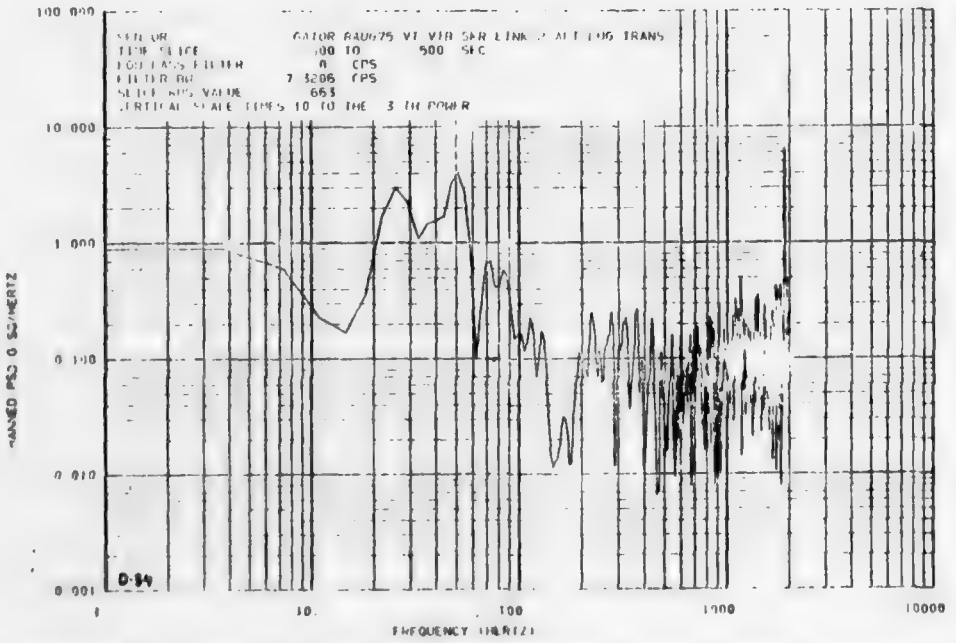

FIGURE D-34. PSD Plot Derived from Data Recorded During Laboratory Vibration Tests in the Vertical Axis of the Weapon.

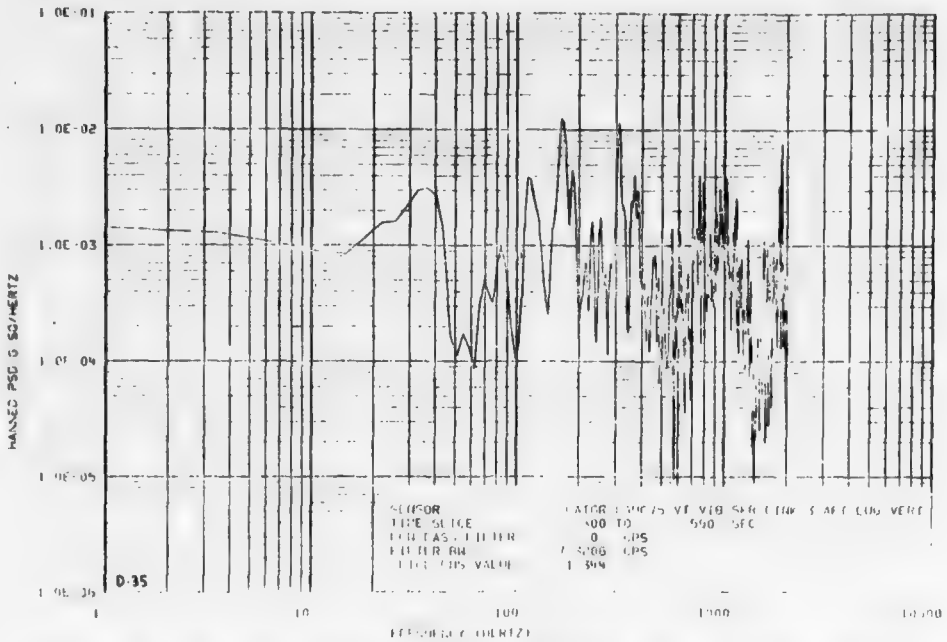

FIGURE D-35. PSD Plot Derived from Data Recorded During Laboratory Vibration Tests in the Vertical Axis of the Weapon.

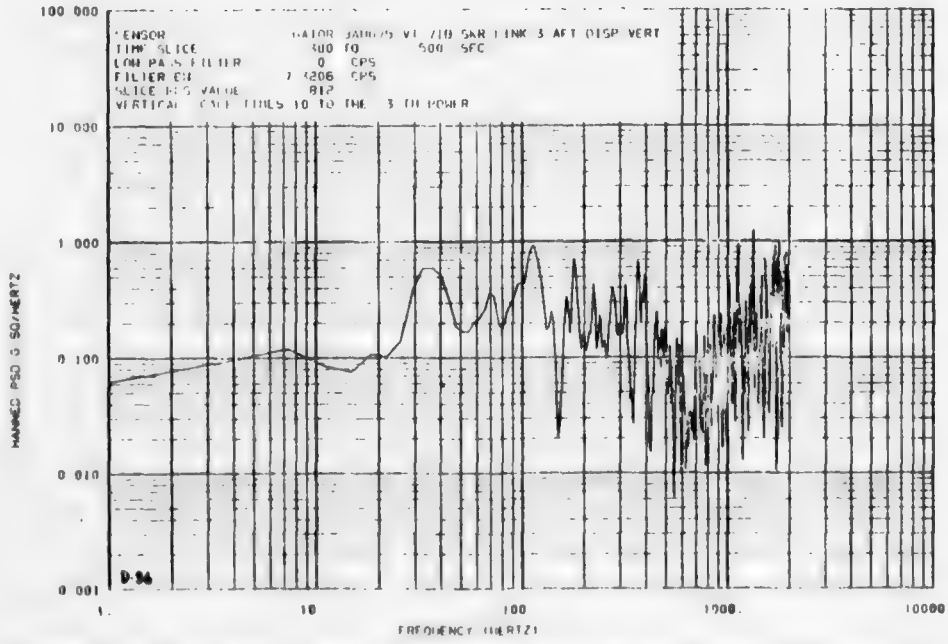

FIGURE D-36. PSD Plot Derived from Data Recorded During Laboratory Vibration Tests in the Vertical Axis of the Weapon.

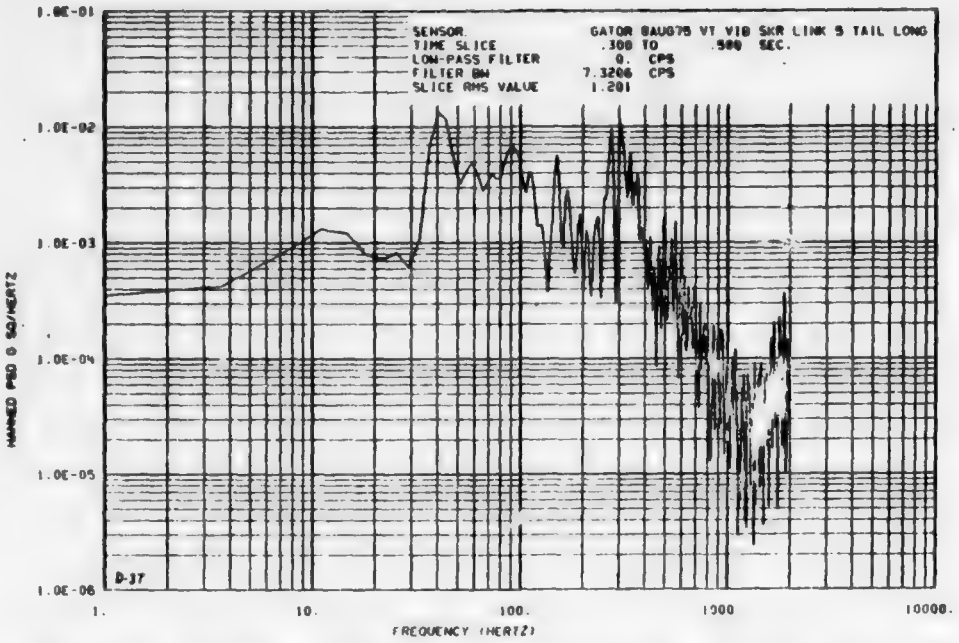

FIGURE D-37. PSD Plot Derived from Data Recorded During Laboratory Vibration Tests in the Vertical Axis of the Weapon.

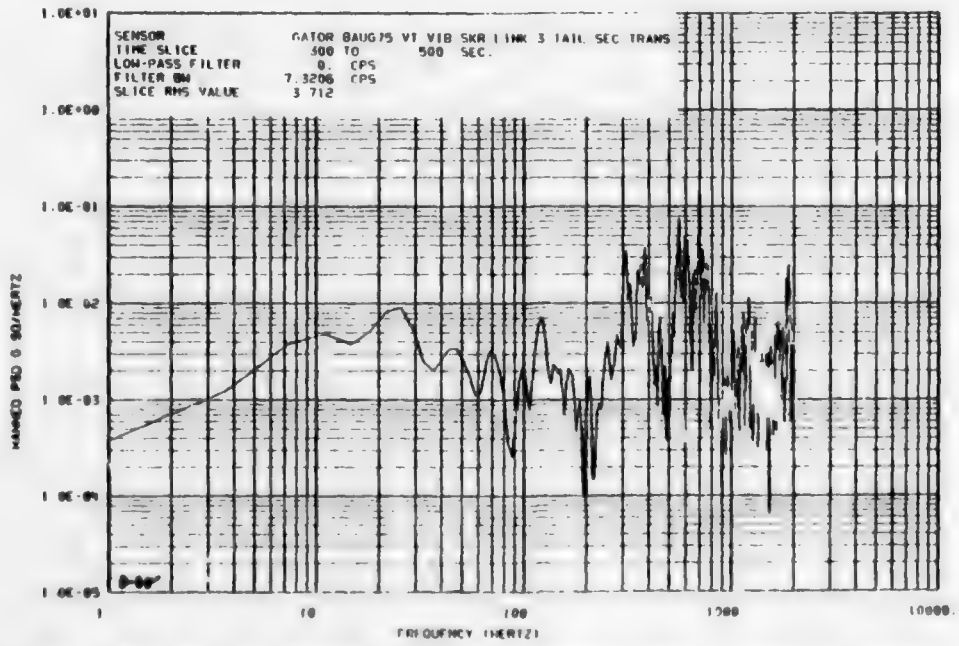

FIGURE D-38. PSD Plot Derived from Data Recorded During Laboratory Vibration Tests in the Vertical Axis of the Weapon.

Appendix E

Overall g RMS Levels During
Selected Flight Conditions
(Tables E-1 through E-9)

TABLE E-1. Overall g RMS Levels Measured During Takeoff at Approximately 2,200-Feet Mean Sea Level (MSL).

Item no.	Location	Sensitivity axis			g level, RMS
		Long. (x)	Trans. (y)	Vert. (z)	
1	Fuze, Mk 339	X			1.795
			X		1.612
				X	1.082
2	Dispenser, forward bulkhead		X		1.137
				X	1.122
3	Strongback, forward lug		X		---
				X	---
4	Strongback, aft lug	X			---
			X		---
				X	2.595
5	Dispenser, aft end		X		1.198
				X	0.992
6	Tail cone, forward bulkhead	X			1.158
			X		1.753
				X	---
11	Forward mine	X			1.148
			X		0.951
				X	0.907
12	Central mine	X			1.120
			X		---
				X	1.536
13	Aft mine	X			0.863
			Y		1.540
				X	1.135

NOTES:
1. Item number assigned to other GATOR system components.
2. "---" indicates no valid data due to equipment malfunction.

AD-A036 498 NAVAL WEAPONS CENTER CHINA LAKE CALIF F/G 1/3
GATOR/AV-8A ENVIRONMENTAL CAPTIVE FLIGHT VIBRATION RESPONSE TES--ETC(U)
FEB 77 K T KATSUMOTO, W W PARMENTER
UNCLASSIFIED NWC-TP-5883 NL

2 OF 2
AD
036 498

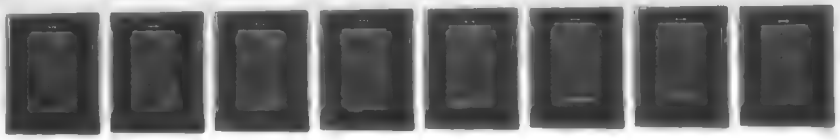

DATE
FILMED
4-13-77
NTIS

TABLE E-2. Overall g RMS Levels Measured During Level Flight at Maximum Speed (Approximately 500 Knots IAS) at 10,000-Feet MSL.

Item no.	Location	Sensitivity axis			g level, RMS
		Long. (x)	Trans. (y)	Vert. (z)	
1	Fuze, Mk 339	X			2.062
			X		1.672
				X	1.060
2	Dispenser, forward bulkhead		X		1.109
				X	1.188
3	Strongback, forward lug		X		1.631
				X	---
4	Strongback, aft lug	X			---
			X		1.649
				X	2.448
5	Dispenser, aft end		X		1.306
				X	0.930
6	Tail cone, forward bulkhead	X			1.171
			X		2.002
				X	---
11	Forward mine	X			0.912
			X		0.812
				X	0.770
12	Central mine	X			0.776
			X		---
				X	0.995
13	Aft mine	X			0.852
			X		1.500
				X	0.888

NOTES:
1. Item number assigned to other GATOR system components.
2. "---" indicates no valid data due to equipment malfunction.

TABLE E-3. Overall g RMS Levels Measured During Level Flight at Maximum Speed (Approximately 540 Knots IAS) at 5,000-Feet MSL.

Item no.	Location	Sensitivity axis			g level, RMS
		Long. (x)	Trans. (y)	Vert. (z)	
1	Fuze, Mk 339	X			2.338
			X		1.800
				X	1.082
2	Dispenser, forward bulkhead		X		1.289
				X	1.272
3	Strongback, forward lug		X		1.777
				X	—
4	Strongback, aft lug	X			—
			X		1.736
				X	2.101
5	Dispenser, aft end		X		1.089
				X	0.815
6	Tail cone, forward bulkhead	X			1.293
			X		1.664
				X	—
11	Forward mine	X			0.901
			X		0.914
				X	0.866
12	Central mine	X			0.713
			X		—
				X	0.963
13	Aft mine	X			0.938
			X		1.014
				X	0.868

NOTES:
1. Item number assigned to other GATOR system components.
2. "—" indicates no valid data due to equipment malfunction.

TABLE E-4. Overall g RMS Levels Measured During Flight at 400 Knots IAS, 5,000-Feet MSL, with Nozzles at 45 Degrees and 80% Power.

Item no.	Location	Sensitivity axis			g level, RMS
		Long. (x)	Trans. (y)	Vert. (z)	
1	Fuze, Mk 339	X			1.808
			X		1.702
				X	0.945
2	Dispenser, forward bulkhead		X		0.547
				X	1.062
3	Strongback, forward lug		X		1.468
				X	—
4	Strongback, aft lug	X			—
			X		1.514
				X	3.336
5	Dispenser, aft end		X		1.750
				X	1.156
6	Tail cone, forward bulkhead	X			0.985
			X		2,583
				X	—
11	Forward mine	X			0.936
			X		0.816
				X	0.714
12	Central mine	X			0.737
			X		—
				X	0.985
13	Aft mine	X			0.766
			X		0.726
				X	0.680

NOTES:
1. Item number assigned to other GATOR system components.
2. "—" indicates no valid data due to equipment malfunction.

TABLE E-5. Overall g RMS Levels Measured During Flight at 250 Knots IAS, 5,000-Feet MSL, with Nozzles at 81 Degrees (except as noted), and 100% Power.

Item no.	Location	Sensitivity axis			g level, RMS
		Long. (x)	Trans. (y)	Vert. (z)	
1	Fuze, Mk 339	X			2.516
			X		2.775
				X	1.681
2	Dispenser, forward bulkhead		X		1.005
				X	1.726
3	Strongback, forward lug		X		2.882
				X	—
4	Strongback, aft lug	X			—
			X		2.835
				X	1.560
5	Dispenser, aft end		X		0.945
				X	0.679
6	Tail cone, forward bulkhead	X			1.971
			X		1.571
				X	—
11	Forward mine	X			2.115
			X		1.704
				X	1.453
12	Central mine	X			1.482*
			X		—
				X	2.234*
13	Aft mine	X			1.111*
			X		1.612*
				X	1.421*

NOTES:

1. Item number assigned to other GATOR system components.
2. "—" indicates no valid data due to equipment malfunction.
3. Readings noted with an asterisk (*) were taken with nozzles at 98.5 degrees vector.

TABLE E-6. Overall g RMS Levels Measured During Flight at 300 Knots IAS, 5,000-Feet MSL, with Nozzles at 81 Degrees (except as noted) and 80% Power.

Item no.	Location	Sensitivity axis			g level, RMS
		Long. (x)	Trans. (y)	Vert. (z)	
1	Fuze, Mk 339	X			1.794
			X		---
				X	0.825
2	Dispenser, forward bulkhead		X		---
				X	0.995
3	Strongback, forward lug		X		1.251
				X	---
4	Strongback, aft lug	X			---
			X		1.245
				X	2.180
5	Dispenser, aft end		X		1.160
				X	0.832
6	Tail cone, forward bulkhead	X			---
			X		1.852
				X	---
11	Forward mine	X			---
			X		---
				X	---
12	Central mine	X			0.477*
			X		---
				X	---
13	Aft mine	X			0.707*
			X		0.702*
				X	0.479*

NOTES:

1. Item number assigned to other GATOR system components.
2. "---" indicates no valid data due to equipment malfunction.
3. Readings noted with an asterisk (*) were taken with nozzles at 98.5 degrees vector.

TABLE E-7. Overall g RMS Levels Measured During Hover and Rolling Landing (as noted).

Item no.	Location	Sensitivity axis			g level, RMS
		Long. (x)	Trans. (y)	Vert. (z)	
1	Fuze, Mk 339	X			1.906
			X		1.470
				X	1.163
2	Dispenser, forward bulkhead		X		0.517
				X	1.346
3	Strongback, forward lug		X		1.757
				X	—
4	Strongback, aft lug	X			—
			X		1.585
				X	1.948*
5	Dispenser, aft end		X		1.020*
				X	0.846*
6	Tail cone, forward bulkhead	X			0.833*
			X		1.484*
				X	—
11	Forward mine	X			0.876
			X		0.736
				X	0.830
12	Central mine	X			0.852
			X		—
				X	0.935
13	Aft mine	X			0.737
			X		0.883
				X	0.776

NOTES:

1. Item number assigned to other GATOR system components.
2. "—" indicates no valid data due to equipment malfunction.
3. Readings noted with an asterisk (*) were taken during rolling vertical landing.

TABLE E-8. Overall g RMS Levels Measured During Laboratory Vibration Test Through the Vertical Axis.

Item no.	Location	Sensitivity axis			g level, RMS
		Long. (x)	Trans. (y)	Vert. (z)	
1	Fuze, Mk 339	X			0.677
			X		1.140
				X	0.814
2	Dispenser, forward bulkhead		X		2.374
				X	1.483
3	Strongback, forward lug		X		0.616
				X	---
4	Strongback, aft lug	X			---
			X		0.663
				X	1.344
5	Dispenser, aft end		X		---
				X	0.812
6	*Tail cone, forward bulkhead*	X			1.201
			X		3.712
				X	---
11	Forward mine	X			1.215
			X		1.267
				X	1.109
12	Central mine	X			2.737
			X		---
				X	0.732
13	Aft mine	X			1.026
			X		1.215
				X	0.644

NOTES:

1. Item number assigned to other GATOR system components.
2. "---" indicates no valid data due to equipment malfunction.

TABLE E-9. Overall g RMS Levels Measured During Laboratory Vibration Test Through the Transverse Axis.

Item no.	Location	Sensitivity axis			g level, RMS
		Long. (x)	Trans. (y)	Vert. (z)	
1	Fuze, Mk 339	X			1.753
			X		1.305
				X	0.932
2	Dispenser, forward bulkhead		X		1.255
				X	1.010
3	Strongback, forward lug		X		2.502
				X	—
4	Strongback, aft lug	X			—
			X		1.745
				X	1.749
5	Dispenser, aft end		X		—
				X	0.787
6	Tail cone, forward bulkhead	X			0.629
			X		2.058
				X	—
11	Forward mine	X			0.748
			X		0.871
				X	2.373
12	Central mine	X			0.728
			X		—
				X	0.726
13	Aft mine	X			1.132
			X		1.782
				X	—

NOTES:

1. Item number assigned to other GATOR system components.
2. "—" indicates no valid data due to equipment malfunction.